

PREDICTING THE EFFECTS OF WEIR MANAGEMENT ON DRAINAGE DISCHARGE OF A  
CONTROLLED DRAINAGE SYSTEM IN A CHANGING CLIMATE

By

Md Sami Bin Shokrana

A DISSERTATION

Submitted to  
Michigan State University  
in partial fulfillment of the requirements  
for the degree of

Biosystems Engineering – Doctor of Philosophy

2022

## ABSTRACT

The widespread adoption of subsurface drainage in the Midwest United States coupled with fertile land and abundant rainfall has made this region the largest producer of corn and soybean in the nation. Although subsurface drainage helps reduce the waterlogging stress on crops by removing nutrient-enriched water from the field, it could contribute to harmful algal blooms in freshwater ecosystems. Controlled drainage (CD) practices can reduce the drainage volume leaving the field and have a positive effect on nutrient load reduction. Although the efficiency of CD under the present climate has been widely studied, it is essential to evaluate its performance in the future to build resilient agricultural systems. In this study, the efficiency of two CD practices was evaluated in reducing drainage discharge for the future based on the height and timing of the weir management.

We used the Root Zone Water Quality Model (RZWQM2) to predict the CD management effects on drainage discharge. To obtain reliable simulation results from the RZWQM2 model, it is important to use measured soil-water characteristic parameters and flow data. We used HYPROP to measure the parameters of the soil water characteristic curve which served as input to the model. Additionally, we developed a stage-discharge equation for an AgriDrain metal-edge sharp-crest 45° V-notch weir to accurately estimate the drainage discharge from the field. A reliable estimate of the drainage discharge was necessary to accurately estimate the nutrient loss.

The recently developed P module of the RZWQM2, known as RZWQM2-P was used in this study to predict drainage discharge and P loss from a subsurface-drained field with clay loam soil. We used the Nash-Sutcliffe model Efficiency (NSE) and percentage bias (PBIAS) statistics to

evaluate model performance. While the model showed “good” and “satisfactory” performance in predicting drainage discharge and total phosphorus (TP) load, respectively, it performed unsatisfactorily in predicting the dissolved reactive phosphorus (DRP) load for both calibration and validation periods. The underperformance of the model in simulating DRP load may be due to the inability of the model to partition fertilizer P into different P pools.

We predicted the efficiency of two CD management scenarios (i.e., common and aggressive management) in reducing drainage discharge for future climate using the calibrated RZWQM2 model. The CD management scenarios were performed by maintaining the weir height at a higher (i.e., 15 cm for non-growing season and 40 cm for growing season) or lower (i.e., 30 cm for non-growing season or 50 cm for growing season) level inside a control structure and by altering the timing of the CD management based on the planting and harvesting dates. While both common and aggressive management was efficient in reducing drainage discharge for both historic and future periods, the percent reduction of drainage discharge with aggressive management was about 11% higher than the common management. The projected increase in precipitation and temperature in the future would cause increased drainage discharge during fall and winter. The aggressive management will be able to completely restrict the flow during the non-growing season which would reduce the nutrient loss of the surface water bodies. In the future, farmers should plant early to benefit from the projected increase in spring rainfall and avoid dry summers. In conclusion, it is evident from the results of this study that both common and aggressive CD management will continue to be effective in reducing drainage discharge in a changing climate.

Copyright by  
MD SAMI BIN SHOKRANA  
2022

To my parents, who sacrificed everything for my education. I would not have come this far without your love and support.

## TABLE OF CONTENTS

LIST OF TABLES.....	viii
LIST OF FIGURES.....	ix
LIST OF ABBREVIATIONS .....	xiii
CHAPTER 1: LITERATURE REVIEW .....	1
REFERENCES.....	6
CHAPTER 2: MEASUREMENT OF SOIL-WATER CHARACTERISTICS INPUT DATA .....	10
2.1    Abstract.....	10
2.2    Method Description.....	10
2.3    Soil Sample Collection .....	12
2.4    Preparing HYPROP2 .....	16
2.5    Starting the Measurements.....	26
2.6    Stopping the Measurements.....	27
2.7    Determining the Dry Weight .....	29
2.8    Method Validation.....	30
2.9    Summary.....	37
REFERENCES .....	38
CHAPTER 3: DEVELOPING A STAGE-DISCHARGE EQUATION FOR A V-NOTCH WEIR TO ESTIMATE THE DRAINAGE DISCHARGE .....	41
3.1    Abstract.....	41
3.2    Introduction .....	41
3.3    Materials and Methods .....	44
3.4    Results and Discussion.....	52
3.5    Conclusions.....	63
REFERENCES .....	64
CHAPTER 4: CALIBRATING THE RZWQM2-P MODEL TO SIMULATE DRAINAGE DISCHARGE AND PHOSPHORUS LOSS IN CLAY LOAM SOIL IN MICHIGAN .....	66
4.1    Abstract.....	66
4.2    Introduction .....	67
4.3    Materials and Methods .....	70
4.4    Results.....	85
4.5    Discussions.....	89
4.6    Conclusions.....	93
REFERENCES .....	94
CHAPTER 5: PREDICTING THE EFFECTS OF TWO CONTROLLED DRAINAGE SCENARIOS ON DRAINAGE DISCHARGE FOR FUTURE CLIMATE.....	100

5.1	Abstract.....	100
5.2	Introduction.....	101
5.3	Materials and Methods .....	104
5.4	Results and Discussions .....	112
5.5	Conclusions.....	127
	REFERENCES .....	128
APPENDIX A: CHAPTER 3.....		134
APPENDIX B: CHAPTER 4.....		141

## LIST OF TABLES

Table 2.1. Saturation time for different types of soils.....	20
Table 4.1. Annual management practices adopted at the Blissfield site [From Shokrana et al. (2022). Used with permission.].....	74
Table 4.2. Input soil hydrologic properties data for Ziegenfuss clay loam soil [From Shokrana et al. (2022). Used with permission.].....	76
Table 4.3. Input data for P pools to initiate the P model [From Shokrana et al. (2022). Used with permission.] .....	78
Table 4.4. Calibrated values of microporosity parameters [From Shokrana et al. (2022). Used with permission.] .....	81
Table 4.5. Calibrated soil hydraulic parameters and their values [From Shokrana et al. (2022). Used with permission.] .....	82
Table 4.6. Other calibrated hydrologic, P loss, soil erosion, and plant parameters and their values. Default values are recorded from Sadhukhan et al. (2019a) [From Shokrana et al. (2022). Used with permission.].....	83
Table 4.7. Model performance statistics for drainage discharge, DRP load, and TP load during the calibration and validation period [From Shokrana et al. (2022). Used with permission.] .....	89
Table 5.1. Summary of CMIP projections obtained from GCMs used in NASA NEX-GDDP database for RCP 4.5 emission scenario (Rojas-Downing et al., 2018) .....	109
Table 5.2. Management of weir height and timing of the common and aggressive managements used in the simulations during (1975-2004) and future (2030-2059) periods. The reference of the weir height is from the ground surface).....	111
Table 5.3. The 30-year average monthly temperature and precipitation under historic (1975-2004) and future (2030-2059) climate scenarios .....	116
Table 5.4. Comparison between historic (1975-2004) and future period (2030-2059) for 30-year average drainage discharge under FD and CD .....	119

## LIST OF FIGURES

Figure 2.1. Soil sampling tools: (a) sampling ring, (b) sample ring insertion tool, (c) rubber mallet, and (d) trowel .....	14
Figure 2.2. (a) hammering to collect soil cores, (b) soil core inserted and ready to collect after hammering, (c) removing soil from the sides of the sample ring to collect undisturbed samples, (d) put a white cap on the sample ring before digging it out with a trowel, (e) digging out the sample ring with trowel and (f) flattening the soil surface with the trowel .....	15
Figure 2.3. Degassing water using a vacuum pump and a vacuum bottle: (a) Assembly of instruments for degassing DI water and (b) Blue tube should be kept in air inside the vacuum bottle while degassing DI water .....	16
Figure 2.4. (a) vacuum pump, (b) beaker mount, (c) vacuum mount and (d) assembly of Hyprop refilling unit .....	18
Figure 2.5. (a) cap is removed from the cutting edge of soil core, (b) Soil core is flipped, and a cheesecloth and perforated tray was put on the soil core, (c) Soil core flipped again with the cap removed, (d) soil core was put in a tray, (e) drainage water was poured in the tray, and (f) drainage water was poured until the cutting edge of the tray .....	21
Figure 2.6. HYPROP 2 sensor unit after implementing the tensio shafts .....	23
Figure 2.7. Shiny surface appears on top of soil core .....	25
Figure 2.8. (a) sensor unit placed on the soil ring, (b) after removing cheesecloth and perforated tray, the user flips the assembled sensor unit and soil core .....	26
Figure 2.9. Assembled sensor unit and soil core is put on a balance to start measurements .....	27
Figure 2.10. An optimal measuring curve for HYPROP measurements (image source: HYPROP Manual) .....	29
Figure 2.11. Tension curve for a clay loam soil. Tension is in units of hectopascal (1 kPa = 10 hPa) .....	31
Figure 2.12. Volumetric water content vs. pF plot using evaporation method and fitted soil water characteristic curve for a clay loam soil .....	32
Figure 2.13. Tension curve for a sandy loam soil. Tension is in units of hectopascal (1 kPa = 10 hPa) .....	35

Figure 2.14. Volumetric water content vs. pF plot using evaporation method and fitted soil water characteristic curve for a sandy loam soil..... 36

Figure 3.1. Top: Diagram of the experimental setup showing water flow through a V-notch weir. Bottom: Sideview photo of the control structure with flowing water [From Shokrana and Ghane (2021). Used with permission.] ..... 48

Figure 3.2. Left: Schematic diagram of a metal-edge sharp-crest 45° V-notch weir. The apex is the point at which both inclined sides of the metal crest meet. The dimensions of the V-notch weir do not include the thickness of the rubber gaskets attached to the board. Right: Photo of the metal-edge sharp-crest 45° V-notch weir [From Shokrana and Ghane (2021). Used with permission.]..... 49

Figure 3.3. Diagram of the side view of a control structure and the distances needed to calculate the head (H) flowing through a V-notch weir using equation (3.5). A Solinst water-depth sensor was used to measure the distance "a" from the top of the structure to the upstream water surface and "f" from the top of the structure to the downstream water surface. A tape measure was used to measure the distance "b" inside the structure, and a meter-stick was used to measure the distance "c" from the top of the structure to the apex of the V-notch weir. Distance "d" was calculated by subtracting "a" from "b" [From Shokrana and Ghane (2021). Used with permission.] ..... 50

Figure 3.4. Measurement of the distance "c" from the top of the control structure to the apex of the V-notch weir. Multiple meter-sticks were glued and riveted together to make a long one. To measure the distance "c": (a) We lowered the meter-stick inside the apex of the V-notch weir, and (b) next, we measured the distance from the apex to the top of the structure by placing another ruler on the top and reading the value on the vertical meter stick [From Shokrana and Ghane (2021). Used with permission.] ..... 51

Figure 3.5. Calibration equation for a metal-edge sharp-crest V-notch weir. We developed this equation for a maximum flow rate of 409.42 L/min with a head of 16.3 cm. We used the weighing method for the low flow rates (16-59 L/min) and the flow meter for the higher flow rates (105-409 L/min). This equation is valid for an H less than the height of the V-notch (i.e., flow through the V-notch). In our experiment, the height of the V-notch was 17.0 cm [From Shokrana and Ghane (2021). Used with permission.] ..... 53

Figure 3.6. Comparison of the V-notch equation developed in this study to those in previous studies [From Shokrana and Ghane (2021). Used with permission.] ..... 55

Figure 3.7. Measurement of water level with water-finding paste. A small amount of paste is applied to a meter stick, which is inserted into water. The dry paste is white but turns red upon contact with water [From Shokrana and Ghane (2021). Used with permission.] ..... 58

Figure 3.8. Measurement of water level using a water-depth sensor: (a) Solinst water-depth sensor; the sensor is located at the middle of the probe. Once the sensor comes in contact with water, sound and light signals will indicate when to take the reading. (b) The sensor probe is lowered inside the control structure through a PVC pipe to reduce the effect of flow turbulence. Once in place, the length of the flat tape along the wall of the control structure indicates the water depth [From Shokrana and Ghane (2021). Used with permission.]..... 59

Figure 3.9. A diagram (not drawn to scale) to represent the water flow inside a 25-cm control structure in agricultural fields. Top diagram: If there is heavy rainfall, the water level in the ditch will rise and the water level in the downstream chamber of the control structure will rise above the apex of the V-notch, causing submerged flow. Bottom diagram: Adding a 17.8 cm (7-inch) bottom board below the V-notch weir would give extra height to the apex of the V-notch weir, so there would be a greater chance of achieving freely flowing water through the V-notch [From Shokrana and Ghane (2021). Used with permission.] ..... 62

Figure 4.1. (a) geographic location of the Blissfield site. This site is part of the River Raisin watershed which directly discharges into the western basin of Lake Erie at Monroe Harbor (b) drainage layout of the study site [From Shokrana et al. (2022). Used with permission.] ..... 73

Figure 4.2. Comparison between observed and simulated drainage discharge during the calibration period (October 1, 2018 – September 30, 2020) [From Shokrana et al. (2022). Used with permission.] ..... 86

Figure 4.3. Comparison between observed and simulated drainage discharge during the validation period (October 1, 2020 – June 30, 2022) [From Shokrana et al. (2022). Used with permission.] ..... 86

Figure 4.4. Comparison between observed and simulated DRP loss through drainage discharge during the calibration period (October 1, 2018 – September 30, 2020) [From Shokrana et al. (2022). Used with permission.]..... 87

Figure 4.5. Comparison between observed and simulated DRP loss through drainage discharge during the validation period (October 1, 2020 – June 30, 2022) [From Shokrana et al. (2022). Used with permission.] ..... 87

Figure 4.6. Comparison between observed and simulated TP loss through drainage discharge during the calibration period (October 1, 2018 – September 30, 2020) [From Shokrana et al. (2022). Used with permission.]..... 88

Figure 4.7. Comparison between observed and simulated TP loss through drainage discharge during the validation period (October 1, 2020 – June 30, 2022) [From Shokrana et al. (2022). Used with permission.] ..... 88

Figure 5.1. Hydrologic boundary of the river raisin watershed. The Blissfield is part of this river raisin watershed which directly discharges into the wester Lake Erie basin at Monroe Harbor ..... 105

Figure 5.2. Change in the 30-year average monthly maximum, minimum, and Mean temperature..... 113

Figure 5.3. Changes in precipitation amount under historical (1975-2004) and future climate scenario (2030-2059) ..... 115

Figure 5.4. 30-year average monthly drainage discharge for historic and future period ..... 119

Figure 5.5. The 30-year average monthly drainage discharge under FD, common management, and aggressive management for the historic period (1975-2004) ..... 122

Figure 5.6. The 30-year average monthly drainage discharge under FD, common management, and aggressive management for the future period (2030-2059) ..... 123

Figure 5.7. The variability in simulated future drainage discharge using 21 GCMs under FD management..... 125

Figure 5.8. The variability in simulated future drainage discharge using 21 GCMs under common management..... 125

Figure 5.9. The variability in simulated future drainage discharge using 21 GCMs under aggressive management ..... 126

## LIST OF ABBREVIATIONS

CD	Controlled Drainage
DRP	Dissolved Reactive Phosphorus
FD	Free Drainage
gSSURGO	Gridded Soil Survey Geographic Database
HYPROP	Hydraulic Property Analyzer
NSE	Nash-Sutcliffe Efficiency
PBIAS	Percentage Bias
RZWQM2	Root Zone Water Quality Model
SWCC	Soil Water Characteristics Curve
TP	Total Phosphorus
WLEB	Western Lake Erie Basin

## CHAPTER 1: LITERATURE REVIEW

The increasing population around the world demands an increase in food production. To meet this demand, agricultural lands have not been increased at the same rate. In many cases, forested and agricultural lands have been transformed into urban areas, thus increasing surface runoff and inundation of low-land areas. Agricultural lands are under heavy stress to increase crop production. Irrigation increases the crop yield but if water does not drain properly from the fields waterlogging might decrease the production of certain crops such as corn and soybean. Therefore, agricultural fields need to be properly drained.

Most of the drainage occurred in the Midwest United States during the 1900s as federal and local government imposed laws regarding drainage and provided the necessary support for farmers to implement it (University of Illinois Extension, 2022). Since then, subsurface drainage practice is widely used in water-abundant areas of the US to improve crop production (King et al., 2014). Subsurface drainage helps reduce crop waterlogging stress by lowering the groundwater table and allowing farmers to perform timely field operations (Blann et al., 2009; Fausey et al., 1995). While the agronomic benefits of subsurface drainage are well documented (Fraser et al., 2001; Gardner et al., 1994; Hill, 1976), downstream environmental problems have been associated with the practice (Jaynes et al., 2001; Sims et al., 1998; Wright & Sands, 2001). A large number of studies have linked subsurface drainage to water quality problems in the receiving surface water bodies, leading to downstream eutrophication and hypoxia problems (Ahiablame et al., 2011; Rabalais et al., 2002). Farmers in the Midwest United States apply Phosphorus (P) and Nitrogen (N) based fertilizers in their fields which are transported to surface

water through surface runoff and subsurface drainage pathways. As a result, the presence of excessive nutrients causes harmful algal blooms (HABs) in freshwater ecosystems.

The golden rule of drainage states: “Drain only the amount of water that is necessary for crop production and not a drop more” – all drainage systems that do not meet this rule most likely transport nutrients and water that is no longer available for crop uptake. Therefore, it is evident that restricting drainage discharge from leaving the field is important to reduce nutrient load. Controlled drainage (CD) is a conservation practice of managing water in the field by changing the outlet level of the drainage system (Evans et al., 1995; Lalonde et al., 1996; Nash et al., 2015; Saadat et al., 2018; Wesstrom & Messing, 2007; Williams et al., 2015b). This practice reduces the drainage volume which in turn reduces the nutrient load coming from the fields. The level is controlled with weir boards or stoplogs inside a control structure. The weir boards are usually lowered a few weeks before planting and harvesting, and then raised after the field operations are completed (Thorp et al., 2008; Youssef et al., 2018). The goal is to keep water inside the field for increased crop uptake during dry periods of the year and also to reduce drainage discharge during the non-growing season.

Several on-farm and on-station replicated plot experiments were conducted to determine the efficiency of CD in reducing drainage discharge and nutrient loss (especially P). Since P is the limiting nutrient for the HABs in freshwater systems, we focused on the studies that worked with the P loss and drainage discharge reduction performance of the CD systems. Williams et al., (2015a) performed an on-farm experiment in Ohio, USA and they found a 7.5 to 33.6% reduction and drainage discharge and a 40 to 68% reduction in dissolved reactive phosphorus (DRP) load under CD management. These findings were in agreement with the findings observed in

Denmark, where the authors found a 37 to 54% reduction in drainage discharge and a 41 to 51% reduction in DRP load (Carstensen et al., 2019). A 60% reduction in drainage discharge and a 66% reduction in total phosphorus (TP) load were obtained from a study in Canada (Sunohara et al., 2016). On the other hand, Saadat et al. (2018) reported no reduction in P loading from Indiana, USA, while a 25 to 39% reduction in drainage discharge was obtained under CD. King et al., (2022) found an insignificant reduction in drainage discharge, but the TP load reduction was significant. The above discussion states that the performance of CD in reducing drainage discharge and P loading varies in different parts of the world and more studies are needed.

While long-term field experiments with CD management can provide the best estimates of drainage discharge and nutrient loss from subsurface-drained fields, they are expensive and time-consuming. On the contrary, field-scale hydrologic models are robust, inexpensive, and can provide results in a cost-effective manner compared to field studies. Therefore, several field-scale models (DRAINMOD, RZWQM2, ICECREAM, etc.) were developed by researchers to predict drainage discharge and nutrient loss from agricultural fields. While a lot of these models can satisfactorily predict the drainage discharge from subsurface-drained fields, their performance in predicting P loss with discharge is still questionable and largely uninvestigated. Therefore, there is a need to assess the performance of these P models in simulating drainage discharge and P loss from fields.

A comprehensive literature review on the P model suggested that ICECREAM is the best model that can predict P loss from surface runoff and subsurface drainage discharge (Qi & Qi, 2016; Radcliffe et al., 2015). However, since ICECREAM lacks a water-table based tile drainage component and uses a simple storage routing concept to mimic tile drainage, there is room to

improve this model (Pferdmenges et al., 2020). To improve the limitations of ICECREAM, Sadhukhan et al. (2019) developed the P module for the Root Zone Water Quality Model (RZWQM2) known as RZWQM2-P. The RZWQM2 is a process-based model that has been widely used in North America (Ahmed et al., 2007; Jiang et al., 2018; Ma et al., 2007; Malone et al., 2014; Thorp et al., 2008), but the P component of this model has been only tested twice by the developers for the same on-station plot experiment under a free drainage scenario. It is important to test the performance of the P model under CD management coupled with different climates, soil types, fertilization, and cropping practices.

The performance of CD in reducing drainage discharge under the present climate has been widely tested around the world (Nash et al., 2015; Saadat et al., 2018; Tolomio & Borin, 2018; Wahba et al., 2001; Wesstrom & Messing, 2007; Williams et al., 2015a), but the efficiency of CD for the future climate is still limited. Pease et al. (2017) conducted a study in Ohio, USA, and reported a reduction in drainage discharge in the future although the climate projections indicated a significant increase in precipitation and temperature for the future. The authors concluded that increased evapotranspiration (ET) due to increased temperature likely has caused reduced drainage discharge in the future. Another study in Poland reported that the most efficient way of reducing drainage discharge with CD management will be to implement it in the early spring (Sojka et al., 2020). Another study investigated the effects of the timing of weir management under CD for future climate (Salla et al., 2022). They found that drainage discharge under differently timed CD management was decreased by 11% to 23% under future climate conditions.

While previous studies concentrated on the timing of weir management (Salla et al., 2022), they ignored the effects on drainage discharge caused by the height of weir management. Those that investigated the height of weir management on CD performance, used the same weir height under CD for both non-growing and growing seasons (Williams et al., 2015), which is not a common practice in the Midwest USA. Only Saadat et al. (2018) performed an on-farm experiment to evaluate the height of weir management on CD performance for existing climate and drainage design. Therefore, it is important to predict the efficiency of CD in reducing drainage discharge under both varying heights and time management for future climate.

The objective of this study is to predict the effects of height and timing of weir management on the drainage discharge of a CD system for future climate conditions in Michigan. The outcome of this study will help farmers make informed decisions on weir management in the future to reduce the waterlogging stress on crops, and to reduce the drainage discharge and nutrient loss from the fields. The following tasks were performed to achieve this objective:

Task 1: Measurement of soil-water characteristics input data

Task 2: Developing a stage-discharge equation for a V-notch weir to estimate the drainage discharge

Task 3: Calibrating the RZWQM2-P model to simulate drainage discharge and phosphorus loss in clay loam soil in Michigan

Task 4: Predicting the effects of two controlled drainage scenarios on drainage discharge for future climate

## REFERENCES

- Ahiablame, L. M., Chaubey, I., Smith, D. R., & Engel, B. A. (2011). Effect of tile effluent on nutrient concentration and retention efficiency in agricultural drainage ditches. *Agricultural Water Management*, 98(8), 1271–1279.
- Ahmed, I., Rudra, R., McKague, K., Gharabaghi, B., & Ogilvie, J. (2007). Evaluation of the Root Zone Water Quality Model (RZWQM) for Southern Ontario: Part II. Simulating Long-Term Effects of Nitrogen Management Practices on Crop Yield and Subsurface Drainage Water Quality. *WATER QUALITY RESEARCH JOURNAL OF CANADA*, 42(3), 219–230. <https://doi.org/10.2166/wqrj.2007.025>
- Blann, K. L., Anderson, J. L., Sands, G. R., & Vondracek, B. (2009). Effects of agricultural drainage on aquatic ecosystems: a review. *Critical Reviews in Environmental Science and Technology*, 39(11), 909–1001.
- Carstensen, M. v, Borgesen, C. D., Ovesen, N. B., Poulsen, J. R., Hvid, S. K., & Kronvang, B. (2019). Controlled Drainage as a Targeted Mitigation Measure for Nitrogen and Phosphorus. *JOURNAL OF ENVIRONMENTAL QUALITY*, 48(3), 677–685. <https://doi.org/10.2134/jeq2018.11.0393>
- Evans, R. O., Skaggs, R. W., & Gilliam, J. W. (1995). CONTROLLED VERSUS CONVENTIONAL DRAINAGE EFFECTS ON WATER-QUALITY. *JOURNAL OF IRRIGATION AND DRAINAGE ENGINEERING-ASCE*, 121(4), 271–276. [https://doi.org/10.1061/\(ASCE\)0733-9437\(1995\)121:4\(271\)](https://doi.org/10.1061/(ASCE)0733-9437(1995)121:4(271))
- Fausey, N. R., Brown, L. C., Belcher, H. W., & Kanwar, R. S. (1995). Drainage and Water-quality in Great-Lakes and Corn-belt States. *Journal of Irrigation and Drainage Monitoring-ASCE*, 121(4), 283–288. [https://doi.org/10.1061/\(ASCE\)0733-9437\(1995\)121:4\(283\)](https://doi.org/10.1061/(ASCE)0733-9437(1995)121:4(283))
- Fraser, H., Fleming, R., & Eng, P. (2001). Environmental benefits of tile drainage. *Prepared for: LICO. Land Improvement Contractors of Ontario. Ridgetown College, University of Guelph.*
- Gardner, W. K., Drendel, M. F., & McDonald, G. K. (1994). Effects of subsurface drainage, cultivation, and stubble retention on soil porosity and crop growth in a high rainfall area. *Australian Journal of Experimental Agriculture*, 34(3), 411–418.
- Hill, A. R. (1976). *The environmental impacts of agricultural land drainage.*
- Jaynes, D. B., Colvin, T. S., Karlen, D. L., Cambardella, C. A., & Meek, D. W. (2001). Nitrate loss in subsurface drainage as affected by nitrogen fertilizer rate. *Journal of Environmental Quality*, 30(4), 1305–1314.

- Jiang, Q. J., Qi, Z. M., Madramootoo, C. A., & Singh, A. K. (2018). Simulating hydrologic cycle and crop production in a subsurface drained and sub-irrigated field in Southern Quebec using RZWQM2. *COMPUTERS AND ELECTRONICS IN AGRICULTURE*, *146*, 31–42. <https://doi.org/10.1016/j.compag.2018.01.021> WE - Science Citation Index Expanded (SCI-EXPANDED)
- King, K. W., Fausey, N. R., & Williams, M. R. (2014). Effect of subsurface drainage on streamflow in an agricultural headwater watershed. *Journal of Hydrology*, *519(A)*, 438–445. <https://doi.org/10.1016/j.jhydrol.2014.07.035>
- King, K. W., Hanrahan, B. R., Stinner, J., & Shedekar, V. S. (2022). Field scale discharge and water quality response, to drainage water management. *Agricultural Water Management*, *264*, 107421.
- Lalonde, V., Madramootoo, C. A., Trenholm, L., & Broughton, R. S. (1996). Effects of controlled drainage on nitrate concentrations in subsurface drain discharge. *Agricultural Water Management*, *29(2)*, 187–199.
- Ma, L., Malone, R. W., Heilman, P., Jaynes, D. B., Ahuja, L. R., Saseendran, S. A., Kanwar, R. S., & Ascough II, J. C. (2007). RZWQM simulated effects of crop rotation, tillage, and controlled drainage on crop yield and nitrate-N loss in drain flow. *Geoderma*, *140(3)*, 260–271.
- Malone, R. W., Nolan, B. T., Ma, L., Kanwar, R. S., Pederson, C., & Heilman, P. (2014). Effects of tillage and application rate on atrazine transport to subsurface drainage: Evaluation of RZWQM using a six-year field study. *Agricultural Water Management*, *132*, 10–22.
- Nash, P. R., Nelson, K. A., Motavalli, P. P., Nathan, M., & Dudenhoeffer, C. (2015). Reducing Phosphorus Loss in Tile Water with Managed Drainage in a Claypan Soil. *JOURNAL OF ENVIRONMENTAL QUALITY*, *44(2)*, 585–593. <https://doi.org/10.2134/jeq2014.04.0146>
- Pease, L. A., Fausey, N. R., Martin, J. F., & Brown, L. C. (2017). Projected climate change effects on subsurface drainage and the performance of controlled drainage in the Western Lake Erie Basin. *Journal of Soil and Water Conservation*. <https://doi.org/10.2489/jswc.72.3.240>
- Pferdmenges, J., Breuer, L., Julich, S., & Kraft, P. (2020). Review of soil phosphorus routines in ecosystem models. *Environmental Modelling & Software*, *126*, 104639.
- Qi, H., & Qi, Z. (2016). Simulating phosphorus loss to subsurface tile drainage flow: a review. *Environmental Reviews*, *25(2)*, 150–162.
- Rabalais, N. N., Turner, R. E., & Wiseman Jr, W. J. (2002). Gulf of Mexico hypoxia, aka" The dead zone". *Annual Review of Ecology and Systematics*, *235–263*.

- Radcliffe, D. E., Reid, D. K., Blombäck, K., Bolster, C. H., Collick, A. S., Easton, Z. M., Francesconi, W., Fuka, D. R., Johnsson, H., & King, K. (2015). Applicability of models to predict phosphorus losses in drained fields: A review. *Journal of Environmental Quality*, *44*(2), 614–628.
- Saadat, S., Bowling, L., Frankenberger, J., & Kladienko, E. (2018). Nitrate and phosphorus transport through subsurface drains under free and controlled drainage. *Water Research*, *142*, 196–207. <https://doi.org/10.1016/j.watres.2018.05.040>
- Sadhukhan, D., Qi, Z., Zhang, T., Tan, C. S., Ma, L., & Andales, A. A. (2019). Development and evaluation of a phosphorus (P) module in RZWQM2 for phosphorus management in agricultural fields. *Environmental Modelling and Software*, *113*, 48–58. <https://doi.org/10.1016/j.envsoft.2018.12.007>
- Salla, A., Salo, H., & Koivusalo, H. (2022). Controlled drainage under two climate change scenarios in a flat high-latitude field. *HYDROLOGY RESEARCH*, *53*(1), 14–28. <https://doi.org/10.2166/nh.2021.058>
- Sims, J. T., Simard, R. R., & Joern, B. C. (1998). Phosphorus loss in agricultural drainage: Historical perspective and current research. *Journal of Environmental Quality*, *27*(2), 277–293.
- Sojka, M., Kozłowski, M., Kesicka, B., Wrozyński, R., Stasik, R., Napierala, M., Jaskula, J., & Liberacki, D. (2020). The Effect of Climate Change on Controlled Drainage Effectiveness in the Context of Groundwater Dynamics, Surface, and Drainage Outflows. Central-Western Poland Case Study. *AGRONOMY-BASEL*, *10*(5). <https://doi.org/10.3390/agronomy10050625>
- Sunohara, M. D., Gottschall, N., Craiovan, E., Wilkes, G., Topp, E., Frey, S. K., & Lapen, D. R. (2016). Controlling tile drainage during the growing season in Eastern Canada to reduce nitrogen, phosphorus, and bacteria loading to surface water. *AGRICULTURAL WATER MANAGEMENT*, *178*, 159–170. <https://doi.org/10.1016/j.agwat.2016.08.030>
- Thorp, K. R., Jaynes, D. B., & Malone, R. W. (2008). Simulating the long-term performance of drainage water management across the Midwestern United States. *Transactions of the ASABE*, *51*(3), 961–976.
- Tolomio, M., & Borin, M. (2018). Water table management to save water and reduce nutrient losses from agricultural fields: 6 years of experience in North-Eastern Italy. *Agricultural Water Management*, *201*(January), 1–10. <https://doi.org/10.1016/j.agwat.2018.01.009>
- University of Illinois Extension. (2022). *Drainage Tile History in the U.S.*
- Wahba, M. A. S., El-Ganainy, M., Abdel-Dayem, M. S., Gobran, A., & Kandil, H. (2001). Controlled drainage effects on water quality under semi-arid conditions in the Western Delta of Egypt. *IRRIGATION AND DRAINAGE*, *50*(4), 295–308. <https://doi.org/10.1002/ird.29>

- Wesstrom, I., & Messing, I. (2007). Effects of controlled drainage on N and P losses and N dynamics in a loamy sand with spring crops. *AGRICULTURAL WATER MANAGEMENT*, 87(3), 229–240. <https://doi.org/10.1016/j.agwat.2006.07.005>
- Williams, M. R., King, K. W., & Fausey, N. R. (2015a). Drainage water management effects on tile discharge and water quality. *AGRICULTURAL WATER MANAGEMENT*, 148, 43–51. <https://doi.org/10.1016/j.agwat.2014.09.017>
- Williams, M. R., King, K. W., & Fausey, N. R. (2015b). Drainage water management effects on tile discharge and water quality. *AGRICULTURAL WATER MANAGEMENT*, 148, 43–51. <https://doi.org/10.1016/j.agwat.2014.09.017>
- Wright, J., & Sands, G. (2001). Planning an agricultural subsurface drainage system. *College of Agricultural, Food and Environmental Sciences, University of Minnesota. BU-07685*, 1–10.
- Youssef, M. A., Abdelbaki, A. M., Negm, L. M., Skaggs, R. W., Thorp, K. R., & Jaynes, D. B. (2018). DRAINMOD-simulated performance of controlled drainage across the U.S. Midwest. *Agricultural Water Management*, 197, 54–66. <https://doi.org/10.1016/j.agwat.2017.11.012>

## **CHAPTER 2: MEASUREMENT OF SOIL-WATER CHARACTERISTICS INPUT DATA**

### **2.1 Abstract**

Soil water characteristic curve (SWCC) has an important relationship with application in drainage, irrigation, soil physical behavior, and modeling hydrology and nutrient transport. However, measurement of the SWCC is often very time consuming, inaccurate and requires a lot of effort. In order to determine an accurate SWCC, we used HYPROP2. This method article extensively describes the topics which were not covered well by the instrument's manual such as collecting soil samples, use of the HYPROP refill unit, degassing water prior to degassing the tensio shafts and other procedures. Advice is provided in terms of better handling of the equipment to receive all four phases of an optimal measuring curve. Following the step-by-step procedure mentioned in this article would provide a high-quality SWCC. Our measurements were performed on both clay loam and sandy loam soils to show differences in the SWCC. We found that the upper tensio shaft took longer to cavitate for sandy loam soil compared to the clay loam soil.

### **2.2 Method Description**

This method explains the use of HYPROP (Hydraulic Property Analyzer) as an alternative technique to the conventional methods of measuring Soil water characteristic curve (SWCC) and unsaturated hydraulic conductivity of soil (METER 2015b; Schindler and Mueller 2006). Measuring SWCCs have always been difficult due to the lack of sufficient data points using conventional methods and the amount of time these methods require to generate these curves. HYPROP2 follows an evaporation method where two tensiometers measure the tension implied by water to the soil column. Also, how the water content of the soil column changes over time at

different tension values is observed (Peters and Durner 2006; Peters et al. 2015; Schindler 1980). However, the limitation of those tensiometers was that they would cavitate at a much smaller pressure typically ranging between 70 to 90 kPa. A new design of tensiometers in the late 2000s allowed withstanding cavitation to a much higher tension values as high as 435 kPa (Peters 2013; Schelle et al. 2013; Schelle, Iden, and Durner 2011; Schindler et al. 2010; Schindler and Müller 2017). HYPROP2 was developed based on those new designs of tensiometers.

HYPROP2 measures water potential at different soil saturation levels with the help of two tensiometers (i.e., one long and one short). This device is a more advanced version of HYPROP that has more robust and precise pressure transducers. It also introduces a faster optical monitoring of the measurements through a LED ring for better visualization of the current status of the device (METER 2015b). In HYPROP2, the soil sample stays on a laboratory balance during the experiment. Water evaporates from the soil over time, and HYPROP2 records the change of water potential during this process. This instrument also records the changing weight of the soil sample. This change of weight helps determine the moisture content of the soil. Finally, HYPROP-Fit program plots water potential against the changes in moisture contents to create a SWCC. The user should know that HYPROP2 can only measure the matric potential of the soil. It can measure water potential at the wet range of the soil, so the curve created with HYPROP2 will not be a complete curve. WP4C instrument can be combined with HYPROP2 to measure water potential in the dry range of the soil sample. WP4C is capable of measuring both matric and osmotic potential that completes the SWCC. However, HYPROP2 has its merits on producing high resolution data at the wet range of a soil sample.

There are studies where results obtained from HYPROP have also been compared with the results from conventional methods or to different models. Öztürk et al. (2013) compared HYPROP outputs with the outputs from sand box (or pressure plate), which validated the use of HYPROP as a potential method for creating SWCC. Another study compared HYPROP with the BEST model (Beerkan Estimation of Soil Transfer Parameters) (Leitinger, Obojes, and Lassabatère 2015), which showed that the retention curves (SWCC) from HYPROP followed a faster and continuous dehydration process compared to the retention curves from the BEST model. Also, their comparison revealed that the results of soil water characteristic may vary based on the methodological approach used between different soil types. A different study evaluated the accuracy of HYPROP Measurement Systems (HMS) with HYDRUS-1D software package (Bezerra-Coelho et al. 2018). HYDRUS-1D can generate virtual pressure head in soil columns as a function of time, and independent tests were performed by this package on HYPROP system using the Van-Genuchten-Mualem model for a wide range of soil textures. The results from HYDRUS-1D showed that accurate estimates of SWCC and other parameters were obtained by HYPROP within the range of available retention measurements. Since HMS failed to operate at a very high pressure range, Wang et al. (2012) evaluated the data points at a high-pressure range using centrifugal method. He added one control point at the high-pressure range of the SWCC already developed by HYPROP. The results showed that adding a control point to the high-pressure range makes the extrapolation of SWCC more reliable.

### **2.3 Soil Sample Collection**

Soil samples were collected from two privately-owned farms. The first one is near Blissfield, Michigan. The soil type is predominantly Ziegenfuss clay loam, which is classified as a

poorly drained soil (reference of NRCS web soil survey). The farmer uses a corn-soybean rotation in this field and applies commercial fertilizer. The second farm is near Palmyra, Michigan. The soil type is Brady and Macomb sandy loam at this farm, which is classified as a somewhat poorly drained soil (reference of NRCS web soil survey). The cropping system is corn-soybean rotation with commercial fertilizer application.

For both farms, soil samples were collected at two different locations with three replicates at each location. It is important to note that soil samples must remain undisturbed during collection. Four tools (Figure 2.1) are needed to collect the soil samples: (i) a soil sampling ring (Meter Group), (ii) a sample ring insertion tool (Meter Group), (iii) a rubber mallet, and (iv) a trowel. Figure 2.2 explains the whole soil sample collection process. Firstly, the soil sampling ring was attached to the sample ring insertion tool in such a way that the cutting edge of the ring was facing the soil surface. Then, the apparatus was hammered using the rubber mallet. The hammering was continued until the sampling ring had completely penetrated the soil. It is important to remember that the sampling ring just holds onto the insertion tool, and it cannot be attached to this without holding the bottom of the ring. Thus, whenever the ring had penetrated the soil, the insertion tool came off leaving the sampling ring inside the soil. Subsequently, a trowel was used to dig around the ring to loosen it up. Each ring comes with two white plastic caps to cover both ends of it. One of the caps were placed on the top surface of the ring. The trowel was put under the cutting edge of the ring, one hand was placed on the top of the ring, and the soil sampling ring with soil sample was taken out and was flipped. The excess soil was removed and levelled along the cutting edge using the trowel. Another cap was placed

to cover the cutting edge of the ring. After collection, soil samples were placed in a box and transported to the lab for further analysis.

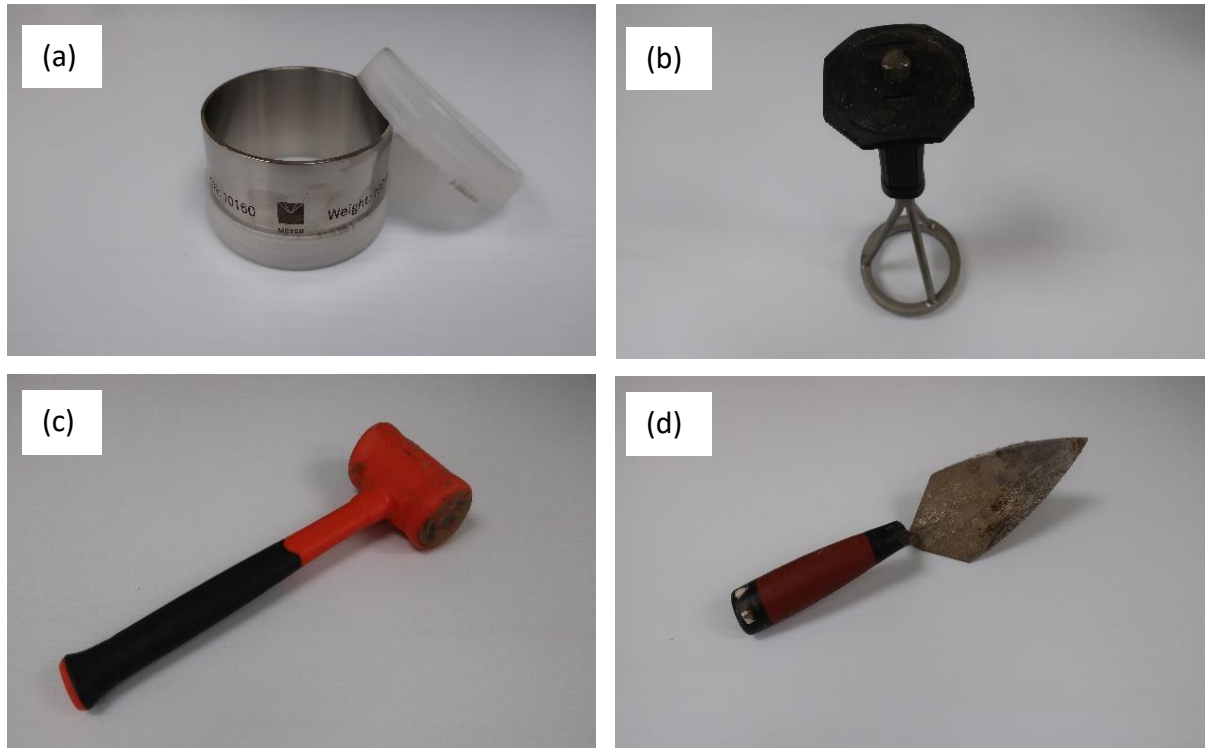


**Figure 2.1. Soil sampling tools: (a) sampling ring, (b) sample ring insertion tool, (c) rubber mallet, and (d) trowel**

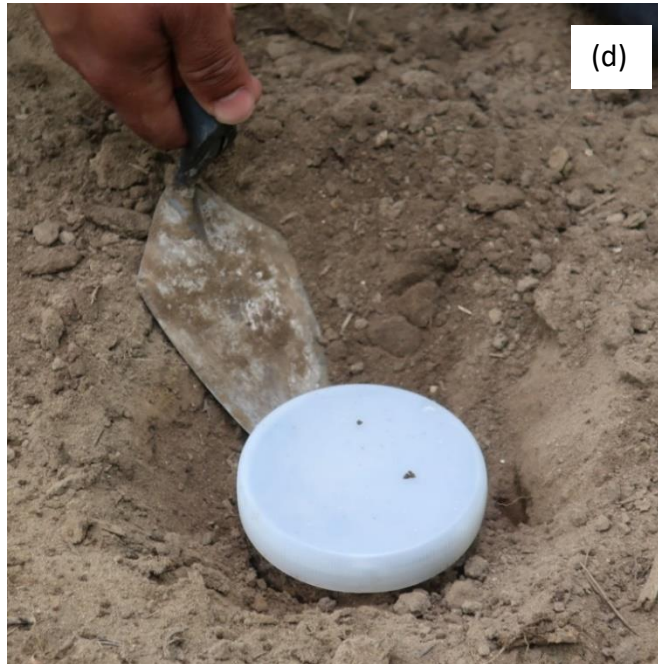


**Figure 2.2. (a) hammering to collect soil cores, (b) soil core inserted and ready to collect after hammering, (c) removing soil from the sides of the sample ring to collect undisturbed samples, (d) put a white cap on the sample ring before digging it out with a trowel, (e) digging out the sample ring with trowel and (f) flattening the soil surface with the trowel**

## 2.4 Preparing HYPROP2

In this section, we will explain the steps required to prepare the HYPROP2 for determining the soil water characteristic curve.

### 2.4.1 Degassing water

The first step in operating HYPROP2 is degassing water. A vacuum bottle was filled with deionized (DI) water. The tube coming out of the vacuum bottle was connected to the vacuum mount of the HYPROP2 system, and the vacuum mount was connected to the vacuum pump (

Figure 2.3a). Then, the pump was turned on to create vacuum in order to evacuate all the bubbles or gas from the DI water. It is important to remember that the tube inside the vacuum bottle needs to stay in the air (not submerged in DI water), so that it can evacuate as much air from the bottle without removing water (

Figure 2.3b). The water was degassed for a couple of hours.

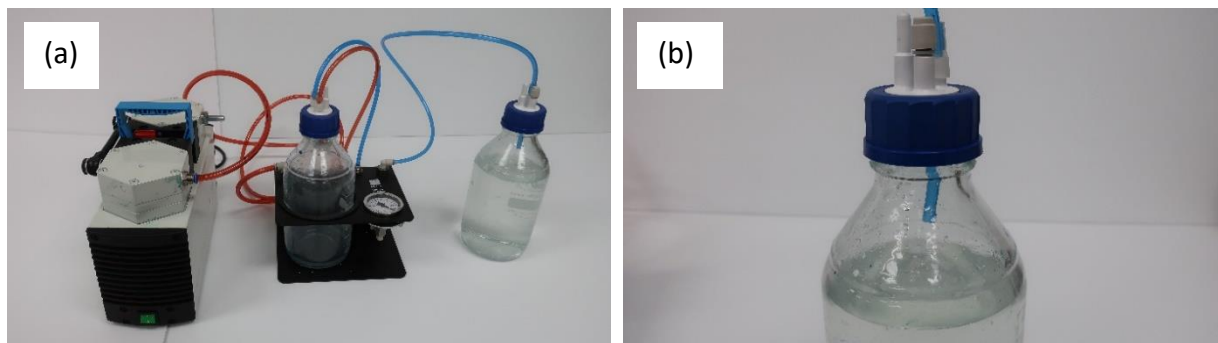


**Figure 2.3. Degassing water using a vacuum pump and a vacuum bottle: (a) Assembly of instruments for degassing DI water and (b) Blue tube should be kept in air inside the vacuum bottle while degassing DI water**

### 2.4.2 Degassing the HYPROP sensor unit

For running a HYPROP experiment, two of the devices need to be degassed completely: the HYPROP sensor unit and the two tensio shafts. There are two ways to perform degassing: (i)

degassing the device using the HYPROP refill unit and (ii) degassing using syringes. Meter Group recommended degassing using the HYPROP refill unit because it is more accurate. Alternative to the HYPROP refill unit is manual degassing using syringes, which creates challenges to degas the water completely. This manual method requires a lot of labor, and chances of error is more than using the automated HYPROP refill unit.

The HYPROP manual gives a fair instruction about how to degas the device manually using syringes but does poorly on explaining the degassing process using HYPROP refill unit. The scope of this article is to give a better understanding of how the HYPROP refill unit works in degassing the tensio shafts and HYPROP sensor unit.

### 2.4.3 Degassing the sensor unit using the HYPROP refill unit

#### 2.4.3.1 Assembly

This method involves the use of a high-performance vacuum pump that can generate a vacuum pressure of around 0.85 to 0.90 bars, which can degas the sensor unit and both of the tensio shafts. The total arrangement consisted of four instruments connected to each other (Figure 2.4). The first instrument was the vacuum pump, which was connected to a vacuum mount. The vacuum mount consisted of a pressure gauge and a vacuum flask. Whenever the pump was running, the vacuum pressure could be monitored looking at the pressure gauge. Also, when the degassing process took place, air bubbles from both tensio shafts and the sensor unit were collected in the vacuum flask to prevent water entering the pump. The vacuum mount was connected to a beaker mount where four tensio shafts can be degassed at the same time. The beaker mount has four ports. Each port is connected to a tube and each tube connects to an adapter. Finally, the beaker mount was connected to the HYPROP sensor unit. The top part of the

HYPROP sensor unit was the acrylic adapter, which was attached to the HYPROP sensor unit base. The beaker mount was connected to the sensor unit with a tube.

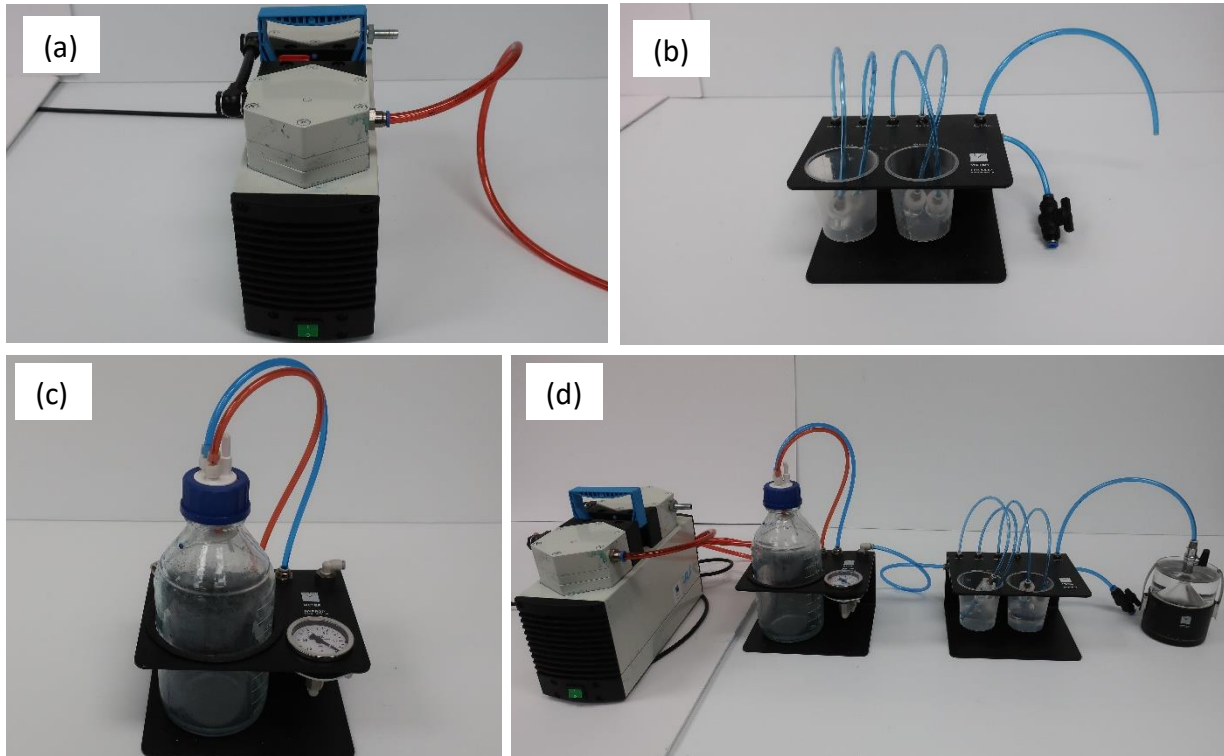


**Figure 2.4. (a) vacuum pump, (b) beaker mount, (c) vacuum mount and (d) assembly of Hyprop refilling unit**

#### 2.4.3.2 Procedure

The degassing process using the HYPROP refill unit should be continued for about 12 to 24 hours. In our case, it was about 20 hours. All the tubes were connected to their respective connections or ports (Figure 2.4d). The color of the tubes should match the color of the connections, so that wrong tubes are not connected to wrong ports. Blind plugs were put in the connections not being used during the experiment. In the beaker mount, the beakers were filled with water from the vacuum bottle which had already been degassed. The tubes in the beaker mount were connected to the glass adapters and then each of the tensio shafts were screwed in

the adapters. Then, the tensio shafts were placed in the beakers. Each beaker had a long and a short tensio shaft submerged in degassed water.

After placing the tensio shafts in the beakers, the black pressure valve attached to the beaker mount was closed by rotating it counterclockwise towards a vertical position of the knob. The pump was turned on for 10 minutes until the system reached full vacuum. Once full vacuum was achieved, the pump was turned off and the system retained the vacuum. The system then kept on degassing for about 2 hours. After 2 hours, the system started losing full vacuum, so the pump needed to be started again for 10 minutes to take the system back to full vacuum. If the user wants to perform this degassing process overnight, purchasing a programmable timer would be very helpful. This timer can run the pump for 10 minutes in every couple of hours and shut it off, thus saving time by running the degassing process overnight and performing the experiments during the daytime.

Getting full vacuum is extremely important for running experiments using HYPROP2. If a vacuum pressure value of around 0.85 to 0.90 bars (85 to 90 kPa) cannot be achieved, proper degassing will not be accomplished. Also, even if the system reaches full vacuum, the user needs to check if it can still hold the vacuum after the pump is turned off. The purpose of using the pump is to allow the system to reach full vacuum and then retain it for a couple of hours even if the pump is not in action. If the system is not able to hold the vacuum, there is definitely a leak in any of the refill unit components. A leak can happen in different ways such as a damaged vacuum bottle, the tubes may not be pushed all the way in through the ports of the vacuum mount and beaker mount, or the pressure valve attached to the beaker mount may be open. Thus, proper attention needs to be directed to these details.

### 2.4.3.3 Saturating the soil sample

After degassing the sensor unit using the HYPROP2 refill unit, the soil sample was saturated with water. The HYPROP manual suggests saturating the soil sample in degassed water. But in reality, the water for saturating soil sample solely depends on the purpose of the experiment. For agricultural applications, the soil core needs to be saturated in subsurface drainage water to simulate water movement in the soil matrix. Thus, we started saturating the soil cores in subsurface drainage water (collected from the on-farm site). The required time of saturating different kinds of soils may vary (Table 2.1).

**Table 2.1. Saturation time for different types of soils**

<b>Soil Texture</b>	<b>Time for saturation</b>
<b>Clay loam</b>	About 1 hour <sup>1</sup>
<b>Sandy loam</b>	About 45 minutes <sup>1</sup>
<b>Coarse sands</b>	About 10 minutes <sup>2</sup>
<b>Fine sands</b>	About 45 minutes <sup>2</sup>
<b>Silt</b>	About 6 hours <sup>2</sup>

*1- Based on our experience.*

*2- Based on HYPROP manual*

A step-by-step saturation process of the soil sample is shown in (Figure 2.5). The white cap from the blunt end of the soil core was removed. The soil core was covered with a cheesecloth, and the perforated tray was placed on top of the soil core. Then, the soil core was flipped, and the white cap was removed from the cutting-edge end of the soil core. Later, the soil core was placed in an empty tray. Drainage water was filled in the tray up to the cutting edge of the soil core. The user should be careful not to pour water on the top surface of the soil core to avoid trapping air. Also, pouring water from the top may immediately create a shiny surface indicating the soil sample is saturated although it may not be saturated in the middle. A white

cap can be placed on top of the cutting edge to prevent evaporation and to protect the soil from solar radiation.

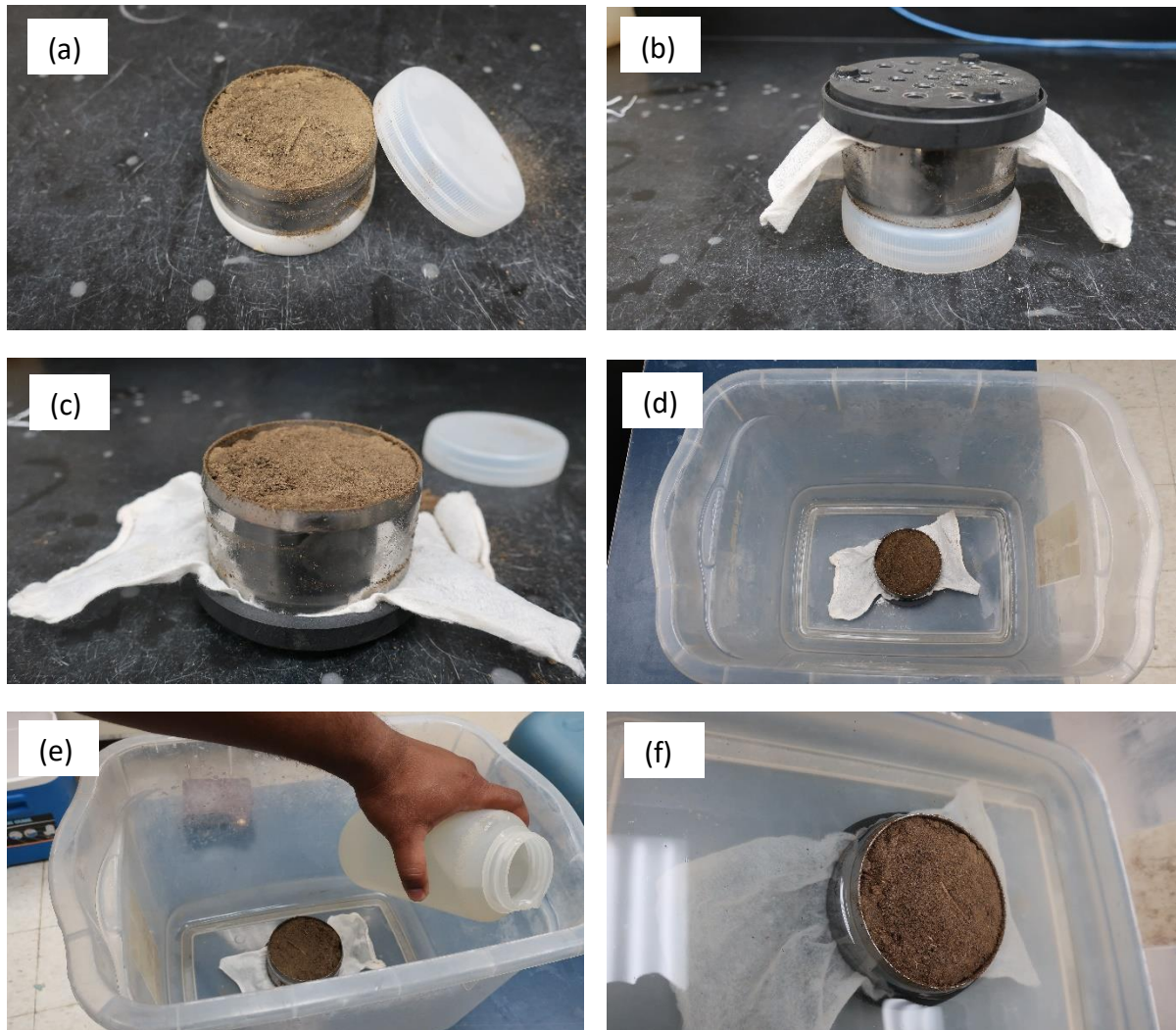


**Figure 2.5. (a) cap is removed from the cutting edge of soil core, (b) Soil core is flipped, and a cheesecloth and perforated tray was put on the soil core, (c) Soil core flipped again with the cap removed, (d) soil core was put in a tray, (e) drainage water was poured in the tray, and (f) drainage water was poured until the cutting edge of the tray**

#### 2.4.3.4 Preparing the programs

Once the soil was saturated, these two programs were used to determine the SWCC: (i) HYPROP-View and (ii) HYPROP-Fit. HYPROP-View was used during the beginning of the experiment to select the saving directories, selection of the HYPROP device, and to determine

the data collection frequency from the sensor unit. HYPROP-Fit was used at a later stage to find the stop point and air entry point of the sample and further evaluation of the results. HYPROP-Fit allowed to select different computational methods for evaluation of results, and to export the results to the computer. Both programs were fairly easy to use, and we recommend using the HYPROP2 manual for more explanation.

#### 2.4.3.5 Implementing tensio shafts in sensor unit

Once degassing was done, the valve connected to the beaker mount was opened very slowly. If the valve was opened too quickly, a sudden pressure shock could damage the pressure sensors in the sensor unit. Then, the tensio shafts were removed from the adapters. Once the tension shafts have been removed from the adapters, it is very important to keep the tensio shafts hydrated, so putting the silicone caps on them is a good practice. The user can also add degassed water on ceramic tips of the tensio shafts from time to time to prevent them from drying. The respective connection ports for each shaft is already drawn on the sensor unit.

When the tensio shafts are completely degassed and their ceramic tips are fully wet, they are ready to be screwed in the sensor unit. The HYPROP manual suggests that it takes about 9 turns for the tensio shafts to get sealed in the ports. From our experience, that was not always the case, or it was hard to measure exact 9 turns (Figure 2.6). Thus, a better practice is to keep an eye on the HYPROP-View program where the refilling wizard shows how much pressure is being exerted by each tensio shaft. At the initial stages of screwing in the shaft, the pressure values remained small or negative, and the pressure started increasing with time. It is advisable to monitor the pressure values while screwing in the tensio shafts. Once it feels that the tensio shafts are close to sealing, they should be screwed in very slowly. Also, monitoring the pressure

values in the HYPROP-View program will help avoid exceeding the maximum limit of 200 kPa (2000 hPa). The pressure values should always remain below this range. Once the shafts were fully screwed in the sensor unit, the silicone caps were removed. Then, a silicone gasket was put on the sensor unit to protect it from dust.

The tensio shafts are very sensitive and can get damaged by the slightest negligence while operating, so it is good to occasionally check whether the tensio shafts are working properly. An easy step to check whether the tensio shafts are functioning is to add small drops of water on the ceramic tip of the tensio shafts. The refilling wizard window in the HYPROP-View program will show the change in pressure due to addition of water droplets. If the pressure for both tensio shafts go back to zero in a little while, then the tensio shafts are functioning properly. This is to check the zero potential of the tensio shafts. Another way to check is to dry the ceramic tip with paper towel and to keep an eye to the pressure values. In this case, the pressure values should readily increase to the atmospheric air pressure.



**Figure 2.6. HYPROP 2 sensor unit after implementing the tensio shafts**

#### 2.4.3.6 Precautions

One important precaution before starting the experiment with HYPROP2 is to check whether offset recalibration is necessary. METER Group sets a narrow range of values for HYPROP sensors to function efficiently. If HYPROP has not been used for some time, the offset values of the electronic sensors may drift from the values set by METER Group. In these circumstances, the user needs to check for offset recalibration. From our experience, it was seen that during consecutive experiments the offset recalibration was unnecessary. However, the user should always check whether calibration is needed. Also, the HYPROP manual does a good job in explaining this calibration process. After degassing the sensor unit, the user needs to connect it with the provided USB adapter. Then, HYPROP-View program needs to be started. After clicking on the “refilling wizard”, the HYPROP sensor should be selected. Then, the software will check whether calibration is required. If calibration is needed, clicking the button “set zero value” will recalibrate the HYPROP sensors.

#### 2.4.4 Assembling sensor unit to the soil sampling ring

When the tensiometers were fully functioning and the soil sample was saturated, i.e., a shiny surface appeared on top of the soil core (Figure 2.7), it was time to attach the tensiometers to the soil core. The USB adapter was removed from the sensor unit, and the sensor unit was ready to be connected to the soil sampling ring. One important advice is to avoid removing the saturated soil sample from the tray filled with drainage water until the user is ready to start the measurements. For sandy soils, water drains through the soil core quickly, so the soil still might not be saturated while implementing the sensor unit to the soil core. A small auger and tensio shaft adapter were used for drilling holes in the soil core. The adapter should be set in such a way

so that the user can remember which holes in the soil core are for long and short tensio shafts. HYPROP manual states that the adapter should be adjusted to the sample ring in such a way, so that the small hole of the adapter aligns with the sample ring number.

Once holes were made with the auger, there was a chance that air would enter those holes, so it was imperative to fill the holes again with water using the droplet syringe. At this stage, the soil was fully saturated and ready to be assembled to the sensor unit. Before assembling the soil core to the sensor unit, the silicone caps from the tensio shafts were removed. Then, the sensor unit was inverted and slowly placed close to the holes in the soil core. Once both tensio shafts were aligned with their respective holes in the soil core, the tensio shafts along with the sensor unit was slowly penetrated to the soil core (Figure 2.8a). Next, the assembled sensor unit and sample ring was flipped (Figure 2.8b) and the perforated bowl along with the cheesecloth was removed. Now, the ring is ready for the experiment.



**Figure 2.7. Shiny surface appears on top of soil core**

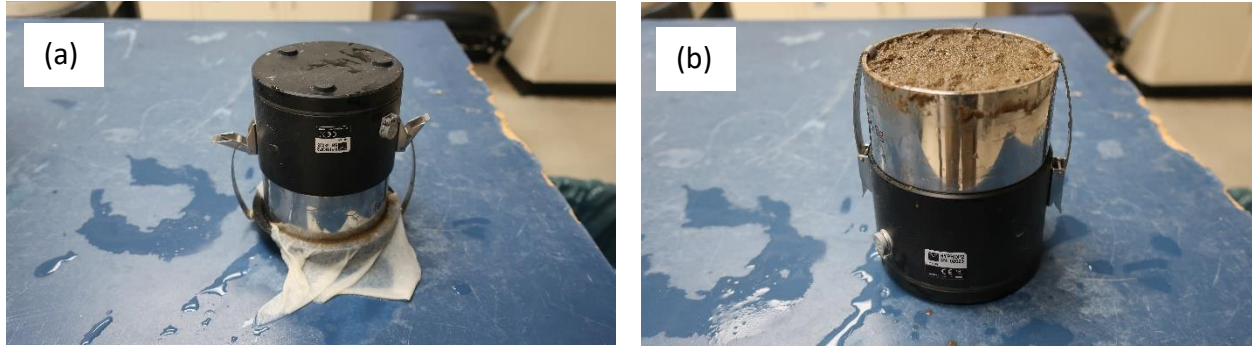


**Figure 2.8. (a) sensor unit placed on the soil ring, (b) after removing cheesecloth and perforated tray, the user flips the assembled sensor unit and soil core**

## **2.5 Starting the Measurements**

After the soil sampling ring was safely attached to the sensor unit, the combined piece was ready to be placed on a balance (Figure 2.9). But before that, the balance was placed on a flat top and made level using the vertical screws and bubble. Next step was to calibrate the balance using the instructions in the HYPROP manual. The sensor unit was then placed on the balance. One end of a magnet clamp (i.e., comes with the HYPROP unit) was connected to the balance and another end to the sensor unit. A white USB cable (i.e., comes with the HYPROP unit) connected the balance to the computer.

Once both the sensor unit and the balance were connected to the computer, HYPROP-View program started recording change of weight of the soil core and pressure potentials at the long and short tensio shafts (METER 2015b). HYPROP-View allows selecting the frequency of the pressure potential data. The default value is 10 minutes, and it is possible to collect higher frequency data at different intervals during the experiment. The weight of the sampling ring (i.e., written on each ring) needs to be entered into the HYPROP-View program for correct evaluation of the results. These weight values are slightly different for each sampling ring. HYPROP-View also allows the user to select the units of pressure potential for example, Hectopascal (hPa) or

Kilopascal (kPa) (1 kPa = 10 hPa). Usually, the experiment keeps on running for 2 to 7 days (depending on the type of soil) and data is collected continuously by the HYPROP-View program. The user can see the data in the HYPROP-Fit program without stopping the measurements. HYPROP-Fit also allows to look for the stopping point or air-entry point in the plot. Once this point is found, the measurements in the HYPROP-View program can be stopped.



**Figure 2.9. Assembled sensor unit and soil core is put on a balance to start measurements**

## **2.6 Stopping the Measurements**

HYPROP measurements should be run for several days to create an optimal measuring curve with time. An ideal measuring curve (Figure 2.10) is composed of 4 phases: (phase 1) regular measurement range, (phase 2) boiling delay phase, (phase 3) cavitation phase and (phase 4) air entry phase (METER 2015b). Phase 1 is the regular measurements where the tension values keep on increasing over time without showing any sign of decrease. In phase 2, tension is increased above the ambient air pressure, and the increase keeps on continuing until the tension value decreases. The boiling delay phase is often very difficult to achieve, but the results are still

valid without this phase. Phase 2 can only be achieved if the user is able to completely degas the tensio shafts and the sensor unit, which would mean no air bubbles should be present in the system. In phase 3, some water vapor starts to form in the tensio shafts, and the tension values will have a sudden drop to the ambient air pressure, which is the point where the curve becomes flat. There will be very small decreases in the tension values after this phase. Air enters the ceramic tube at phase 4, and tension values instantly drop to zero.

After the tension values in the tensio shafts start dropping, a measurement can be manually stopped in three ways. First, using the stop point where the long tensio shaft reaches the cavitation phase, so the tension values do not increase anymore. The curve will become almost flat or reduce very little after this point. Second, using the air-entry point when the tension values at the long tensio shaft reduce to zero as air enters the ceramic tip. Third, using the air entry point when the tension values at both the long and short tensio shafts reaches zero due to air entrapment in the ceramic tip.

To automatically stop the measurements, the user needs to click on the “search stop point” button in the HYPROP-Fit measurements tab. This program will detect a stop point in the tension curve of the top tensio shaft whenever it starts cavitating. It is important to remember that one should only use this “search stop point” option if the tensio shafts have been fully degassed and boiling delay phase have been achieved.

For our experiments, we were not able to achieve a boiling delay phase for both soil types due to presence of water bubbles in the tensio shafts even after degassing them for more than 20 hours. When it is not possible to get a boiling delay phase, suboptimal curves develop, and the tension values will not go through a rapid drop. Instead, the tension values will become flat

after increasing for some time. In this case, the automatic stop point detection using the HYPROP-Fit program may not be reliable. The user should manually find the stop point using the stop point cursor by moving right or left in the measurement tab of the HYPROP-Fit program. It is advisable to select the stop point at such a point where the slope of the tension curve is positive. In this paper, the same concept has been used to identify the stop point of tension curves for both clay and sandy loam soils.

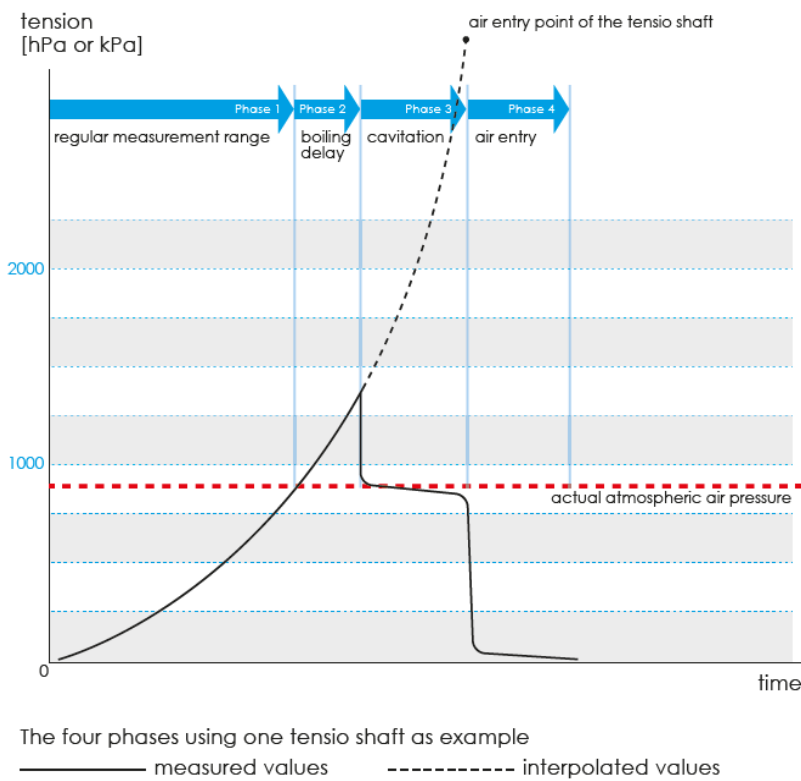


**Figure 2.10. An optimal measuring curve for HYPROP measurements (image source: HYPROP Manual)**

## 2.7 Determining the Dry Weight

After the experiment was ended, we determined the dry weight of the soil sample (METER 2015b). This dry weight helped to measure the volumetric water content based on how much weight was lost from the soil core due to evaporation. First, the soil core was detached from the

HYPROP sensor unit, which required care because the tensio shafts were strongly attached to the soil core and a little extra force in the wrong direction could break them.

Once the soil core was detached from the sensor unit, it was placed in an aluminum tray. The weight of the empty tray was measured beforehand. It is normal that after several days of drying within ambient temperature, the soil becomes very crumbly (especially sandy soils), and the soil will easily fall off the sampling ring. To address this, the sampling ring was cleaned properly with a brush so that the tray could catch all the grains of the soil sample. The tray was placed in an oven for 24 hours at 105°C. After drying, the soil sample were weighed again. The dry soil weight was calculated by subtracting the empty aluminum tray weight from the combined weight of soil and tray after drying. This dry weight was recorded in the HYPROP-Fit program to measure the volumetric water content (METER 2015a). There are several soil hydraulic models available in the HYPROP-Fit program including Brooks-Corey, Fredlund-Xing, Kosugi, and van Genuchten models. The user can use any of these models, but the van Genuchten model is the most popular and the default model in the HYPROP-Fit program (Brooks and Corey 1966; Fredlund and Xing 1994; Van Genuchten 1980; Kosugi 1996).

## **2.8 Method Validation**

HYPROP measurements were conducted for both clay loam and sandy loam soil. The results for both soils are shown in figures 2.11 to 2.14 as part of our method validation. After finishing measurements, HYPROP produced one spreadsheet in Excel Worksheet (.xlsx) and five plots in image format (.png). The spreadsheet kept record of all the data measured during the experiment. The plots featured (i) change in tension values obtained from tensio shafts over time, (ii) retention or change in volumetric water content with change in pressure head (pF), (iii) change

in unsaturated hydraulic conductivity with pressure head (pF), (iv) change in unsaturated hydraulic conductivity with volumetric water content, and (v) weight loss of undisturbed soil core over time.

### 2.8.1 Clay loam soil

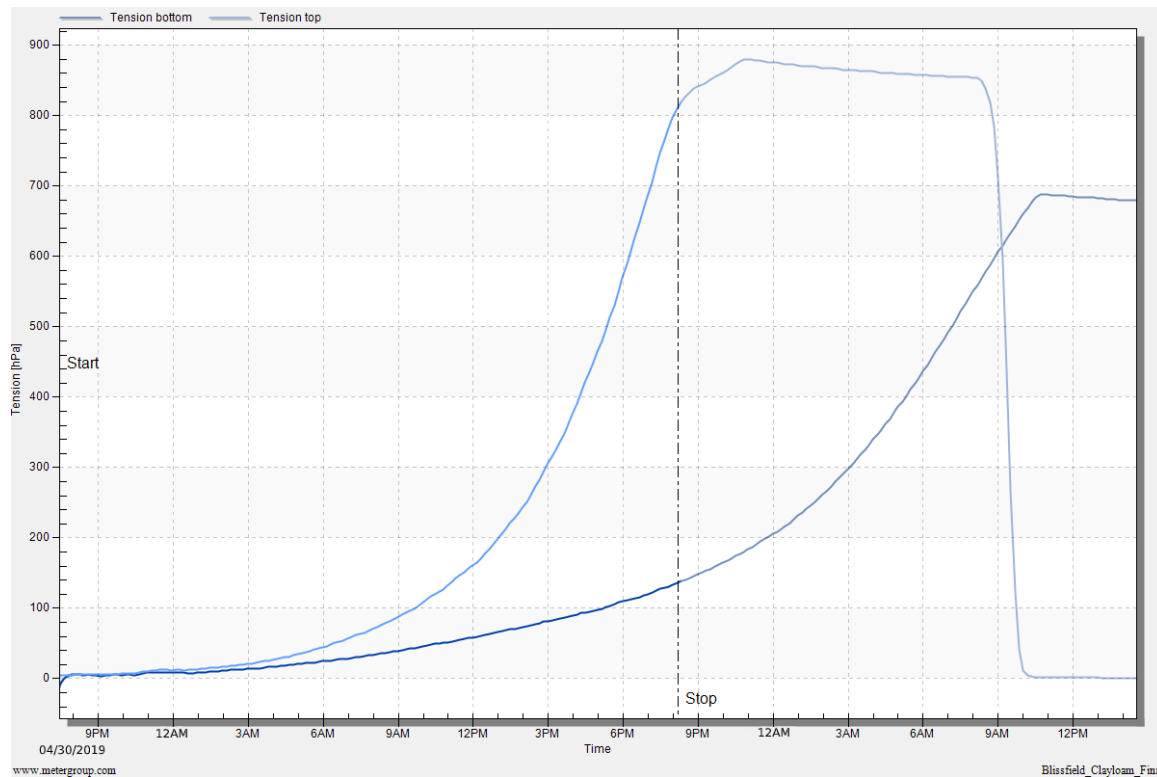


**Figure 2.11. Tension curve for a clay loam soil. Tension is in units of hectopascal (1 kPa = 10 hPa)**

The water tension did not rise immediately at the beginning of the measurements, but rather both tensio shafts showed a very gradual increase and it was difficult to distinguish their pressure difference until about first 3 hours of the measurements (Figure 2.11). At 2 kPa (20 hPa), the tensio shafts were far enough away to determine the hydraulic conductivities. After 6 hours of measurements, the tension values increased more rapidly than the beginning of the measurements and formed two gradually increasing curves. At this stage of gradual increment of

curves, tension at the top shaft was higher than the tension at the bottom shaft. Both tension curves kept on increasing and after a day of measurements, the top tensio shaft reached its cavitation phase and air bubbles started entering the tensio shaft. This is the stage where the experiment should have been stopped, but measurements were not stopped, and the experiment was continued. Since the measurements were not stopped, the tension at the bottom shaft kept on rising and it started cavitating after 12 hours. At this point, the soil sample had lost 9% of water over the drying process (Figure 2.12). Since experiment was not stopped automatically using the “search stop point” option of the HYPROP-Fit program, the experiment was stopped by manually finding a stop point before the cavitation phase until where the slope of the tension curve of top tensio shaft kept on increasing without showing any sign of decrease (method 1 explained in section 1.4).

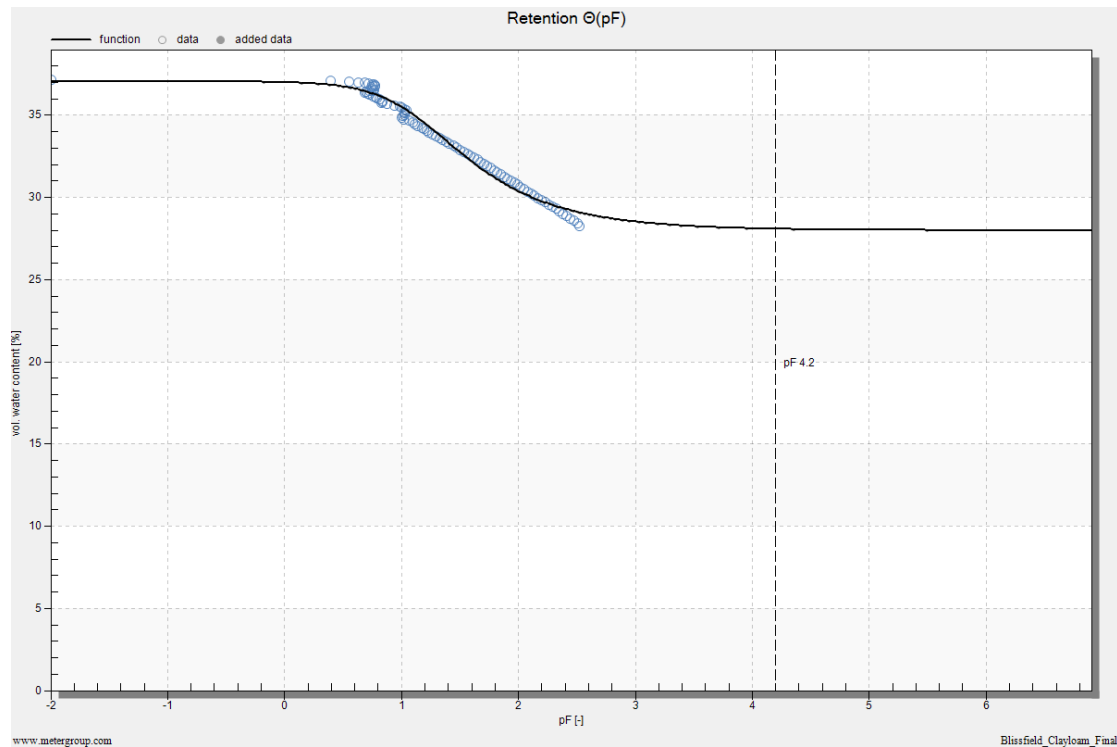


**Figure 2.12. Volumetric water content vs. pF plot using evaporation method and fitted soil water characteristic curve for a clay loam soil**

HYPROP-Fit program lets the user choose different models to analyze the HYPROP2 measurements. The default is Van Genuchten model (1980) where volumetric water content of the soil is calculated by the following equations

$$S_e = \frac{\Theta - \Theta_r}{\Theta_s - \Theta_r} \quad (2.1)$$

$$\text{and } S_e = \left[ \frac{1}{1 + (\alpha h)^n} \right]^m \quad (2.2)$$

where  $S_e$  is effective saturation ( $\text{cm}^3/\text{cm}^3$ ),  $h$  is pressure head (cm),  $\Theta$  is volumetric water content ( $\text{cm}^3/\text{cm}^3$ ; multiply by 100 to get in percentage),  $\Theta_r$  is residual water content ( $\text{cm}^3/\text{cm}^3$ ) and  $\Theta_s$  is saturated water content ( $\text{cm}^3/\text{cm}^3$ ). Additionally,  $\alpha$  is the shape parameter related to the inverse of the air entry pressure ( $\text{cm}^{-1}$ ),  $n$  is the shape parameters that controls both the bending of the retention curve at the air-entry region and the asymptotic curvature towards the residual water content and  $m$  is the additional shape parameter which equals to  $1 - (1/n)$ .

It is also possible to select 4 other models (Brooks-Corey, Freudland-Xing, Kosugi and Van Genuchten mvar) in HYPROP2 for analysis, but we used the Van Genuchten (1980) model also known as the traditional constrained Van Genuchten-Mualem model for our study. After running this model by HYPROP-Fit program for a clay loam soil, values for the following parameters were generated as outputs:

$$\alpha = 0.0730, n = 1.661, m = 1 - (1/n) = 0.398, \Theta_s = 0.371 \text{ and } \Theta_r = 0.280$$

Thus, the equation of volumetric water content for clay loam soil is calculated as

$$\Theta = 0.091 \left[ \frac{1}{1 + (0.0730 * h)^{1.661}} \right]^{0.398} + 0.280 \quad (2.3)$$

HYPROP-Fit program also provides estimates of field capacity and permanent wilting point. Field capacity is estimated at 33 kPa matric potential. The water content at permanent

wilting point is estimated at 1500 kPa. The above model provides the water content at 6 kPa ( $h = 63.1$  cm, and  $pF=1.8$ ), 33 kPa ( $h = 316.2$  cm, and  $pF=2.5$ ) and 1500 kPa ( $h = 15848.9$  kPa, and  $pF=4.2$ ) to be 31.3%, 29.1% and 28.1%, respectively. These values are important for irrigation timing, and can be used as an input for hydrological models such as DRAINMOD (Skaggs et al. 2012).

### 2.8.2 Sandy loam soil

At the beginning of the experiment, the water tension at both tensio shafts followed a gradual increase for the first 3 days (Figure 2.13), and both the tensio shafts showed the same tension values during this time. At about 140 hPa (14 kPa), the tensio shafts were far enough away to determine the hydraulic conductivities. After about 4 days of measurements, the tension values increased at a greater slope. Top shaft showed higher tension value than the bottom shaft. The measurements were completed by the failure of upper tensio shaft after more than four days. At this point, the soil sample had lost about 25% of water over the drying process (Figure 2.14). The experiment was stopped by manually finding a stop point on the top tension curve as explained in section 1.4.

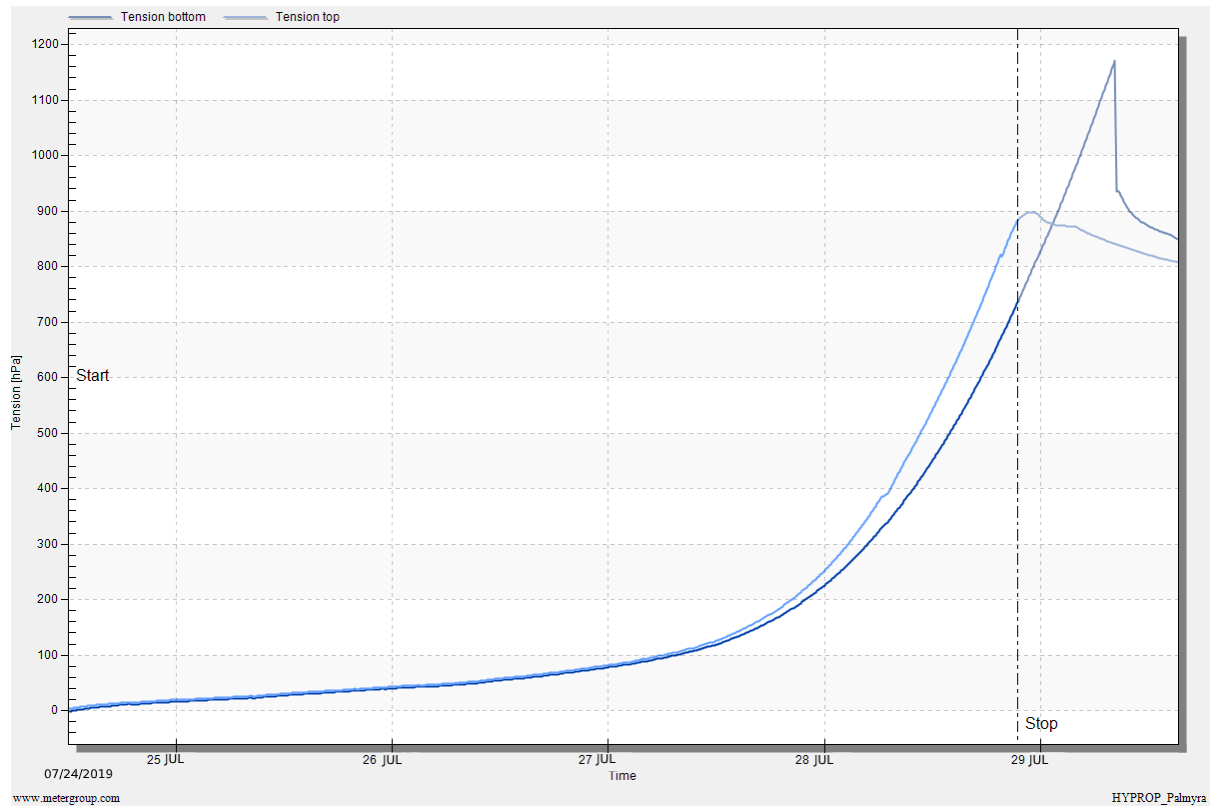


**Figure 2.13. Tension curve for a sandy loam soil. Tension is in units of hectopascal (1 kPa = 10 hPa)**

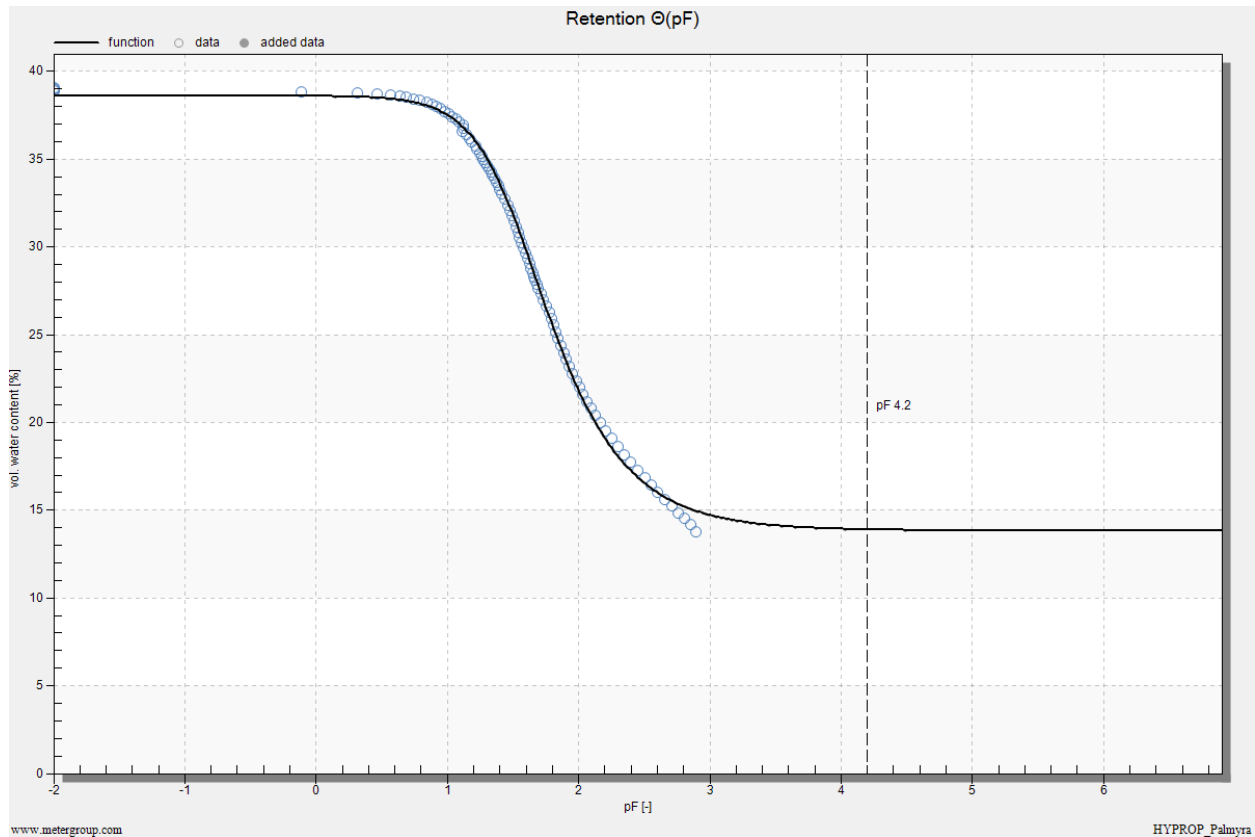


**Figure 2.14. Volumetric water content vs. pF plot using evaporation method and fitted soil water characteristic curve for a sandy loam soil**

After collecting the data for the sandy loam soil, HYPROP-Fit program gave parameter values as follows:

$$\alpha = 0.0302, n = 1.975, m = 1 - (1/n) = 0.494, \Theta_s = 0.386 \text{ and } \Theta_r = 0.138$$

Using the Van Genuchten-Mualem (1980) model, the equation for this soil is calculated as:

$$\Theta = 0.248 \left[ \frac{1}{1 + (0.0302 * h)^{1.975}} \right]^{0.494} + 0.138 \quad (2.4)$$

This model gives the water content at 6 kPa ( $h = 63.1$  cm, and  $pF=1.8$ ), 33 kPa ( $h = 316.2$  cm, and  $pF=2.5$ ) and 1500 kPa ( $h = 15848.9$  kPa, and  $pF=4.2$ ) to be 31.3%, 29.1% and 28.1%, respectively.

## **2.9 Summary**

This chapter provides an extensive guideline for using HYPROP2 including collecting an undisturbed soil sample and using the instrument to determine an accurate SWCC. The HYPROP2 manual does not give good instructions on how the samples should be collected and how to saturate those samples in water based on one's research needs. Also, this article talks about the degassing process using the HYPROP refill unit. Even though the optimal curve is expected from HYPROP2 based on the instrument manual, a suboptimal curve can also be used to determine the SWCC. This method is highly efficient in degassing water and to generate good results. Anyone correctly following this method article should be able to replicate the results obtained in this study.

## REFERENCES

- Bezerra-Coelho, Camila R., Luwen Zhuang, Maria C. Barbosa, Miguel Alfaro Soto, and Martinus Th Van Genuchten. 2018. "Further Tests of the HYPROP Evaporation Method for Estimating the Unsaturated Soil Hydraulic Properties." *Journal of Hydrology and Hydromechanics* 66(2):161–69.
- Brooks, Royal Harvard and Arthur T. Corey. 1966. "Properties of Porous Media Affecting Fluid Flow." *Journal of the Irrigation and Drainage Division* 92(2):61–90.
- Fredlund, Delwyn G. and Anqing Xing. 1994. "Equations for the Soil-Water Characteristic Curve." *Canadian Geotechnical Journal* 31(4):521–32.
- Van Genuchten, M. Th. 1980. "A Closed-Form Equation for Predicting the Hydraulic Conductivity of Unsaturated Soils 1." *Soil Science Society of America Journal* 44(5):892–98.
- Kosugi, Ken'ichirou. 1996. "Lognormal Distribution Model for Unsaturated Soil Hydraulic Properties." *Water Resources Research* 32(9):2697–2703.
- Leitinger, Georg, Nikolaus Obojes, and Laurent Lassabatère. 2015. "Assessing Soil Hydraulic Characteristics Using HYPROP and BEST: A Comparison." in *EGU General Assembly Conference Abstracts*. Vol. 17.
- METER. 2015a. *HYPROP-Fit User User Manual*. 2015-01, 96 pp, UMS GmbH, Gmunder Strasse 8, 81379 Munich, Germany. URL: <http://www.meter-group.com/hyprop-2/#support>.
- METER. 2015b. *Manual HYPROP*. Version 2015-01, 96 pp, UMS GmbH, Gmunder Strasse 37, Munich, Germany. URL: <http://www.meter-group.com/hyprop-2/#support>.
- Öztürk, Hasan S., Wolfgang Durner, Amir Haghverdi, and Birgit Walter. 2013. "Comparison of Soil Moisture Retention Characteristics Obtained by the Extended Evaporation Method and the Pressure Plate/Sand Box Apparatus." P. 3911 in *EGU General Assembly Conference Abstracts*. Vol. 15.
- Peters, A. and W. Durner. 2006. "Improved Estimation of Soil Water Retention Characteristics from Hydrostatic Column Experiments." *Water Resources Research* 42(11).
- Peters, Andre. 2013. "Simple Consistent Models for Water Retention and Hydraulic Conductivity in the Complete Moisture Range." *Water Resources Research* 49(10):6765–80.
- Peters, Andre, Sascha C. Iden, and Wolfgang Durner. 2015. "Revisiting the Simplified Evaporation Method: Identification of Hydraulic Functions Considering Vapor, Film and Corner Flow." *Journal of Hydrology* 527:531–42.

- Bezerra-Coelho, Camila R., Luwen Zhuang, Maria C. Barbosa, Miguel Alfaro Soto, and Martinus Th Van Genuchten. 2018. "Further Tests of the HYPROP Evaporation Method for Estimating the Unsaturated Soil Hydraulic Properties." *Journal of Hydrology and Hydromechanics* 66(2):161–69.
- Brooks, Royal Harvard and Arthur T. Corey. 1966. "Properties of Porous Media Affecting Fluid Flow." *Journal of the Irrigation and Drainage Division* 92(2):61–90.
- Fredlund, Delwyn G. and Anqing Xing. 1994. "Equations for the Soil-Water Characteristic Curve." *Canadian Geotechnical Journal* 31(4):521–32.
- Van Genuchten, M. Th. 1980. "A Closed-Form Equation for Predicting the Hydraulic Conductivity of Unsaturated Soils 1." *Soil Science Society of America Journal* 44(5):892–98.
- Kosugi, Ken'ichirou. 1996. "Lognormal Distribution Model for Unsaturated Soil Hydraulic Properties." *Water Resources Research* 32(9):2697–2703.
- Leitinger, Georg, Nikolaus Obojes, and Laurent Lassabatère. 2015. "Assessing Soil Hydraulic Characteristics Using HYPROP and BEST: A Comparison." in *EGU General Assembly Conference Abstracts*. Vol. 17.
- METER. 2015a. *HYPROP-Fit User User Manual*. 2015-01, 96 pp, UMS GmbH, Gmunder Strasse 8, 81379 Munich, Germany. URL: <http://www.meter-group.com/hyprop-2/#support>.
- METER. 2015b. *Manual HYPROP*. Version 2015-01, 96 pp, UMS GmbH, Gmunder Strasse 37, Munich, Germany. URL: <http://www.meter-group.com/hyprop-2/#support>.
- Öztürk, Hasan S., Wolfgang Durner, Amir Haghverdi, and Birgit Walter. 2013. "Comparison of Soil Moisture Retention Characteristics Obtained by the Extended Evaporation Method and the Pressure Plate/Sand Box Apparatus." P. 3911 in *EGU General Assembly Conference Abstracts*. Vol. 15.
- Peters, A. and W. Durner. 2006. "Improved Estimation of Soil Water Retention Characteristics from Hydrostatic Column Experiments." *Water Resources Research* 42(11).
- Peters, Andre. 2013. "Simple Consistent Models for Water Retention and Hydraulic Conductivity in the Complete Moisture Range." *Water Resources Research* 49(10):6765–80.
- Peters, Andre, Sascha C. Iden, and Wolfgang Durner. 2015. "Revisiting the Simplified Evaporation Method: Identification of Hydraulic Functions Considering Vapor, Film and Corner Flow." *Journal of Hydrology* 527:531–42.

- Schelle, H., L. Heise, K. Jänicke, and W. Durner. 2013. "Water Retention Characteristics of Soils over the Whole Moisture Range: A Comparison of Laboratory Methods." *European Journal of Soil Science* 64(6):814–21.
- Schelle, H., S. C. Iden, and W. Durner. 2011. "Combined Transient Method for Determining Soil Hydraulic Properties in a Wide Pressure Head Range." *Soil Science Society of America Journal* 75(5):1681–93.
- Schindler, U. 1980. "Ein Schnellverfahren Zur Messung Der Wasserleitfähigkeit Im Teilgesättigten Boden and Stechzylinderproben." *Archiv Fur Acker-Und Pflanzenbau Und Bodenkunde*.
- Schindler, U., W. Durner, G. von Unold, and L. Mueller. 2010. "Evaporation Method for Measuring Unsaturated Hydraulic Properties of Soils: Extending the Measurement Range." *SOIL SCIENCE SOCIETY OF AMERICA JOURNAL* 74(4):1071–83.
- Schindler, Uwe Georg and Lothar Müller. 2017. "Soil Hydraulic Functions of International Soils Measured with the Extended Evaporation Method (EEM) and the HYPROP Device." *Open Data Journal for Agricultural Research* 3.
- Schindler, Uwe and Lothar Mueller. 2006. "Simplifying the Evaporation Method for Quantifying Soil Hydraulic Properties." *JOURNAL OF PLANT NUTRITION AND SOIL SCIENCE* 169(5):623–29.
- Skaggs, R. Wayne, M. A. Youssef, and G. M. Chescheir. 2012. "DRAINMOD: Model Use, Calibration, and Validation." *Transactions of the ASABE* 55(4):1509–22.
- Wang, Xiao-Lei, Shuang Huang, J. S. Huang, and Zi-yun Peng. 2012. "Using HYPROP System and centrifugal method to measure soil Water characteristic curve." *China Rural Water and Hydropower* 6(4):7.

## **CHAPTER 3: DEVELOPING A STAGE-DISCHARGE EQUATION FOR A V-NOTCH WEIR TO ESTIMATE THE DRAINAGE DISCHARGE**

### **3.1 Abstract**

A reliable empirical flow equation for V-notch weirs will provide flow estimates that can be used to calculate nutrient loads leaving fields with subsurface drainage. The objective of this study was to develop such an equation for an AgriDrain metal-edge sharp-crest 45° V-notch weir. In this undertaking, we measured flow rate with a combination of the weighing method for low flow and a turbine flow meter for high flow. The head of water (H) was measured inside a 25-cm AgriDrain control structure with a three-step method. First, we measured the water level (a) and height of the control structure (b). Second, we measured the height of the V-notch apex (c). Third, we calculated head using this equation:  $H=(b-a) - (b-c)$ . Based on the flow meter readings (Q) and H measurements, we developed the following stage-discharge equation:  $Q = 0.749H^{2.25}$ , with Q in liters per minute and H in centimeters. This equation is valid for an H less than the height of the V-notch (i.e., flow through the V-notch) with unsubmerged flow. Based on field experience, we provide a standard procedure for accurate estimation of drainage discharge. In conclusion, the stage-discharge equation developed in this study can provide reliable flow estimates for subsurface drainage studies.

### **3.2 Introduction**

Subsurface drainage is a widely used practice that removes excess water from poorly drained soils (King et al., 2014; Konyha et al., 1992; Mourtzinis et al., 2021; Schilling and Helmers, 2008) and is implemented by installing perforated plastic drainage pipes below the soil surface. In addition to removing water, these pipes allow nitrogen and phosphorus to drain out of the

soil. These can accumulate in lakes and oceans and cause eutrophication (Fausey et al., 1995; Ghane et al., 2016; King et al., 2015; Pease et al., 2018).

Several drainage best management practices (BMPs: controlled drainage, saturated buffer, denitrifying bioreactor, etc.) have the potential to mitigate this issue of nutrient transport. Some of these BMPs require installation of an in-line water-level control structure, which manages drainage discharge at the edge of the field (Christianson et al., 2012; Ghane et al., 2012; Jaynes and Isenhardt, 2014; Williams et al., 2015). To assess the effectiveness of the BMPs in reducing nutrient loads, it is necessary to estimate drainage discharge, and an accurate method for doing so is needed.

Researchers have used various devices and methods, including weirs, sump pumps, tipping buckets, and ultrasonic flow measurements to estimate flow rate (Chun and Cooke, 2008; Kanwar et al., 1999). Calculating flow rate with a weir is one of the most inexpensive and reliable methods available to assess subsurface drainage systems. Weirs are placed inside a control structure to measure drainage discharge from the field. Researchers use different types of weirs (e.g., rectangular, triangular or V-notch, or trapezoidal) to develop flow equations (Walkowiak, 2006). These equations are mostly empirical and vary based on the design and dimension of the weir.

In 2018, AgriDrain introduced a new type of metal-edge sharp-crest V-notch weir. The reason for the new design was to manufacture a standard sharp-crest V-notch weir as opposed to a broad-crest V-notch weir (Huffman et al., 2013). The advantage of a sharp-crest V-notch weir is to prevent the jet of water leaving the weir apex from adhering to any part of the weir's downstream side (Walkowiak, 2006). Instead, the jet of water would spring free of the apex, with

minimal contact with the downstream side of the weir. As a result, the new design improves the accuracy of flow measurements. Christianson et al. (2019) calibrated these sharp-crest V-notch weirs for 15- and 25-cm AgriDrain control structures. These dimensions “15- and 25-cm” refer to the diameter of the drainage pipe connected to the control structure. The equation developed from their experiment for flow rate as related to the depth of water from the apex of the V-notch, often called the head of water, is:

$$Q = 0.66H^{2.28} \quad (3.1)$$

where

Q = flow rate (L/min), and

H = head of water (cm)

Christianson et al. (2019) also calibrated the flow rate measured with these different-sized (15- and 25-cm) V-notch weirs at three different placements inside the control structure: on the bottom of the structure, 48 cm above it, and 97 cm above it. They found no significant differences in the equations they developed to calculate flow rate, regardless of placement or the size of the weir. The authors developed their flow equation with a weighing method of flow measurement. Due to the importance of V-notch equations in subsurface drainage studies, there is a need to verify the V-notch equation in another setting. Also, Christianson et al. (2019) developed their equation for a head of about 14 cm, which does not cover the entire height of a standard metal-edge sharp-crest 45° V-notch weir.

The objective of this study was to develop a stage-discharge relationship for an AgriDrain metal-edge sharp-crest 45° V-notch weir. In our calibration method, we used a combination of the weighing method and a flow meter to measure flow rates. The stage-discharge equation that

we developed should accurately estimate drainage discharge when water is flowing through the V-notch weir. This equation will aid in evaluating the effectiveness of BMPs in reducing nutrient load.

### 3.3 Materials and Methods

#### 3.3.1 Commonly used V-notch equations

The triangular or V-notch weirs are popular in drainage studies because of their high accuracy at low flow rates (Chanson and Wang, 2013; Haan et al., 1994; Trokolanski, 1960; USGS, 1982). The estimation of flow through V-notch weir follows a stage-discharge relationship. The discharge is directly proportional to the head. The discharge equation for a sharp-crest V-notch weir with an apex angle  $\theta$  is written as (World Meteorological Organization, 1971):

$$Q = \frac{8}{15} C_d (2g)^{0.5} \tan\left(\frac{\theta}{2}\right) H^{2.5} \quad (3.2)$$

where

Q = flow rate (L/min),

H = head of water (cm),

g = acceleration due to gravity, and

$C_d$  = discharge coefficient. For a triangular sharp-crest weir with an angle of  $90^\circ$ ,  $C_d$  is assumed to be 0.61 (Bijankhan and Ferro, 2017).

A simplified equation was developed (USGS, 1982) to calculate flow rate through thin-plate V-notch weirs when the angle of V-notch was less than or equal to  $90^\circ$ . For a metal-edge sharp-crest  $45^\circ$  V-notch weir, the United States Geological Survey (USGS) equation is:

$$Q = 0.343H^{2.5} \quad (3.3)$$

where

$Q$  = flow rate (L/min), and

$H$  = head of water (cm)

Since the area of the V-notch weir is quite small compared to the cross-sectional area of the channel, it is safe to neglect the approach velocity for V-notch angles of 90° or less (USGS, 1982). While this may be true for open channel flow but may not apply to the subsurface drainage control structures. Depending on the diameter of the pipe and the slope leading into the control structure, the approach velocity can be enough to create turbulence inside the structure. Another study suggested that if two criteria are satisfied, it is acceptable to ignore the approach velocity in a V-notch weir (World Meteorological Organization, 1971). Those criteria are met if  $H/P < 0.4$  (where  $H$  is the head of water,  $P$  is the distance from the bottom of the structure to the apex of the V-notch weir) and  $H/B < 0.2$  (where  $B$  is the width of the V-notch board). These criteria may be invalid in subsurface drainage control structures, so we cannot use the USGS equation. Therefore, there is a need to calibrate the V-notch weir inside a control structure.

In our experiment, we fitted flow and head data to a simplified version of equation 3.2. This equation is written as:

$$Q = aH^b \quad (3.4)$$

where  $a$  and  $b$  are fitted parameters from a regression analysis.

### 3.3.2 Experimental setup and flow measurement

Our experiment to develop a flow equation was conducted in September 2021 near a pond located south campus of Michigan State University. The setup is shown in figure 3.1 (Supplementary information: figure S1). We used a Flomec GPI turbine flow meter (model

number: TM20NQ9GMB) with a flow measurement range of 75-757 L/min (20-200 gallons/min, with a  $\pm 3\%$  accuracy). This flow meter was factory calibrated by the manufacturer.

It is important to note that the experimental flow range (16-409 L/min) from this study was determined based on experience and literature review. For a 25-cm control structure, 17 cm is the maximum head that can be obtained when water is flowing through an Agri Drain metal-edge sharp-crest 45° V-notch weir. Therefore, this experimental flow range mentioned above approximately covers the entire flow range through a V-notch weir.

For the lower flow rates (16-59 L/min), we used a weighing method. In this method, we held a 5-gallon bucket at the outlet of the control structure, recorded the time required to collect a specific volume of water in the bucket, weighed the bucket on a portable scale (Brecknell PS-USB), then calculated the flow rate. We took three weight readings (triplicate readings) for each flow rate and used their mean value as our final flow reading. It is important to note that the weighing scale was calibrated with known weights before and after the experiment. For the higher flow rates (105-409 L/min), we used the Flomec GPI turbine flow meter mentioned above.

The upstream chamber of the control structure was connected to a 25-cm (10 inches) SDR-35 pipe. We reduced the pipe size to 5 cm (2 inches) to accommodate the flow meter. We pumped (Pacer pumps, model number: SEB2ULE51C) water out of a pond with a flexible PVC pipe. The benefit of using a pond as the water source is that the water level in the pond does not drop as compared to a water tank, which reduces the fluctuation of the pumped water. Nevertheless, we still saw minor fluctuation in the pumped water, as is expected with the pump. To reduce the effect of flow fluctuation, we took numerous (at least 4) flow meter readings for each measurement and took an average of those readings as our final flow.

The discharge side of the pump was connected to a 100-ft long blue lay flat discharge hose, which supplied water to the flow meter. The V-notch weir (figure 3.2) was placed on top of a 17.8-cm tall (7-in; height does not include the thickness of compressed rubber gasket) bottom board inside the control structure.

It is important to note that there was a minor difference (17.0 vs. 16.5 cm) in the height of the V-notch in our experiment compared to the one used by Christianson et al. (2019), even though both are standard V-notch weirs from the same manufacturer. The total height and angle of the V-notch board were the same for both studies. Therefore, any calibrated stage-discharge equation is still valid when the angle of the sharp-crest V-notch weir is the same.

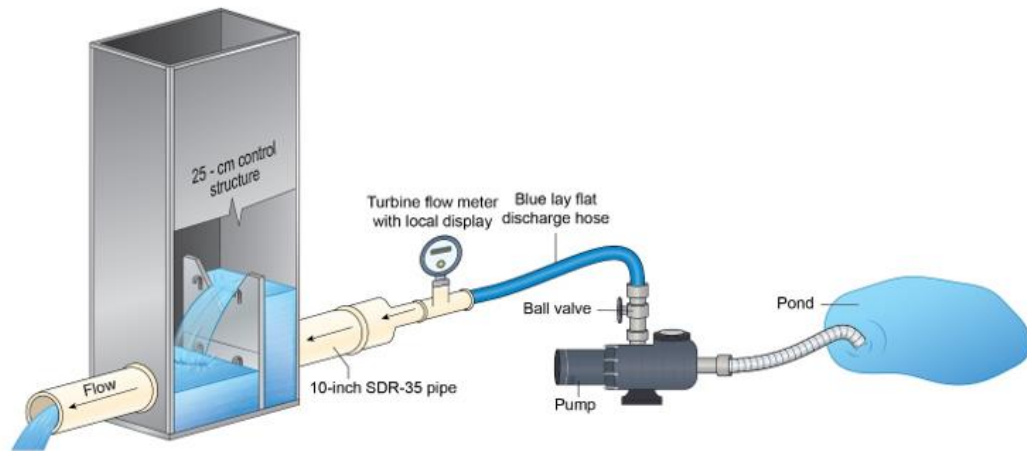


**Figure 3.1. Top: Diagram of the experimental setup showing water flow through a V-notch weir. Bottom: Sideview photo of the control structure with flowing water [From Shokrana and Ghane (2021). Used with permission.]**

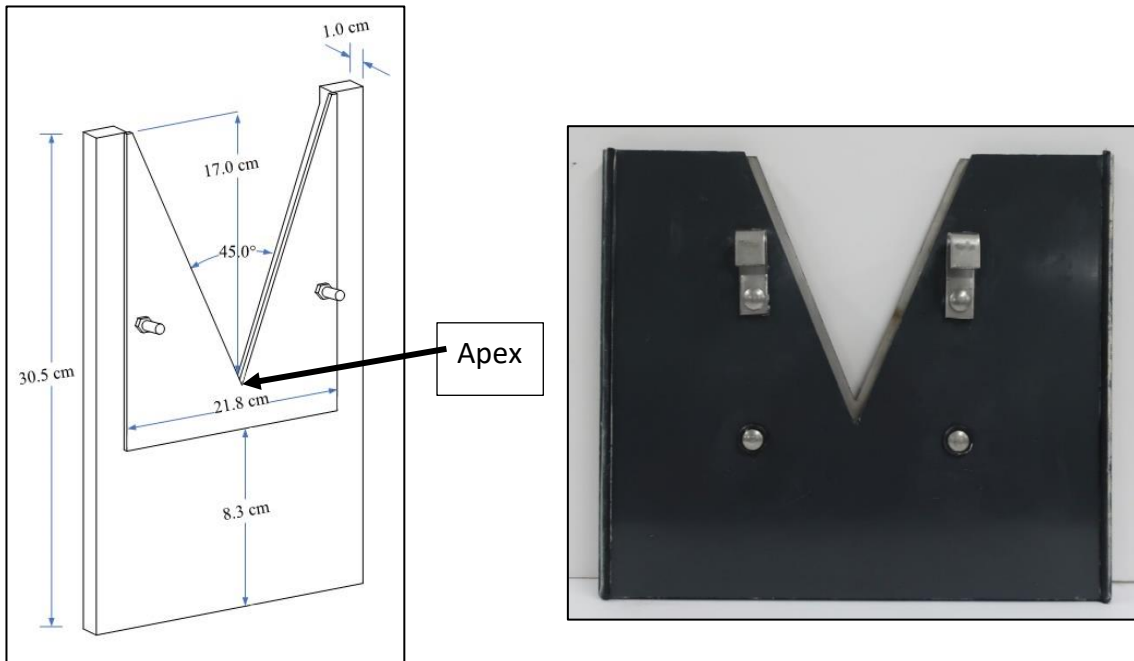


**Figure 3.2. Left: Schematic diagram of a metal-edge sharp-crest 45° V-notch weir. The apex is the point at which both inclined sides of the metal crest meet. The dimensions of the V-notch weir do not include the thickness of the rubber gaskets attached to the board. Right: Photo of the metal-edge sharp-crest 45° V-notch weir [From Shokrana and Ghane (2021). Used with permission.]**

### 3.3.3 Head measurement procedure

#### Phase 1. Water-level and measurement of the height of the structure

To determine the head of water inside the V-notch weir, we put a PVC pipe along the wall of the control structure and made holes in it so that water can seep through that hole and maintain the same head as the control structure inside that pipe, but with less instability. Afterwards, we lowered a water-depth sensor (model 101 P2, Solinst Canada Ltd.) inside the PVC pipe to measure the head for each flow reading obtained from the flow meter and the weighing method (figure 3.3). This water-depth sensor provided the distance from the top of the control structure to the upstream water surface (distance “a”). We also measured the distance from the top to the bottom of the control structure (distance “b”) with a tape measure.

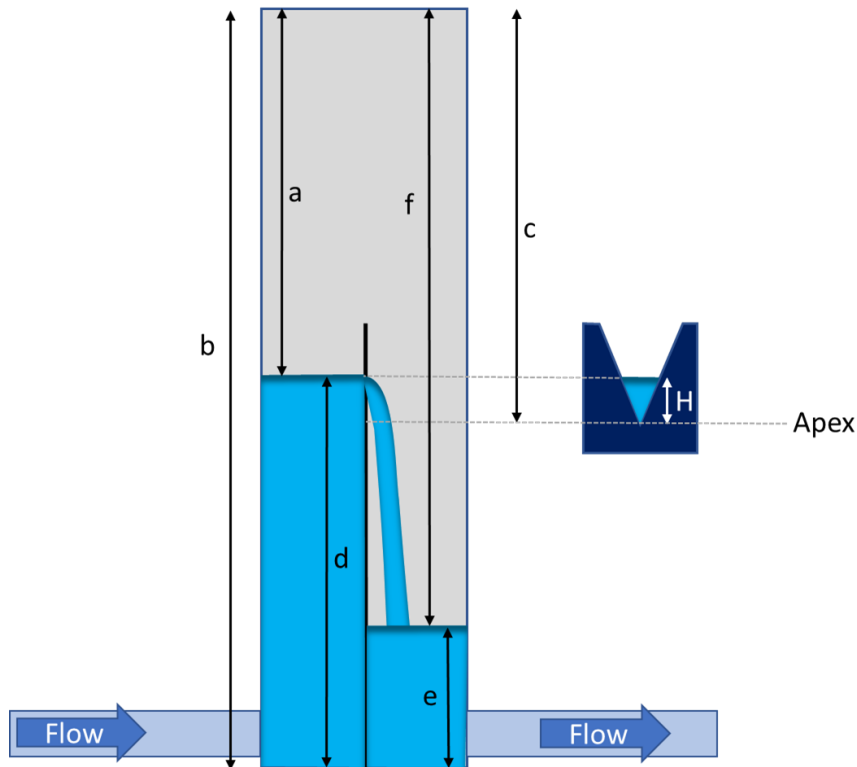


**Figure 3.3. Diagram of the side view of a control structure and the distances needed to calculate the head (H) flowing through a V-notch weir using equation (3.5). A Solinst water-depth sensor was used to measure the distance "a" from the top of the structure to the upstream water surface and "f" from the top of the structure to the downstream water surface. A tape measure was used to measure the distance "b" inside the structure, and a meter-stick was used to measure the distance "c" from the top of the structure to the apex of the V-notch weir. Distance "d" was calculated by subtracting "a" from "b" [From Shokrana and Ghane (2021). Used with permission.]**

Phase 2. Measurement of the height of the apex of the V-notch and the procedure for its verification

We measured the height of the apex of the V-notch using a top-down approach. In this approach, we measured the distance from the top of the control structure to the apex of the V-notch (distance "c" in figure 3.3) with a meter-stick (figure 3.4). Then, the distance from the top of the structure to the apex of the V-notch was measured by placing another ruler on the top and reading the value on the vertical meter stick (figure 3.4 (b)). The height of the V-notch apex was calculated by estimating the distance "b-c", shown in figure 3.3.

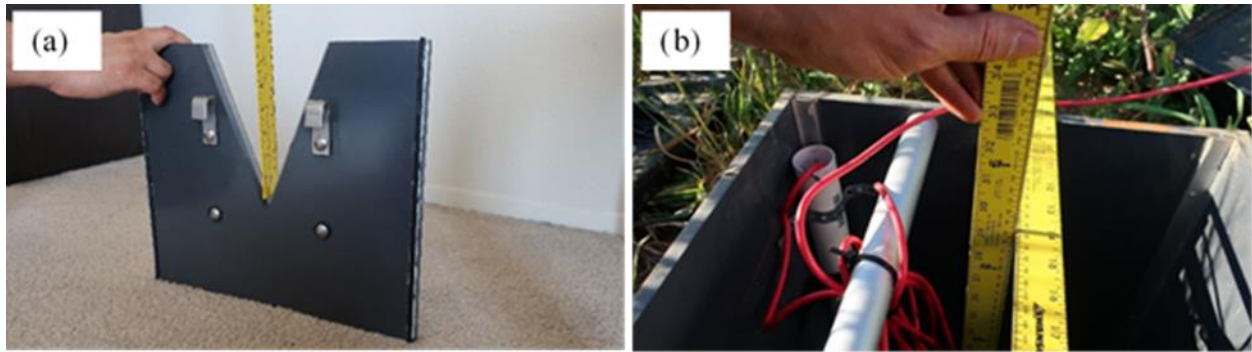


**Figure 3.4. Measurement of the distance “c” from the top of the control structure to the apex of the V-notch weir. Multiple meter-sticks were glued and riveted together to make a long one. To measure the distance “c”: (a) We lowered the meter-stick inside the apex of the V-notch weir, and (b) next, we measured the distance from the apex to the top of the structure by placing another ruler on the top and reading the value on the vertical meter stick [From Shokrana and Ghane (2021). Used with permission.]**

### Phase 3. Equation for head calculation

Based on the measured distances in phases 1 and 2 (figure 3.3), head was calculated as:

$$H = (b - a) - (b - c) \quad (3.5)$$

where

a = distance from the top of the control structure to the upstream water surface (cm),

b = distance from the top of the control structure to the bottom (the height of the structure, cm),

c = distance from the top of the control structure to the apex of the V-notch weir (cm), and

H = head of water (cm)

#### 3.3.4 Quality control measures

We ensured high-quality data collection by taking cautionary steps throughout the experiment. These are listed below.

1. According to the manufacturer’s user manual, we maintained the optimum pipe length for the turbine flow meter. Based on the turbine flow meter manual, the upstream and

downstream pipe lengths of the flow meter should be at least ten (10) times and five (5) times the diameter of the turbine (i.e., 5 cm), respectively. In our experiment, the upstream pipe length of the flow meter was 101.6 cm (20 times the turbine's diameter) and the downstream pipe length was 50.8 cm (10 times the turbine's diameter).

2. We checked the level of the whole setup before and during the experiment, including the control structure and the pipes, to ensure that the setup was horizontal.
3. We made sure that the turbine of the flow meter was not clogged with algae. We disconnected the flow meter from the pipes before, during, and after the experiment. Then, we visually checked for algae, and we did not find any algae in the turbine of the flow meter.

### 3.3.5 Developing the empirical flow equation with regression analysis

We used a least squares regression to develop the empirical flow equation for this experiment. Measured flow rates were plotted against the corresponding head measurements, and the coefficient of determination (*R*-squared) was used to evaluate the goodness of fit.

## 3.4 Results and Discussion

### 3.4.1 V-notch apex height measurement using top-down approach

We measured the distances “b” and “c” (figure 3.3) with the top-down approach. Distance “b” was 149.8 cm and distance “c” was 118.1 cm, so that the distance “b-c” was 31.7 cm, which is the height of the V-notch apex, that is, the distance from the structure bottom to the V-notch apex, as measured with the top-down approach. The distance “b-c” was constant for all head measurements. It is important to mention that the distance “b-c” represented the field condition

where the V-notch board was placed on top of a 17.8-cm (7-in) bottom board, and the rubber gaskets attached to those boards were compressed.

### 3.4.2 Calibrated V-notch weir equation

The least squares regression showed a strong relationship ( $R$ -square= 0.999) between head and flow rate (figure 3.5). The empirical stage-discharge relationship equation is written as:

$$Q = 0.749H^{2.25} \tag{3.6}$$

where

$Q$  = flow rate (L/min), and

$H$  = head of water (cm)

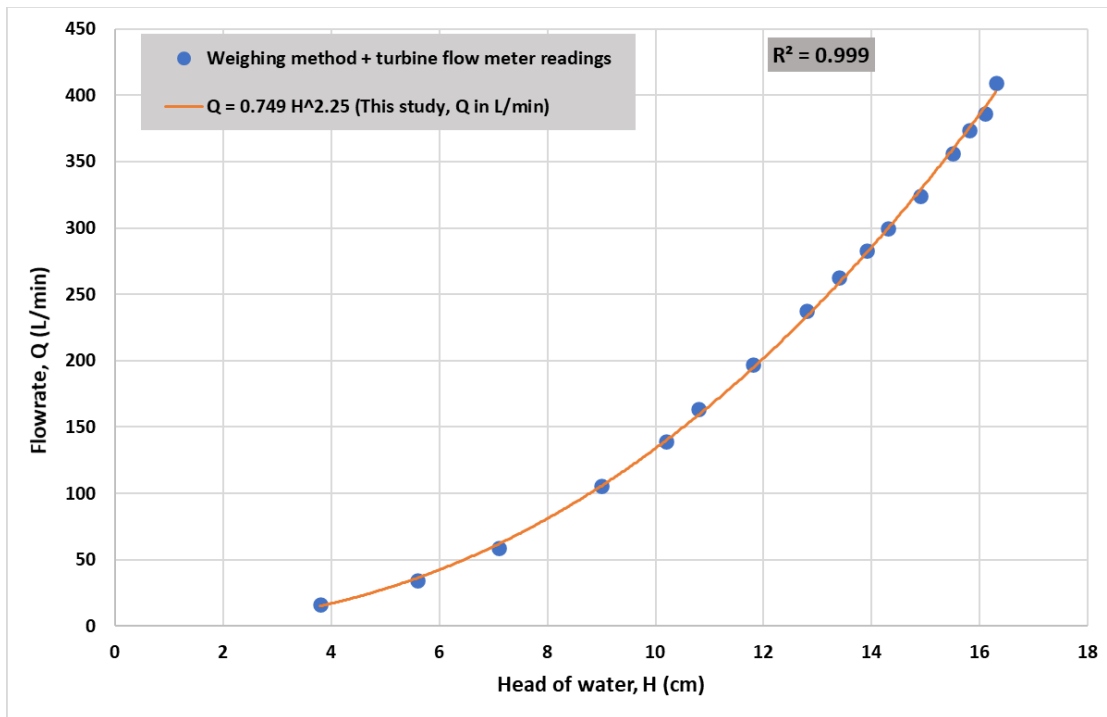


**Figure 3.5. Calibration equation for a metal-edge sharp-crest V-notch weir. We developed this equation for a maximum flow rate of 409.42 L/min with a head of 16.3 cm. We used the weighing method for the low flow rates (16-59 L/min) and the flow meter for the higher flow rates (105-409 L/min). This equation is valid for an H less than the height of the V-notch (i.e., flow through the V-notch). In our experiment, the height of the V-notch was 17.0 cm [From Shokrana and Ghane (2021). Used with permission.]**

Christianson et al. (2019) tested their V-notch flow equation for two different control structure sizes (15 cm and 25 cm). The authors concluded that the V-notch flow equation could be used for other control structures, regardless of their size. They also tested their equation by placing the V-notch weir at three different heights inside each of the different sized structures. They found no statistically significant difference in the flow equations among three different V-notch weir placements. Consequently, we expect that our empirical equation will be valid for structures of different sizes when the same AgriDrain metal-edge sharp-crest 45° V-notch weir is used.

#### 3.4.3 Comparison with previously reported V-notch weir equations

We compared the V-notch equation of this study to that of previous studies (figure 3.6). The USGS (1982) equation (eq. 3.3) underestimated the flow rates for all the head measurements. This may be explained by the differences in the scope for application of these two equations. The equation developed in this study can estimate flow rates for 45° V-notch weirs inside a 25-cm AgriDrain control structure, whereas the USGS equation is used in different applications in an open-channel flow.

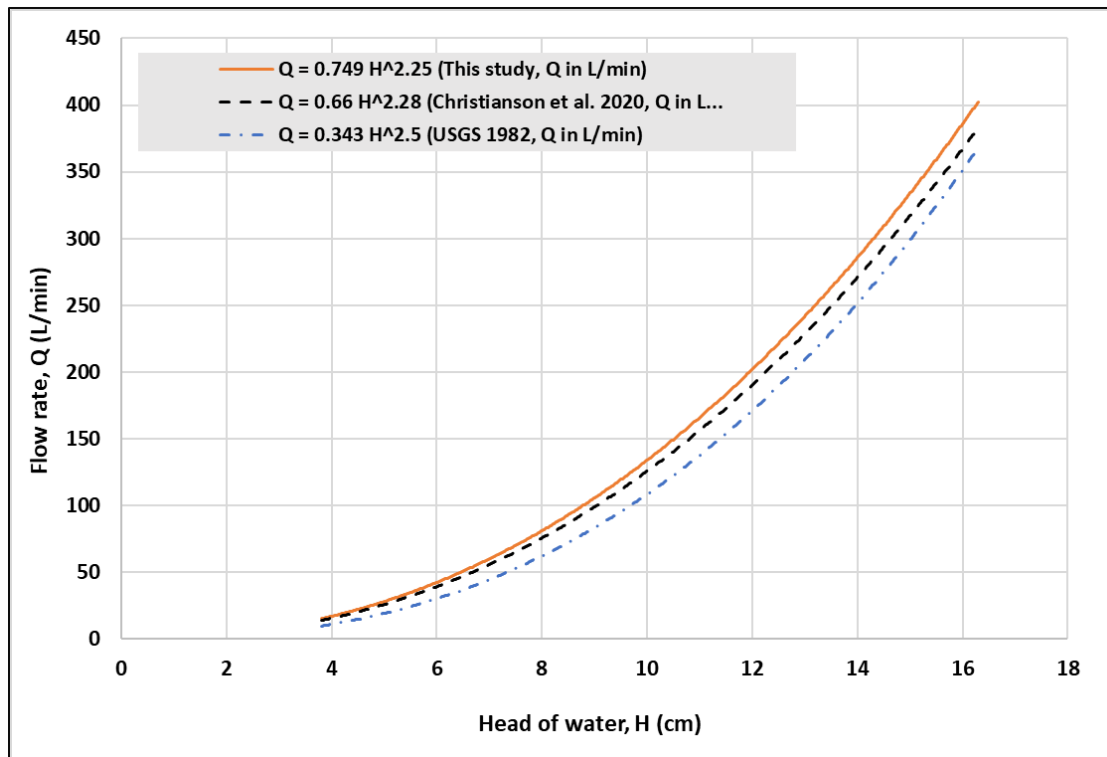


**Figure 3.6. Comparison of the V-notch equation developed in this study to those in previous studies [From Shokrana and Ghane (2021). Used with permission.]**

We developed our equation for a maximum flow rate of 409.42 L/min with a head of 16.3 cm. Our equation is valid for an H less than the height of the V-notch (i.e., flow through the V-notch). In our experiment, the height of the V-notch was 17.0 cm. The flow rates obtained from the equation developed in this study (eq. 6) are consistently higher than the equation developed by Christianson et al. (2019) (figure 3.6). Christianson et al. (2019) used one method (weighing) of flow rate reading to develop their equation, but they did not calibrate and verify their weighing scale as reported in Christianson et al. (2021). Figure 3.6 shows that the equation from Christianson et al. (2019) underestimates the higher flow rates compared to the equation obtained in our study. This could be because their weighing scale was not calibrated and verified.

To assure the reliability of our equation (eq. 3.6), we obtained stage-discharge relationship data from a separate experiment conducted in Farrall Hall at Michigan State University. In that experiment, we used two turbine flow meters (one for low flow and one for high flow), different from the one used to develop equation 3.6. Comparison between that experiment (two flow meters) and the one conducted herein shows that stage-discharge data closely agreed with each other (Supplementary information: figure S2). Therefore, the two-turbine experiment verifies the stage-discharge equation 3.6. For more information, refer to the supplementary information.

#### 3.4.4 Standard procedure for accurately measuring flow rate

Based on our combined results and experiences, we provided a standard procedure for accurately estimating drainage discharge. These steps can be used for rectangular or cylindrical structures.

Step 1: Measure the height of the control structure (distance “b” in figure 3.3)

Measure the distance from the top to the bottom of the control structure with a tape measure, making sure that the tape measure is in contact with the structure wall so that it doesn’t bend.

Step 2: Measure the depth of the V-notch apex (distance “c” in figure 3.3)

Measure the distance from the top of the control structure to the V-notch apex, distance “c”, by first placing a long, thin measuring stick inside the apex. Then, carefully measure distance “c” by placing another ruler on the top of the control structure and reading the value on the vertical meter stick (figure 3.4).

Step 3: Measure the upstream water-level from top or bottom of the structure (distance “a” or “d” in figure 3.3, respectively)

There are at least two methods for measuring the water level from the bottom of the control structure (distance “d” in figure 3.3): a pressure transducer or a water-finding paste.

The pressure transducer method is useful for measuring the water level when continuous flow rates will be measured. The pressure transducer is placed inside a polyvinyl chloride (PVC) pipe and lowered to the bottom of the upstream chamber of the structure. The PVC pipe reduces the effects of flow turbulence on the pressure transducer. To ensure accurate water-level measurements, the pressure transducer reading is verified with manual water-level measurements regularly (e.g., with water-finding paste) and sediments are removed from the pressure transducer as they accumulate.

The second method is useful for measuring water level when the instantaneous flow rate will be measured. This method requires a meter stick and water-finding paste. The water-finding paste is applied on a meter stick and then slowly lowered to the bottom of the control structure. The meter stick is lowered along the wall of the upstream chamber of the control structure to ensure that it does not bend. The paste will turn red upon contact with water (figure 3.7).

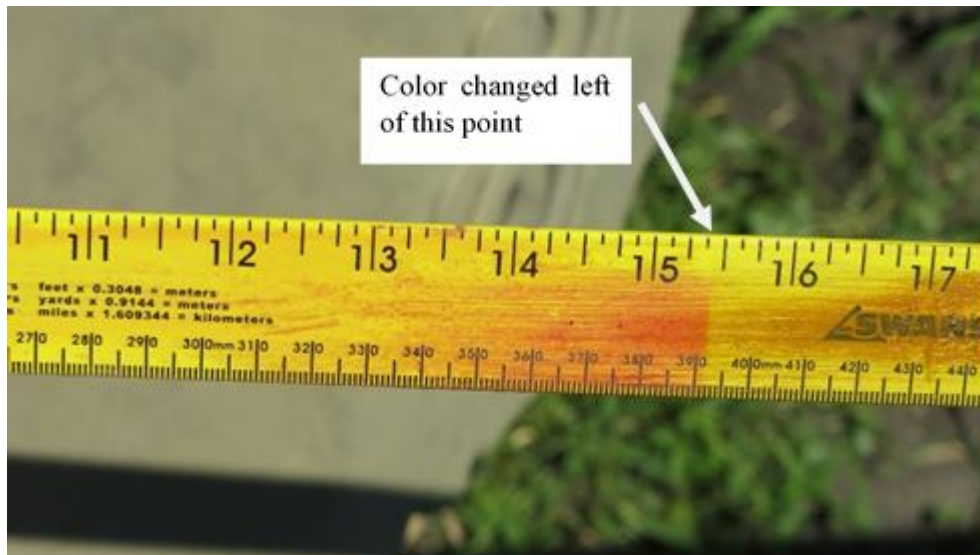


**Figure 3.7. Measurement of water level with water-finding paste. A small amount of paste is applied to a meter stick, which is inserted into water. The dry paste is white but turns red upon contact with water [From Shokrana and Ghane (2021). Used with permission.]**

Various water-depth sensors are available to measure the water depth from the top of the structure (distance “a” in figure 3.3) as performed in this study. Some of them need to contact water to measure the depth (figure 3.8 (a)). These types of sensors can be acquired from Solinst, Geotech, and Heron, Inc. Others are contactless, for example, an ultrasonic level sensor. Both methods are used when measuring instantaneous flow rate. The sensors that need to contact water for depth measurements (e.g., the one from Solinst) usually consist of a probe connected to a flat tape measure. When using this type of sensor, the probe is lowered into the upstream chamber of the control structure near the wall (figure 3.8 (b)). Once the probe meets the water surface, the unit will emit both sound and light signals. At that time, the value on the flat tape, read by looking at the marked numbers vertically, is an estimate of the water depth inside the control structure, distance “a” in figure 3.3. Another sensor for measuring water depth from the top of the structure is an ultrasonic sensor, which is currently being investigated by researchers to determine if it works with the AgriDrain control structures.

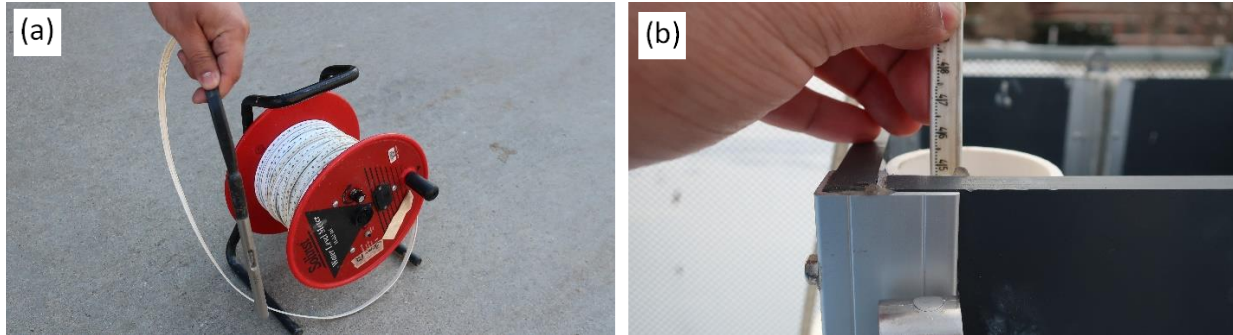


**Figure 3.8. Measurement of water level using a water-depth sensor: (a) Solinst water-depth sensor; the sensor is located at the middle of the probe. Once the sensor comes in contact with water, sound and light signals will indicate when to take the reading. (b) The sensor probe is lowered inside the control structure through a PVC pipe to reduce the effect of flow turbulence. Once in place, the length of the flat tape along the wall of the control structure indicates the water depth [From Shokrana and Ghane (2021). Used with permission.]**

Step 4: Measure the downstream water-level from structure top or bottom (distance “f” or “e” in figure 3.3)

It is important to measure the water level in the downstream chamber of the control structure to ensure flow impedance (i.e., submerged flow) does not occur. This means that the water level in the downstream chamber must not rise above the V-notch apex. The downstream water depth can be measured from the structure top (distance “b-f”) using a water-depth meter. It is also possible to measure the downstream water level from the bottom (distance “e”) with a pressure transducer or water-finding paste. The details about these measurement procedures are explained in step 3. Our calibrated equation will not be valid under submerged flow conditions.

Step 5: Calculate head inside the V-notch weir

To calculate head inside the structure when the height of the water level in the upstream chamber (distance “d” in figure 3.3) can be identified from a pressure transducer or from the water-finding-paste method, use the following equation:

$$H = d - (b - c) \quad (3.7)$$

To calculate head when the depth of water in the upstream chamber (distance “a” in figure 3.3) can be determined from a water-depth meter, use equation 3.5.

Step 6: Calculate flow rate

Use equation 3.6 to calculate flow rate based on a measured head when the following two conditions are met: (1) water must be flowing through the V-notch weir and not flowing over the weir (that is,  $H < 17.0$  m for this study) and (2) the height of the water level in the downstream chamber (distance “e” in figure 3.3) must not exceed the V-notch apex (distance “b-c” in figure 3.3), so that submerged flow is avoided.

3.4.5 Things to avoid when following the standard procedure

3.4.5.1 Avoid adding nominal board sizes to measure height of V-notch apex

A common method of estimating the height of the V-notch apex (distance “b-c” in figure 3.3) is to add the nominal sizes of boards, which could introduce errors. When adding nominal board sizes, the thickness of the rubber gaskets will be neglected. To demonstrate this point, we estimated the height of the V-notch apex by adding two nominal 5-in boards, one nominal 7-in board, one nominal 7-in bottom-board, and a standard metal-edge sharp-crest 45° V-notch board. Based on adding nominal board sizes, the height of the V-notch apex was 74.5 cm. Based on the top-down approach, we determined the height of the V-notch apex to be 74.9 cm; there is a difference of 0.4 cm between the two measurements, perhaps due to the thickness of the rubber gaskets, or variations between the nominal and actual board sizes. If not considered, these factors could result in an error in the measurement of the V-notch apex height. At the end of 2013, AgriDrain replaced the traditional boards with foam gaskets (or foam O-rings) with the

injection-molded boards with rubber gaskets. The compressed thickness of the new rubber gaskets may not be the same as the foam ones. This error would be even greater if more boards were used inside the control structure. Therefore, nominal board sizes should not be used to estimate the height of the V-notch apex (distance “b-c” in figure 3.3), unless the height of each board is carefully measured, and the thickness of compressed rubber gaskets is included.

#### 3.4.5.2 Avoid using a V-notch weir board without a bottom board

During heavy rainfall, the water level in a ditch may rise and create outlet submergence (figure 3.9). In this situation, the water level in the downstream chamber of the structure can rise above the V-notch apex, thus preventing the use of equation 3.6 because water is no longer freely flowing through the V-notch. However, if a bottom board is used, the equation 3.6 can be used to calculate flow as long as the water level in the downstream chamber remains below the V-notch apex. If the downstream water level rises higher, equation 3.6 cannot be used. Overall, the benefit of using a bottom board is that it gives extra height to the apex of the V-notch weir, so there is a greater chance of achieving freely flowing water through the V-notch.

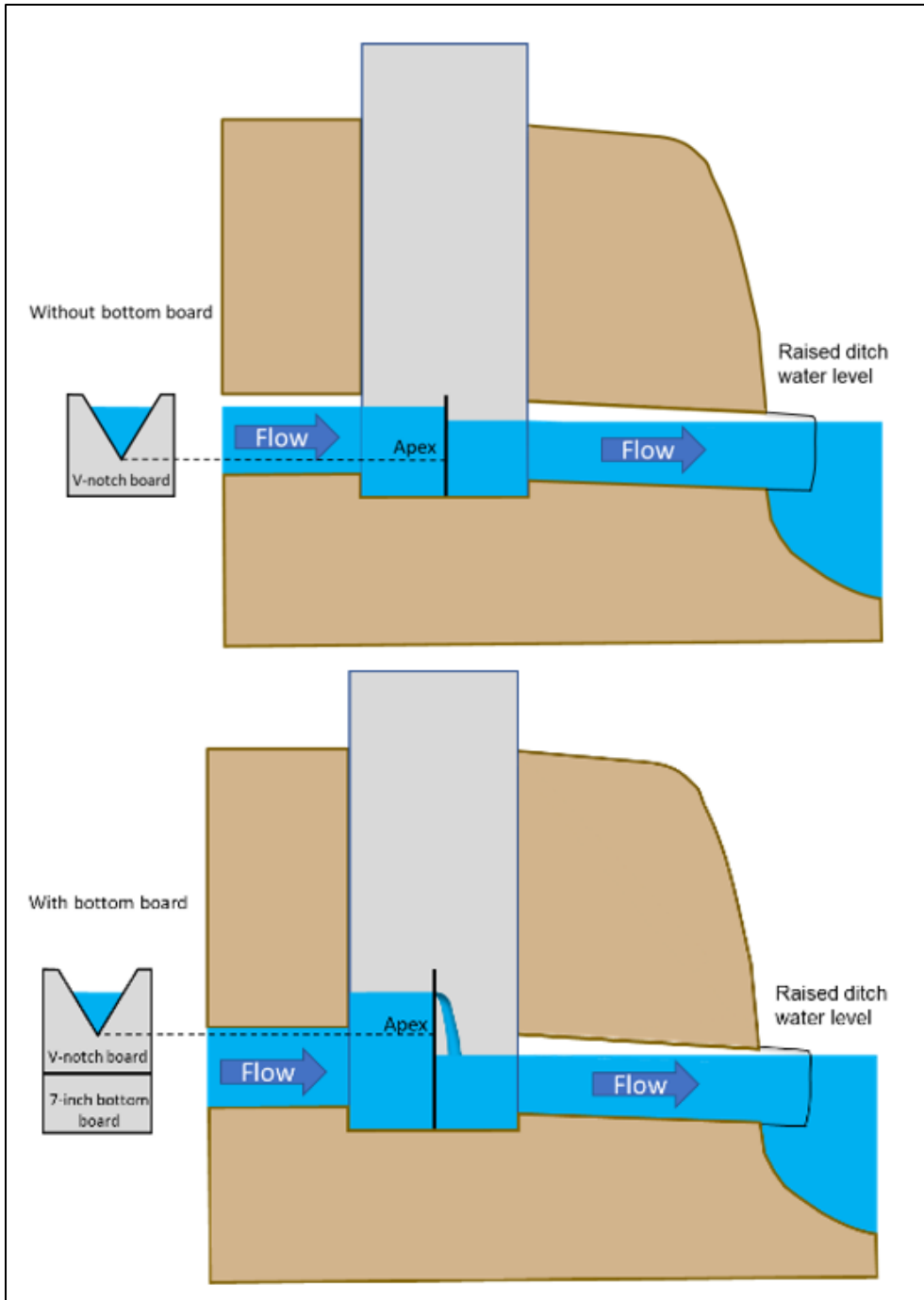


Figure 3.9. A diagram (not drawn to scale) to represent the water flow inside a 25-cm control structure in agricultural fields. Top diagram: If there is heavy rainfall, the water level in the ditch will rise and the water level in the downstream chamber of the control structure will rise above the apex of the V-notch, causing submerged flow. Bottom diagram: Adding a 17.8 cm (7-inch) bottom board below the V-notch weir would give extra height to the apex of the V-notch weir, so there would be a greater chance of achieving freely flowing water through the V-notch [From Shokrana and Ghane (2021). Used with permission.]

### 3.5 Conclusions

We measured head and flow rate for a metal-edge sharp-crest 45° V-notch weir inside a 25-cm AgriDrain control structure. Based on those measurements, we developed an empirical stage-discharge equation while following quality-control procedures. In our calibration method, we used a weighing method for the lower flow rates and a turbine flow meter for the higher flow rates. The empirical metal-edge sharp-crest 45° V-notch weir equation can be used for any AgriDrain control structure, as long as the water is flowing through the V-notch weir and there is no flow submergence. If using a cylindrical control structure, we recommend developing a stage-discharge equation before drainage monitoring. Based on field experience, we provide a standard procedure to accurately estimate drainage discharge. In conclusion, the V-notch weir equation developed in this study can provide reliable flow estimates that can be used for nutrient load reductions in subsurface drainage studies.

## REFERENCES

- Bijankhan, M., Ferro, V. (2017). Dimensional analysis and stage-discharge relationship for weirs: a review. *Journal of Agricultural Engineering*, 48(1), 1–11. <https://doi.org/10.4081/jae.2017.575>
- Chanson, H., Wang, H. (2013). Unsteady discharge calibration of a large V-notch weir. *Flow Measurement and Instrumentation*, 29, 19–24. <https://doi.org/10.1016/j.flowmeasinst.2012.10.010>
- Christianson, L., Bhandari, A., Helmers, M., Kult, K., Sutphin, T., Wolf, R. (2012). Performance evaluation of four field-scale agricultural drainage denitrification bioreactors in Iowa. *Transactions of the ASABE*, 55(6), 2163–2174. <https://doi.org/10.13031/2013.42508>
- Christianson, L. E., Christianson, R. D., Lipka, A. E., Bailey, S. B., Chandrasoma, J., McCoy, C., Fontes, G. P., Roh, J., Bailon, A. P. S. B., Wickramaratne, N. M., Cooke, R. A. (2019). Calibration of stainless steel-edged v-notch weir stop logs for water level control structures. *Applied Engineering in Agriculture*, 35(5), 745–749. <https://doi.org/10.13031/aea.13350>
- Chun, J. A., Cooke, R. A. (2008). Calibrating agridrain water level control structures using generalized weir and orifice equations. *Applied Engineering in Agriculture*, 24(5), 595–602. <https://doi.org/10.13031/2013.25274>
- Fausey, N. R., Brown, L. C., Belcher, H. W., Kanwar, R. S. (1995). Drainage and Water-quality in Great-Lakes and Corn-belt States. *Journal of Irrigation and Drainage Monitoring-ASCE*, 121(4), 283–288. [https://doi.org/10.1061/\(ASCE\)0733-9437\(1995\)121:4\(283\)](https://doi.org/10.1061/(ASCE)0733-9437(1995)121:4(283))
- Ghane, E., Fausey, N. R., Shedekar, V. S., Piepho, H. P., Shang, Y., Brown, L. C. (2012). Crop yield evaluation under controlled drainage in Ohio, United States. *Journal of Soil and Water Conservation*, 67(6), 465–473. <https://doi.org/10.2489/jswc.67.6.465>
- Ghane, E., Ranaivoson, A. Z., Feyereisen, G. W., Rosen, C. J., Moncrief, J. F. (2016). Comparison of Contaminant Transport in Agricultural Drainage Water and Urban Stormwater Runoff. *Plos One*, 11(12). <https://doi.org/10.1371/journal.pone.0167834>
- Haan, C. T., Barfield, B. J., Hayes, J. C. (1994). *Design hydrology and sedimentology for small catchments*. Elsevier.
- Jaynes, D. B., Isenhardt, T. M. (2014). Reconnecting Tile Drainage to Riparian Buffer Hydrology for Enhanced Nitrate Removal. *Journal of Environment Quality*, 43(2), 631–638. <https://doi.org/10.2134/jeq2013.08.0331>
- Kanwar, R. S., Bjerneberg, D., Baker, D. (1999). An automated system for monitoring the quality and quantity of subsurface drain flow. *Journal of Agricultural Engineering Research*, 73(2), 123–129. <https://doi.org/10.1006/jaer.1998.0398>

- King, K. W., Fausey, N. R., Williams, M. R. (2014). Effect of subsurface drainage on streamflow in an agricultural headwater watershed. *Journal of Hydrology*, 519(A), 438–445. <https://doi.org/10.1016/j.jhydrol.2014.07.035>
- King, K. W., Williams, M. R., Fausey, N. R. (2015). Contributions of Systematic Tile Drainage to Watershed-Scale Phosphorus Transport. *Journal of Environmental Quality*, 44(2), 486–494. <https://doi.org/10.2134/jeq2014.04.0149>
- Konyha, K. D., Skaggs, R. W., Gilliam, J. W. (1992). Effects of Drainage and Water-management Practices on Hydrology. *Journal of Irrigation and Drainage Engineering*, 118(5), 807–819. [https://doi.org/10.1061/\(ASCE\)0733-9437\(1992\)118:5\(807\)](https://doi.org/10.1061/(ASCE)0733-9437(1992)118:5(807))
- Mourtzinis, S., Andrade, J. F., Grassini, P., Edreira, J. I. R., Kandel, H., Naeve, S., Nelson, K. A., Helmers, M., Conley, S. P. (2021). Assessing benefits of artificial drainage on soybean yield in the North Central US region. *Agricultural Water Management*, 243. <https://doi.org/10.1016/j.agwat.2020.106425>
- Pease, L. A., King, K. W., Williams, M. R., LaBarge, G. A., Duncan, E. W., Fausey, N. R. (2018). Phosphorus export from artificially drained fields across the Eastern Corn Belt. *Journal of Great Lakes Research*, 44(1), 43–53. <https://doi.org/10.1016/j.jglr.2017.11.009>
- Schilling, K. E., Helmers, M. (2008). Effects of subsurface drainage tiles on streamflow in Iowa agricultural watersheds: Exploratory hydrograph analysis. *Hydrological Processes*, 22(23), 4497–4506. <https://doi.org/10.1002/hyp.7052>
- Troskolanski, A. T. (1960). *Hydrometry: Theory and practice of hydraulic measurements*. Pergamon Press.
- USGS. (1982). Measurement and computation of streamflow, vol. 2, Computation of discharge. *US Geological Survey Water Supply Paper 2175, Page 32*.
- Walkowiak, D. K. (2006). *ISCO open channel flow measurement handbook*.
- Williams, M. R., King, K. W., Fausey, N. R. (2015). Drainage water management effects on tile discharge and water quality. *Agricultural Water Management*, 148, 43–51. <https://doi.org/10.1016/j.agwat.2014.09.017>
- World Meteorological Organization. (1971). Use of Weirs and Flumes in Stream Gauging, WMO Technical Note No. 117.

## CHAPTER 4: CALIBRATING THE RZWQM2-P MODEL TO SIMULATE DRAINAGE DISCHARGE AND PHOSPHORUS LOSS IN CLAY LOAM SOIL IN MICHIGAN

### 4.1 Abstract

Phosphorus (P) loss and transport through subsurface drainage systems is a primary focus for addressing harmful algal blooms in freshwater systems. The recent development of the phosphorus (P) routine of the Root Zone Water Quality Model (RZWQM2-P) has the potential to enhance our understanding of the fate and transport of P from subsurface-drained fields to surface water. However, there is a need to test the model under different fertilization, soil, climate, and cropping conditions. The objective of this study was to test the model's performance with daily drainage discharge, dissolved reactive phosphorus (DRP), and total phosphorus (TP) load collected from a subsurface-drained field with a clay loam soil. We calibrated RZWQM2-P using two years of measured data. Subsequently, we validated RZWQM2-P using a year and nine months of measured data. We used the Nash-Sutcliffe model efficiency (NSE) and percentage bias (PBIAS) statistics for the RZWQM2-P model evaluation. Results showed that the model performance was “good” (daily NSE = 0.66 and PBIAS = -7.16) in predicting hydrology for the calibration period. For the validation period, the hydrology prediction of the model was “very good” (daily NSE = 0.76), but it had a “satisfactory” underestimation bias (PBIAS = 23.57). The model’s performance was “unsatisfactory” in simulating DRP for both calibration (daily NSE = 0.31 and PBIAS = -61.50) and validation (daily NSE = 0.32 and PBIAS = 43.68) periods. The P model showed “satisfactory” performance in predicting TP load for both calibration (daily NSE = 0.46 and PBIAS = -32.41) and validation (daily NSE = 0.39 and PBIAS = 42.90) periods, although both periods showed “unsatisfactory” percent bias. The underperformance may have been due to the model’s inability to partition fertilizer P into different P pools under high water table or ponding

conditions when using daily data. In conclusion, the RZWQM2-P model performed well for drainage discharge with daily data, but further investigation is needed to improve the P component of the model.

## **4.2 Introduction**

Phosphorus (P) is extensively used in agriculture in the forms of fertilizer and manure to facilitate crop production and high yields (Sharpley et al., 2001). Precipitation and irrigation events cause significant P loss from agricultural lands to surface water, thus making it one of the major non-point sources of eutrophication in freshwater bodies (Dubrovsky et al., 2010; Kleinman et al., 2011). Eutrophication stimulates harmful algal blooms (HABs) in surface water which poses severe ecological, economic, and health concerns (Pierzynski et al., 2005). Although nitrogen (N) and P play a significant role in causing HABs in lakes and oceans, P is considered to be the limiting nutrient freshwater systems (Sharpley et al., 1994).

In agricultural landscapes, P loss to surface water occurs in two pathways: surface runoff and subsurface drainage discharge (Ghane et al., 2016). P can be lost from both pathways in dissolved (i.e., dissolved reactive phosphorus, DRP) and particulate (i.e., particulate phosphorus, PP) forms, but DRP is considered to be the primary driver of HABs in freshwater systems due to its bioavailability (Macrae et al., 2021). While the current knowledge can efficiently explain P loss pathways (Pierzynski et al., 2005), it was not always the case. Due to the high P sorption capacity of agricultural soils, P was largely considered immobile (Baker et al., 1975; Radcliffe & Cabrera, 2006). Therefore, P transport via surface runoff was seen as the primary pathway, and research was focused on developing management strategies to reduce soil erosion (Ryden et al., 1974). However, in the 1990s, Sims et al. (1998) found that a significant amount of P can be lost via

subsurface drainage discharge, and they suggested developing management strategies that reduce subsurface transport of P. Although the installation of subsurface drainage increases the total drained water volume from a field, it significantly reduces surface runoff volume and sediment loss compared to an undrained field (Dolezal et al., 2001; Robinson & Rycroft, 1999; Skaggs et al., 1994). While the installation of subsurface drains reduces P loss in surface runoff, their role in increasing P loss from subsurface pathways cannot be overlooked (Bengston et al., 1995; King et al., 2015).

Long-term field experiments employing management practices can investigate P loss from subsurface drainage discharge, but they are expensive and time-consuming. On the other hand, field-scale hydrologic models are inexpensive, and they provide results in a shorter time than field experiments. Models can use field experimental data as inputs and extrapolate the results across spatial and temporal scales. Over the years, significant progress has been made in developing P modules to incorporate into both field-scale and watershed-scale hydrologic models. A robust and sophisticated P model should be able to predict: (i) DRP and PP loss from both surface and subsurface pathways, (ii) P loss through macropores, (iii) plant uptake P, (iv) P transformation in soil, and (v) the effects of management practices on P loss. Although many P models exist, only a few of those can fulfill the criterion mentioned above.

Askar et al., (2021) developed and tested a P module for DRAINMOD known as DRAINMOD-P that fulfills the requirements mentioned above. The authors tested their model in a site in Ohio for clay soil, which showed promising results in predicting P loss from subsurface-drained fields. In addition to developing the P module, the authors modified the macropore flow

component of DRAINMOD using the Hagen-Poiseuille law to accurately estimate the water and P transport through preferential flow pathways.

A comprehensive literature review on P models (Qi & Qi, 2016; Radcliffe et al., 2015) suggested that ICECREAM is the most promising model to accurately predict P loss from surface runoff and subsurface drainage discharge (Tattari et al., 2001). However, ICECREAM does not have a water table based tile drainage component as estimated by Hooghoudt's equation (Hooghoudt, 1940; Smedema et al., 2004). Instead, it estimates the sum of the water flux from the macropore and micropore at the tile drain depth to imitate tile drainage (Qi & Qi, 2016; Sadhukhan et al., 2019a). Additionally, the storage routing concept that ICECREAM uses cannot simulate upward flow, which is a problem for soils with a shallow water table (Pferdmenges et al., 2020). ICECREAM also simulates the soil matrix flow using the simple storage routing concept, but this can be improved by implementing the Richards equation (Pachepsky et al., 2003).

To improve the limitations of the ICECREAM model mentioned above, Sadhukhan et al. (2019a) have developed a P module for the Root Zone Water Quality Model (RZWQM2). RZWQM2 is a field-scale process-based model that uses more robust and sophisticated approaches than ICECREAM to simulate subsurface drainage discharge from an agricultural field (Ma et al., 2011; Ma et al., 2012). RZWQM2 has been widely tested and validated across North America (Ahmed et al., 2007; Jiang et al., 2018; Ma et al., 2007; Malone et al., 2014; Thorp et al., 2008). The RZWQM2-P model performs as a single tool to simulate hydrology and P loss through surface runoff and subsurface drainage discharge pathways.

Although RZWQM2-P has been tested and validated by the developers (Sadhukhan et al., 2019a), further testing is needed to evaluate the model's performance under different soil types,

climate, management practices, and crop varieties. The objective of this study is to test and validate the performance of RZWQM2-P model in predicting DRP and PP loss in a clay loam soil. The outcome of this study will help RZWQM2-P model developers identify processes and subroutines within the model that need to be improved for predicting P loss from a subsurface-drained field.

### **4.3 Materials and Methods**

#### **4.3.1 Overview of RZWQM2-P**

The RZWQM2-P (version 4.2) is a field-scale, process-based, and one-dimensional (i.e., vertical in the soil profile) model that can simulate major physical, chemical, and biological processes occurring in an agricultural field. The RZWQM2-P combines two distinct models: (i) the RZWQM2 model and (ii) the P model (Sadhukhan et al., 2019a). The RZWQM2 model was first developed and then further improved by the USDA-ARS to simulate soil hydrological processes, crop production, and water quality effects under different agricultural management practices (Ahuja et al., 2000). The P routine has been recently developed and integrated with the RZWQM2 to simulate P loss through hydrologic pathways (Sadhukhan et al., 2019a).

The RZWQM2 uses several mathematical equations to simulate the physical processes in the model (Ma et al., 2011; Ma et al., 2012). The modified forms of Brooks-Corey equations are used to describe the soil water characteristic curve (Brooks & Corey, 1964). The infiltration process due to rainfall, snowmelt, or irrigation event is described by the Green-Ampt equation (Green & Ampt, 1911). Richards equation is used to simulate the redistribution of water following infiltration (Richards., 1931). Subsurface drainage discharge is simulated using the Hooghoudt's steady-state equation (Bouwer & Van Schilfgaarde, 1963; Smedema et al., 2004) and Poiseuille's

law is used to simulate the macropore flow. Daily potential evapotranspiration (PET) is estimated using the Shuttleworth-Wallace equation (Farahani & DeCoursey, 2000). Crop growth can be simulated using three crop growth simulation models which are: (i) the generic crop growth model (Hanson, 2000), (ii) the DSSAT crop growth model (Nielsen et al., 2002), and (iii) the HERMES crop growth model (Malone et al., 2017).

For the simulation of P, RZWQM2-P separates the P cycle into five different soil P pools. Three of those are inorganic and two organic P pools (Jones et al., 1984). The inorganic P pools comprise the labile P pool, active inorganic P pool, and stable inorganic P pool. Among these inorganic P pools, the labile P pool is in dissolved form and it is the only pool from which P is available for plant uptake. The labile P pool is in rapid equilibrium with the active inorganic P pool, where the P is present in solid form but easily released to the soil solution. A slow adsorption and desorption process occurs between the active inorganic P and stable inorganic P. The P present in the inorganic P pool is very insoluble, therefore this pool maintains a slow equilibrium with the active inorganic P pool. The two organic P pools are the fresh organic P pool and the stable organic P pool. Mineralized P from the fresh organic P pool is added to the labile P pool and stable organic P pool. A slowly mineralized P is also added from the stable organic P pool to the labile P pool. The P model can also simulate P dynamics from manure and fertilizer application by creating four surface manure P pools and two surface fertilizer P pools.. More details on how the P model works are described by Sadhukhan et al. (2019a).

#### 4.3.2 Site description

The on-farm monitoring site is located near Blissfield, Michigan (figure 4.1). The grade of the field is 0.1%. The field area is 6.7 hectares (16.6 Acres). The soil type is Ziegenfuss clay loam, classified

as a poorly drained soil. The farmer uses a corn-soybean rotation in this field and applies commercial inorganic fertilizer. The date of cropping and management practices are shown in Error! Reference source not found.. The depth of subsurface drains is about 81 cm, and the spacing is about 1005 cm. The effective radius of the four-row perforated drain pipe is estimated to be 0.7 cm (Ghane., 2022). The average soil test phosphorus (STP) concentration was 35 ppm (Bray-P) on 18 March 2018.

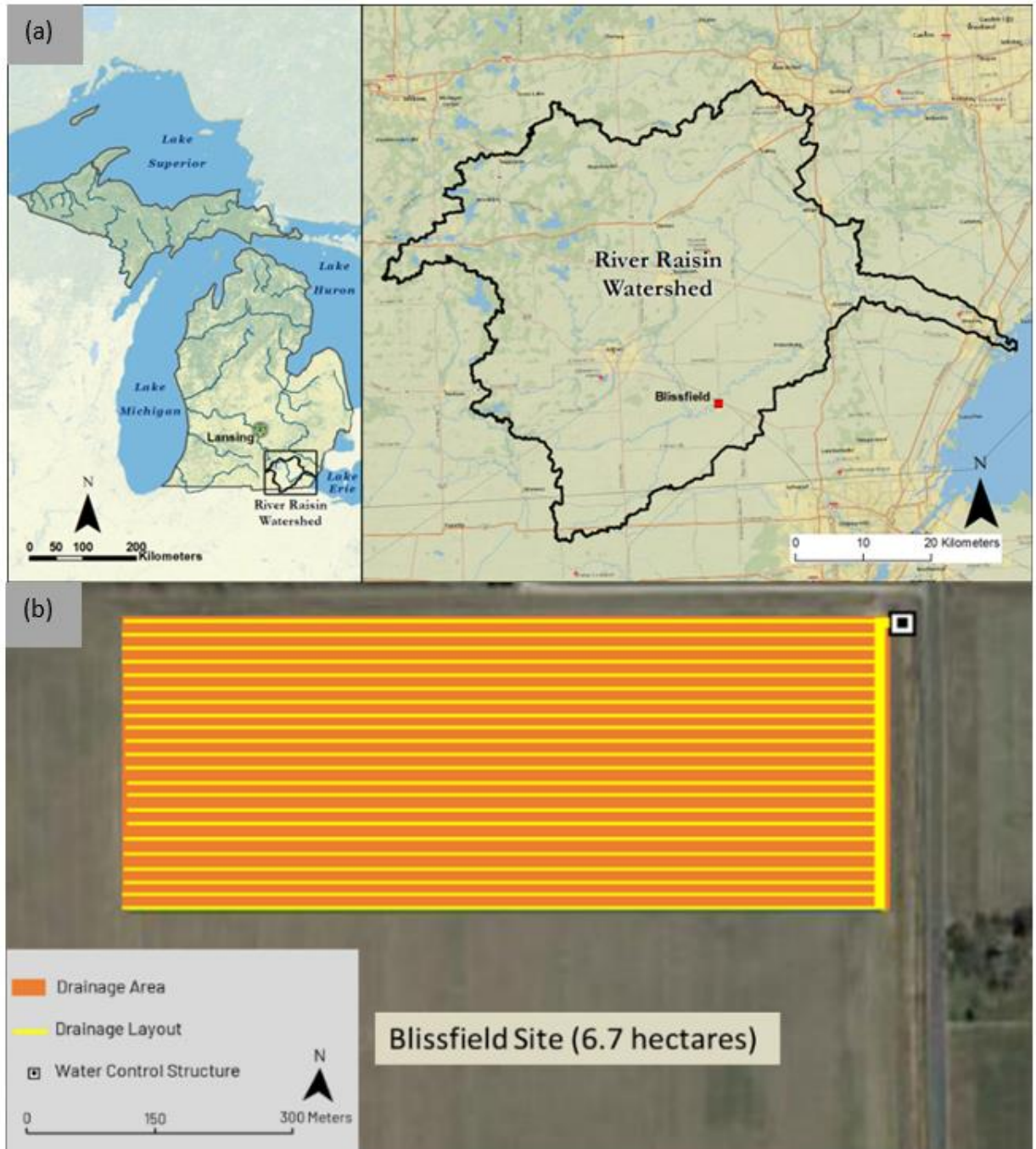


Figure 4.1. (a) geographic location of the Blissfield site. This site is part of the River Raisin watershed which directly discharges into the western basin of Lake Erie at Monroe Harbor (b) drainage layout of the study site [From Shokrana et al. (2022). Used with permission.]

**Table 4.1. Annual management practices adopted at the Blissfield site [From Shokrana et al. (2022). Used with permission.]**

Year	Date	Management practices	Comments
2018	18-May	Soybean planting	150,000-175,000 seeds/ac
	15-October	Soybean harvest	
2019 <sup>[a]</sup>	09-April	Inorganic fertilizer application	Inorganic fertilizer applied at 20.2 kg/ha nitrogen, 22.5 kg/ha phosphorus, 111.8 kg/ha potassium
	24-October	Winter wheat planting	
2020 <sup>[b]</sup>	07-May	Winter wheat termination	Planting density was 70lb/ac. Wheat planted with a grain drill
	12-May	No-till corn planting	
	12-May	Inorganic fertilizer application	
	18-June	Inorganic fertilizer application	
	17-October	Corn harvest	
	19-October	Cereal rye planting	
	2021 <sup>[c]</sup>	15-May	
2021 <sup>[c]</sup>	21-May	Soybean planting	150,000 seeds/ac
	20-October	Soybean harvest	
2022	03-June	Soybean planting	190,000 seeds/ac

<sup>[a]</sup>No crop was planted in 2019 due to wet spring. Inorganic fertilizers include nitrogen, phosphorus, and potassium fertilizers.

<sup>[b]</sup>Urea ammonium nitrate was applied on 12-May 2020 and anhydrous ammonia was applied on 18-June 2020. The planting density of cereal rye is unknown. In the model, we used the same planting density as winter wheat to represent cereal rye. P fertilizer was applied in the form of P<sub>2</sub>O<sub>5</sub>.

<sup>[c]</sup>The fall 2021 season was very wet, so no cover crop was planted during that time.

### 4.3.3 Data collection

Soil water characteristic information is one of the most important inputs for the simulation of hydrology in RZWQM2. Overall, the soil profile is delineated into five layers. We used the HYPROP2 instrument (Meter Group, Inc.) to automatically determine the output parameters of the soil water characteristics curve (SWCC) for the topsoil layer (Shokrana & Ghane, 2020). However, it was challenging to collect undisturbed soil samples from deeper layers using the soil sampling tools provided with HYPROP. Therefore, we acquired the soil physical and chemical properties data from the GSSURGO database for the deeper soil layers (table 4.2) (Soil Survey Staff, Natural Resources Conservation Service, n.d.). The bulk densities ( $\rho_b$ ) of the first three layers were measured in the lab by the scoop method (Peck, 2015) and the last two layers were collected from the GSSURGO database. The specific density of soil was assumed to be a constant value of  $2.65 \text{ g/cm}^3$  (Jury & Horton, 2004). In addition, soil texture data were analyzed by the Bray-P method in the soil, plant, and nutrients (SPNL) lab at Michigan State University. All the SWCC parameters such as residual water content, saturated water content, field capacity, permanent wilting point, and initial saturated hydraulic conductivity were acquired from the GSSURGO database.

**Table 4.2. Input soil hydrologic properties data for Ziegenfuss clay loam soil [From Shokrana et al. (2022). Used with permission.]**

Depth of soil layer <sup>[a]</sup> (cm)	Bulk density <sup>[b]</sup> , $\rho_b$ (g/cm <sup>3</sup> )	Porosity (cm <sup>3</sup> /cm <sup>3</sup> )	Sand (%)	Silt (%)	Clay (%)	Residual water content, $\Theta_r$ (cm <sup>3</sup> /cm <sup>3</sup> )	Saturated water content, $\Theta_s$ (cm <sup>3</sup> /cm <sup>3</sup> )	Field capacity, $\Theta_{fc}$ (cm <sup>3</sup> /cm <sup>3</sup> )	Permanent wilting point, $\Theta_{pwp}$ (cm <sup>3</sup> /cm <sup>3</sup> )
0-23	1.37	0.483	27.2	35.8	37.0	0.113	0.390	0.282	0.195
23-76	1.46	0.449	27.2	37.3	35.5	0.110	0.360	0.267	0.195
76-102	1.50	0.434	25.7	40.8	33.5	0.108	0.350	0.282	0.211
102-170	1.72	0.351	35.0	33.0	32.0	0.104	0.320	0.268	0.208
170-205	1.90	0.283	34.0	37.0	29.0	0.098	0.240	0.195	0.157

<sup>[a]</sup> The depth to the impermeable layer is 170 cm.

<sup>[b]</sup> The  $\rho_b$  of the first three layers were measured in our lab and the last two layers were collected from the GSSURGO database. The depth to the impermeable layer is 170 cm.

We started monitoring at the on-farm site on October 1<sup>st</sup>, 2018 and continued until June 30<sup>th</sup>, 2022 (i.e., the study duration is 3 years and 9 months). The hourly weather data used to run the RZWQM2-P are precipitation, air temperature, solar radiation, wind speed, and relative humidity. All these data were collected from our on-site ATMOS-41 weather station (Meter Group, Inc.). Missing weather data due to equipment malfunctioning were replaced from the Enviroweather database (<https://enviroweather.msu.edu/>). In case both ATMOS-41 and Enviroweather databases failed to provide data, those were collected from the National Oceanic and Atmospheric Administration (NOAA) database (<https://www.ncei.noaa.gov/>). We used the NOAA station at Lenawee County Airport (Adrian, MI, USA) to collect weather data.

A control structure was installed to regulate the water table inside the field using stop logs or weir boards (Gilliam et al., 1979). HYDROS-21 sensors were placed both upstream and downstream of the control structure to collect water level data. Daily water samples were collected year-round in 1000-mL plastic containers using a Teledyne ISCO autosampler based on a daily composite sampling strategy with six aliquots per day (Dialameh & Ghane, 2022). The water samples were retrieved and brought back to the lab on a weekly basis. Afterward, the

samples were analyzed for DRP within 24 hours of retrieval. The samples were first filtered with a 0.45- $\mu\text{m}$  filter before analyzing for DRP. The TP analysis was performed on unfiltered water samples within 7 days of retrieval, using the alkaline persulfate digestion procedure (Patton & Kryskalla, 2003). We used the Gallery Discrete Analyzer (Thermo Fisher Scientific) which uses the colorimetric technique for analyzing samples.

Estimation of subsurface drainage discharge is one of the essential parts of this study because the nutrient load is a function of the drainage discharge. We used our own calibrated V-notch weir discharge equation as the primary method for estimating drainage discharge (Shokrana & Ghane., 2021). This equation is used until the head of water reaches the maximum height of the V-notch (i.e., 22.1 cm). Once the head of water goes above the maximum height of the V-notch, an area-velocity sensor (TIENET 350 area velocity sensor) was used to estimate the drainage discharge.

#### 4.3.4 Initialization of P pools

Once the SWCC parameters and drainage discharge data were collected, the next step was to initialize the P pools before starting the model simulations. The soil samples were collected from the Blissfield site and were sent to the Soil and Plant Nutrient Laboratory (SPNL) at Michigan State University for nutrient analysis. The soil samples were collected up to 90 cm from the surface. The results from the laboratory provided an initial estimate of the amount of Bray-P in the top 90 cm of the soil. Afterward, the initial amount of labile P pool for the first two layers (0-23 cm and 23-76 cm) were estimated from the total amount of Bray-P present in the top 30 cm of the soil. For the third (76-102 cm) and fourth layer (102-170 cm), we assumed that the concentration of Bray-P was 1 ppm and 0.25 ppm, respectively. We also assumed that the

initial amount of labile P pool in a specific layer is the same as the Bray-P amount in that layer. Since we did not have any soil test data for the deepest soil layer (170 cm - 205 cm), the initial amount of labile P was assumed as zero for that layer. This value is important in estimating the active P amount in a soil layer. The stable inorganic P pool is assumed to be 4 times the active P amount in a soil layer (Jones et al., 1984). RZWQM2-P assumes that 90% of the crop residue remains on the surface or first layer, and the remaining 10% goes to the second layer. The fresh organic P pool in a soil layer was assumed to be 0.03% of the crop residue amount in a soil layer (Noack et al., 2012). A detailed description of the method used to calculate different P pools can be found in (Sadhukhan & Qi, 2018). The input data provided for the initialization of P pools are shown in table 4.3.

**Table 4.3. Input data for P pools to initiate the P model [From Shokrana et al. (2022). Used with permission.]**

Depth of soil layer (cm)	Soil organic matter (%)	Soil organic carbon (%)	Amount of Carbon (kg/ha)	Initial labile P (kg/ha) <sup>[a]</sup>	P sorption coefficient <sup>[b]</sup>	Active P amount (kg/ha)	Crop residue amount (kg/ha) <sup>[c]</sup>	Initial stable inorganic P pool (kg/ha)	Initial stable organic P (kg/ha)	Fresh organic P (kg/ha)
0-23	3.00	1.74	54827	65.1	0.36	114.0	4500	455.8	548	1.35
23-76	0.75	0.44	48268	19.8	0.36	34.5	500	138.0	483	0.15
76-102	0.50	0.29	44370	3.9	0.36	7.0	0	28.3	444	0
102-170	0.50	0.29	84796	2.9	0.36	5.0	0	21.2	848	0
170-205	0.43	0.25	97141	0	0.36	0	0	0	971	0

<sup>[a]</sup>The initial labile P in a specific layer was assumed to be the same as Bray-P for that layer. The total amount of Bray-P for the top 30-cm soil layer was 84.94 kg/ha. The initial labile P amounts for the third and fourth layers (i.e., 76-102 cm) were calculated from the Bray-P concentrations for those layers based on field measurements. The initial labile P for the last layer (i.e., 176-205 cm) was assumed to be zero.

<sup>[b]</sup>This P sorption coefficient is a unitless parameter that was estimated from the (Williams et al., 2008).

<sup>[c]</sup>We assumed that 90% of the crop residue remains on the surface or the first layer and the remaining 10% remain on the second layer. Since corn was planted in the year before the warm-up period of simulation, we assumed the corn residue amount as 5000 kg/ha.

#### 4.3.5 Model calibration and validation

Our two-year calibration period started on October 1, 2018 and ended on September 30, 2020. The validation period was one year and nine months, ranging from October 1, 2020 until

June 30, 2022. While choosing the calibration period, we ensured that it covered both wet and dry years of the study period (Skaggs et al., 2012). The annual precipitation for the water year (i.e., water years started from October 1 of the current year and ended on September 30 of the following year) 2019, 2020, and 2021 were 112.65, 73.83, and 85.71 cm, respectively. The calibration was performed in the following order: soil water dynamics, surface runoff, drainage discharge, evapotranspiration, plant water uptake parameters, and then recalibrated in the same order (Ma et al., 2012). Once we were satisfied with the hydrology calibration, we started calibrating DRP and TP loss through surface runoff and drainage discharge.

#### 4.3.5.1 Model performance statistics

We used the Nash-Sutcliffe efficiency (NSE) and percent bias (PBIAS) values to evaluate our model performance. Each model component was evaluated and categorized as very good, good, satisfactory, and unsatisfactory (Moriassi et al., 2007, 2015). For hydrology calibration and validation, the model performance was considered “very good” when  $NSE > 0.75$  and  $PBIAS < \pm 10\%$ , “good” when  $0.65 < NSE \leq 0.75$  and  $\pm 10\% \leq PBIAS < \pm 15\%$ , and “satisfactory” when  $0.50 < NSE \leq 0.65$  and  $\pm 15\% \leq PBIAS < \pm 25\%$  (Moriassi et al., 2007). For DRP and TP simulation, the model performance was considered “very good” when  $NSE > 0.65$  and  $PBIAS < \pm 15\%$ , “good” when  $0.50 < NSE \leq 0.65$  and  $\pm 15\% \leq PBIAS < \pm 20\%$ , and “satisfactory” when  $0.35 < NSE \leq 0.50$  and  $\pm 20\% \leq PBIAS < \pm 30\%$  (Moriassi et al., 2015). All the recommended model performance statistics mentioned above are of monthly time step.

#### 4.3.5.2 Soil water dynamics module

The two most important parameters that we calibrated for the soil water balance module were the bubbling pressure and the pore size distribution index. These two parameters were

initially set to the values (i.e., 25.89 cm for bubbling pressure and 0.194 for the pore-size distribution index) mentioned in (Ma et al., 2011) and later adjusted to better predict the water balance of the field data. The greater the bubbling pressure, the greater the affinity of water to the soil. The bubbling pressure was more sensitive to soil water content than the pore size distribution index. We observed an increase in the soil water content when the bubbling pressure was increased. In contrast, the soil water content was reduced by increasing the pore size distribution index.

#### 4.3.5.3 Surface runoff module

The surface runoff was sensitive to the saturated hydraulic conductivity ( $K_{sat}$ ) at the surface layer, the total macroporosity, the width of cracks, and the average radius of cylindrical pores. In our field site, a buffer strip is located on a mound between the field and the drainage ditch. This high elevation of the buffer strips prevents any surface runoff from reaching the drainage ditch. In addition, we installed time-lapse cameras at different locations of the field in late 2019 to observe potential surface runoff. Since surface runoff was not observed, we tried to keep the surface runoff to a minimum during the model calibration. Additionally, observation wells were installed midway between the laterals for water table monitoring. We observed a decrease in the simulated surface runoff volume with increased  $K_{sat}$  at the surface layer. The bubbling pressure and pore size distribution index parameters played an important role in surface runoff calibration. The macroporosity parameters were not as sensitive to the surface runoff simulation as the  $K_{sat}$  at the surface layer. Additionally, we calibrated the crust conductivity for surface runoff simulation, but the simulated surface runoff appeared to be insensitive to this parameter. The calibrated macropore parameters are shown in table 4.4.

**Table 4.4. Calibrated values of macroporosity parameters [From Shokrana et al. (2022). Used with permission.]**

Depth of soil layer (cm)	Total macroporosity (cm <sup>3</sup> /cm <sup>3</sup> )	Fraction dead-end macropores	Average radius of cylindrical pores (cm)	Width of cracks (cm)	Length of cracks (cm)	Depth of cracks (cm)
0-23	0.05	0.50	0.1	0	0	0
23-76	0.05	0.50	0	0.5	10.0	10.0
76-102	0.05	0.50	0	0.5	10.0	10.0
102-170	0.05	0.50	0	0.5	10.0	10.0
170-205	0.05	0.50	0	0.5	10.0	10.0

#### 4.3.5.4 Subsurface drainage discharge module

Subsurface drainage discharge was mostly influenced by the air entry pressure or bubbling pressure, pore size distribution index, Ksat, and lateral Ksat. Drainage discharge was more sensitive to the air entry pressure compared to the pore-size distribution index. We observed a decrease in drainage discharge with an increase in air entry pressure whereas it did not show any specific increasing or decreasing trend with the increase of pore size distribution index. The drainage discharge was influenced by an interaction effect of air entry pressure and pore size distribution index. Drainage discharge showed an increasing trend with an increase in the Ksat. The magnitudes of Lateral Ksat were adjusted as 2 multiplied by the vertical Ksat (Qi et al., 2015; Sadhukhan et al., 2019a; Thorp et al., 2009) and they also had a greater influence on the drainage discharge calibration. The calibrated values of the sensitive drainage discharge parameters are shown in table 4.5.

**Table 4.5. Calibrated soil hydraulic parameters and their values. [From Shokrana et al. (2022). Used with permission.]**

Depth of soil layer (cm)	Soil bubbling pressure (cm)	Pore size distribution index	Saturated hydraulic conductivity ( $K_{sat}$ ) (cm/h)	Lateral saturated hydraulic conductivity ( $LK_{sat}$ ) (cm/h)
0-23	-25.0	0.190	1.25	2.50
23-76	-19.0	0.162	1.05	2.10
76-102	-30.5	0.138	0.97	1.94
102-170	-34.0	0.120	0.75	1.50
170-205	-18.2	0.130	0.01	0.02

#### 4.3.5.5 Evapotranspiration module

Evapotranspiration (ET) was greatly influenced by the albedo parameters. Initial albedo values were adopted from Sadhukhan et al. (2019a) and later those values were adjusted to match the historical monthly ET values observed in Michigan and the observed drainage discharge. RZWQM2 has four albedo parameters, and the calibrated values are shown in table 4.6. The ET was also sensitive to the surface soil resistance parameter. An increase in this parameter reduced ET and increased drainage discharge. Additionally, the minimum leaf stomatal resistance parameter had an important influence on the ET module. Decreasing the leaf stomatal resistance increased ET, especially the transpiration component of the ET module.

**Table 4.6. Other calibrated hydrologic, P loss, soil erosion, and plant parameters and their values. Default values are recorded from Sadhukhan et al. (2019a). [From Shokrana et al. (2022). Used with permission.]**

Parameters	Calibrated Value	Default Value (Range)
<b>Hydraulic parameters</b>		
Crust conductivity (cm/h)	0.35	0.01 (0.01-20)
Water table leakage rate (cm/h)	$1 \times 10^{-5}$	-
<b>ET parameters</b>		
Albedo of dry soil (unitless)	0.35	0.20 (0.01-0.90)
Albedo of wet soil (unitless)	0.63	0.30 (0.02-0.90)
Albedo of crop at maturity (unitless)	0.15	0.70 (0.01-0.90)
Albedo of fresh residue (unitless)	0.75	0.22 (0.01-0.90)
Surface soil resistance for the S-W PET (s/m)	285	37 (0-500)
<b>P parameters</b>		
Replenishment rate coefficient (g/(m <sup>2</sup> d))	0.75	0.20 (0.00-1.00)
Detachability coefficient (g/(J mm))	0.95	0.40 (0.00-1.00)
Filtration coefficient (1/m)	0.002	0 (0.000-1.000)
Extraction coefficient (unitless)	0.35	1.00 (0.10-1.00)
Initial DRP in groundwater (GW) reservoir (kg/ha)	10	20
Initial PP in groundwater (GW) reservoir (kg/ha)	18	20
<b>Soil erosion parameters</b>		
Management and practice factor (PFACT)	0.85	0.50 (0.01-1.00)
Contouring factor (CFACT)	0.85	0.50 (0.01-1.00)
Manning's n (NFACT)	0.02	0.01 (0.01-0.40)
<b>Plant parameters</b>		
<b>P uptake distribution parameter (unitless)</b>		
Corn	10	10 (1-15)
Soybean	10	10 (1-15)
Winter wheat	10	10 (1-15)
<b>Minimum leaf stomatal resistance (s/m)</b>		
Corn	200	-
Soybean	130	-
Winter wheat	100	-

<sup>[a]</sup>Ranges are collected from Sadhukhan et al. (2019a) and RZWQM2 manual

#### 4.3.5.6 P transport module

The most important parameters for DRP calibration were the surface S-W resistance, macropore parameters, and the initial level of DRP in GW (groundwater) reservoir. Reducing the S-W resistance parameter improved model performance statistics by increasing the model

predictions during high flow events. Slightly adjusting the bubbling pressure and pore size distribution index for the deeper soil layers improved the DRP loss prediction of the model. DRP calibration was most sensitive to the initial DRP in the GW reservoir. Reducing this value increased DRP load during the high flow events. The DRP loss simulation of the model was also sensitive to the average radius of cylindrical macropores and the width of the cracks. Both parameters were positively correlated to the DRP load.

Macropore parameters had an important effect on the calibration for particulate phosphorus (PP). The PP loss through surface runoff was calibrated by adjusting the soil loss parameters (e.g., soil erodibility factor, cover and management factor, support practice factor, and Manning's  $n$ ). Decreasing soil filtration coefficients had a very small increase in PP load through drainage discharge. On the contrary, increasing the soil replenishment rate coefficient and soil detachability coefficient improved the model performance statistics for PP load through drainage discharge.

It is important to note that we evaluated the P model's performance by comparing simulated DRP and TP loss with the observed data. RZWQM2-P does not directly predict TP loss, rather it predicts DRP and PP loss separately. Since we did not analyze for PP in the lab, we used TP instead of PP to evaluate the P model's performance. Simulated TP loss was estimated by adding PP loss to the DRP loss. Theoretically, TP is a combination of DRP, DUP (dissolved unreactive phosphorus), and PP. We assumed the DUP to be zero while estimating simulated TP.

## 4.4 Results

### 4.4.1 Prediction of Subsurface drainage discharge

The performance of the model during the calibration period was “good” in predicting daily drainage discharge (Figure 4.2). The NSE and PBIAS performance statistics were calculated based on the daily observed and simulated data. The NSE value was 0.66 (i.e., good) and the PBIAS was -7.16 (i.e., very good) (table 4.7) (Moriassi et al., 2007). The negative PBIAS value indicated that the model had a slight overestimation bias. Based on individual events, the model generally underpredicted the drainage discharge for the calibration period, but there were two events in August 2019 and September 2019 that overpredicted the drainage discharge. The overprediction of these two flow events caused the overall performance of the model to have an overestimation of drainage discharge for the calibration period.

The model did a “very good” job (figure 4.3) in predicting the drainage discharge during the validation period. The NSE and PBIAS values for the validation period were 0.76 (i.e., very good) and 23.57 (i.e., satisfactory) (table 4.7). The positive PBIAS value indicated a high underestimation bias of the model. This means that the drainage discharge was generally underestimated. A scatterplot of the drainage discharge for calibration and validation period is in supplementary figure S3.

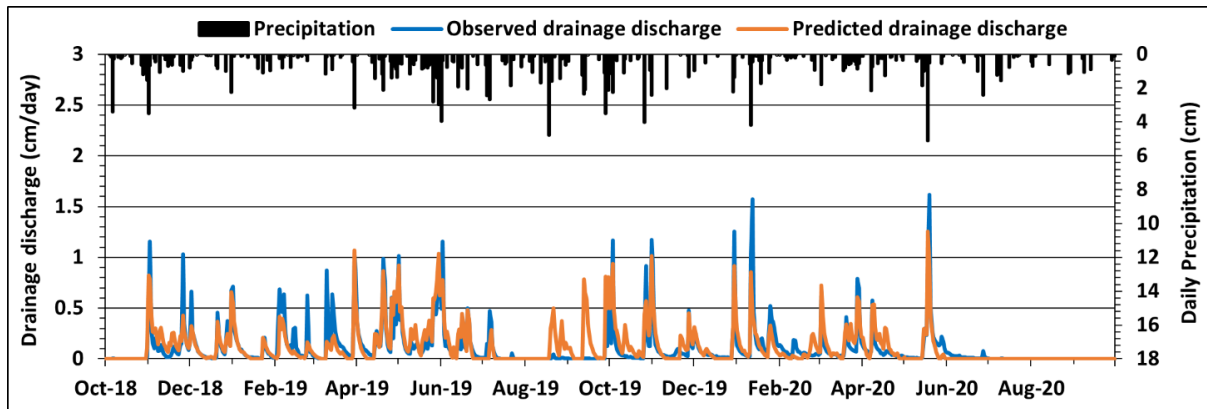


Figure 4.2. Comparison between observed and simulated drainage discharge during the calibration period (October 1, 2018 – September 30, 2020)

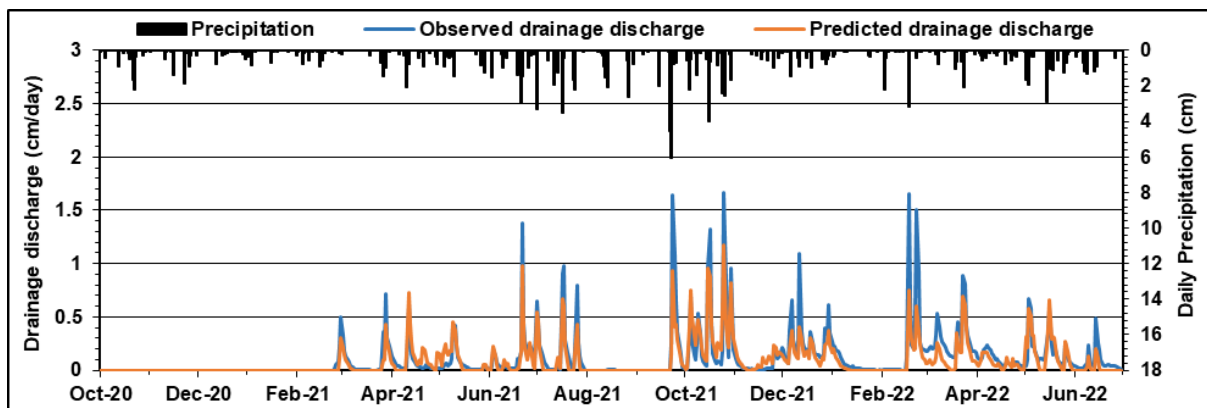


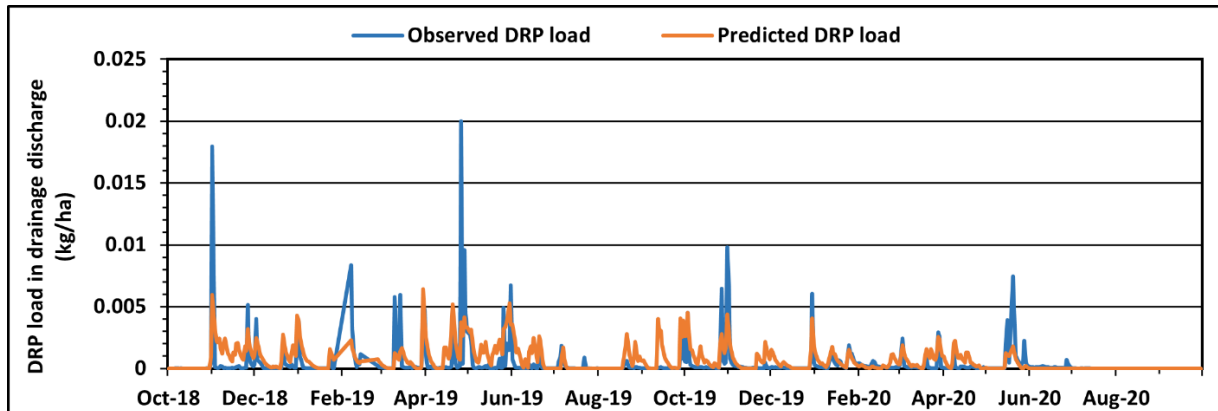
Figure 4.3. Comparison between observed and simulated drainage discharge during the validation period (October 1, 2020 – June 30, 2022) [From Shokrana et al. (2022). Used with permission.]

#### 4.4.2 Prediction of DRP load

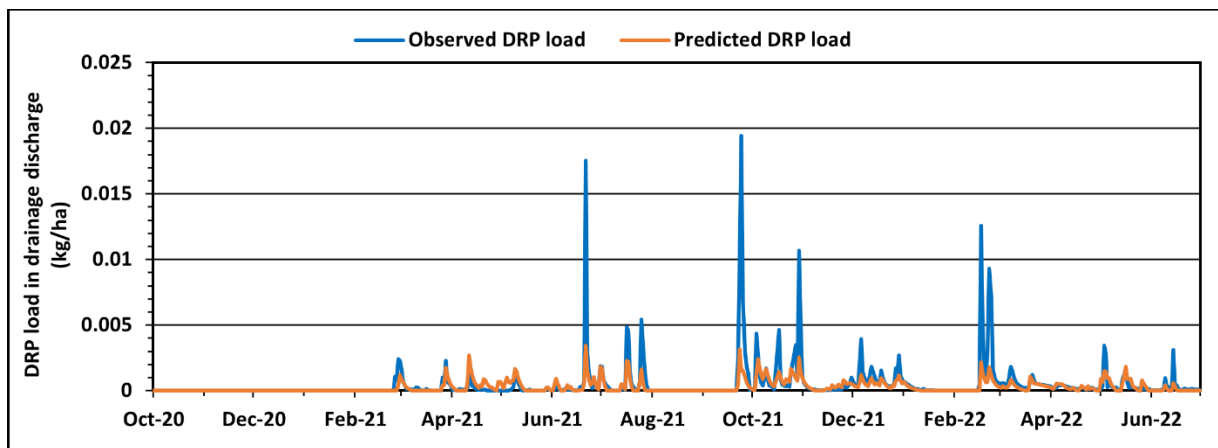
The model was unable to satisfactorily predict the DRP loss through drainage discharge (figure 4.4). The model performance statistics revealed that the NSE and PBIAS values for the calibration period based on daily data were 0.31 and -61.50, respectively (

Table 4.7) (Moriasi et al., 2015). The NSE value indicated an “unsatisfactory” performance of the model simulation. The negative PBIAS value indicated an “unsatisfactory” overestimation bias of the simulated DRP load. For the validation period, the model performance was also

“unsatisfactory” with an NSE value of 0.32 and a PBIAS value of 43.68 (Figure 4.5). Also, the model showed an underestimation bias for most of the large flow events during the validation period.



**Figure 4.4. Comparison between observed and simulated DRP loss through drainage discharge during the calibration period (October 1, 2018 – September 30, 2020) [From Shokrana et al. (2022). Used with permission.]**



**Figure 4.5. Comparison between observed and simulated DRP loss through drainage discharge during the validation period (October 1, 2020 – June 30, 2022) [From Shokrana et al. (2022). Used with permission.]**

#### 4.4.3 Prediction of DRP load

The model performance was “satisfactory” in simulating TP loss through drainage discharge (figure 4.6). The NSE value based on daily data (table 4.7) was 0.46 (i.e., satisfactory performance) and PBIAS was -32.41 (i.e., unsatisfactory performance with a small overestimation

bias) for the calibration period (Moriassi et al., 2015). Compared to the DRP simulation, the model performance was better in predicting TP loss. During the validation period, the NSE was 0.40 which meant a “satisfactory” performance of the simulation. The PBIAS was 42.90 which meant an “unsatisfactory” performance with an underestimation bias (figure 4.7).

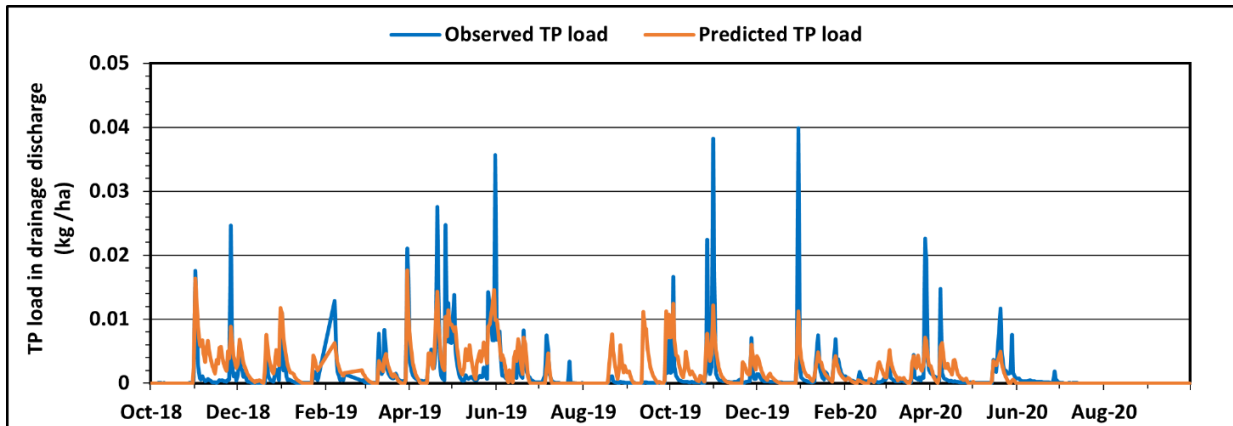


Figure 4.6. Comparison between observed and simulated TP loss through drainage discharge during the calibration period (October 1, 2018 – September 30, 2020) [From Shokrana et al. (2022). Used with permission.]

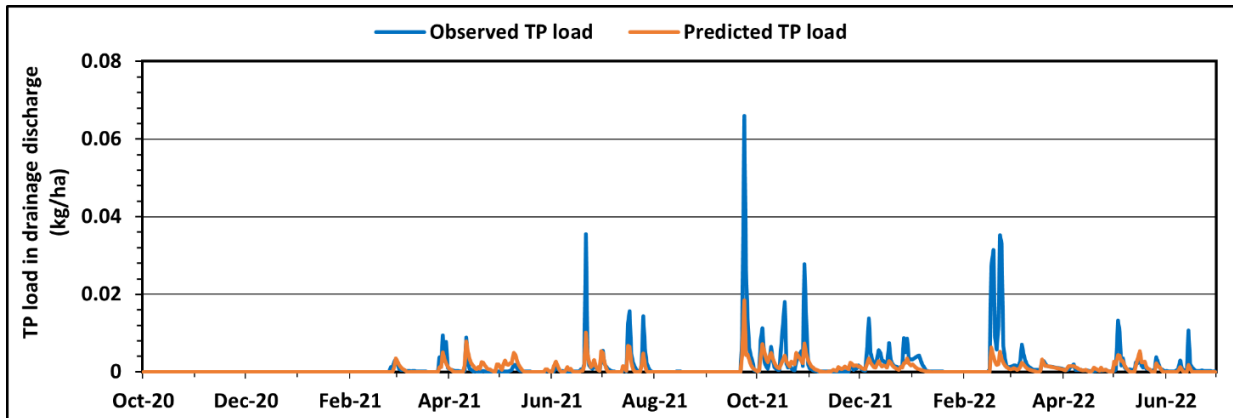


Figure 4.7. Comparison between observed and simulated TP loss through drainage discharge during the validation period (October 1, 2020 – June 30, 2022) [From Shokrana et al. (2022). Used with permission.]

**Table 4.7. Model performance statistics for drainage discharge, DRP load, and TP load during the calibration and validation period [From Shokrana et al. (2022). Used with permission.]**

	Subsurface drainage discharge		DRP load		TP load	
	NSE	PBIAS	NSE	PBIAS	NSE	PBIAS
<b>Calibration period (October 1, 2018 – September 30, 2020)</b>	0.66	-7.2	0.31	-61.5	0.46	-32.4
<b>Validation period (October 1, 2020 – June 30, 2022)</b>	0.76	23.6	0.32	43.7	0.39	42.9

## 4.5 Discussions

### 4.5.1 Underperformance of the model Prediction

Our observed data from the field experiment showed that all the P was transported through subsurface drainage discharge. This was because of the relatively flat slope of the field and the presence of a buffer strip on a mound that prevented any surface runoff to reach the drainage ditch. It is important to note that although there was no surface runoff, there were instances when a high water table was present in the field and sometimes surface ponding was observed. A combination of reasons explains the unsatisfactory performance of the P model predictions. These reasons are: (i) the insensitivity of the model to fertilizer applications and (ii) the use of high-resolution daily data as model input.

First, the unsatisfactory performance of the P model can be explained by the insensitivity of the model to fertilizer application. The farmer applied P fertilizer in the field in April 2019 (solid diammonium phosphate, DAP fertilizer) and May 2020 (liquid fertilizer with sulfur and zinc) at an application rate of 22.5 and 9.5 kg/ha, respectively. Theoretically, more P fertilizer application should result in more P loss through subsurface drainage discharge. The observed DRP loss from figure 4.4 follows this trend. The simulated DRP loss should also be higher for the April 2019

fertilization event than that of May 2020. A detailed description of how the RZWQM2-P model estimates loss of P through drainage discharge after fertilizer application may be helpful to understand the underperformance of the model in transporting P load to drainage discharge.

Once the fertilizer is applied in the field, the RZWQM2-P model immediately divides the applied fertilizer P between two surface fertilizer pools: (i) available fertilizer P pool and (ii) residual fertilizer P pool. The majority (75%) of the applied fertilizer P is added to the available fertilizer pool and the rest (25%) is added to the residual fertilizer pool. When the first rainfall occurs, all the P in the available fertilizer pool is released. For the second rainfall, 40% of the P is released from the residual fertilizer pool. From the third and onwards rainfall, 7.5% of the P from the residual fertilizer pool is released until all the P in that pool is depleted. We increased the P fertilizer application rate 15-fold (10 kg-P/ha to 150 kg-P/ha) to check for the model's sensitivity to P fertilizer application on May 13, 2020. We found that all the P were lost through surface runoff and P loss through drainage discharge did not change. The time-lapse images (supplementary figure S1) showed the occurrence of ponding conditions near the edge of the field on May 18 - 20, 2020, caused by a rainfall event that started on the same day.

Apart from the time-lapse images, we also had observation wells installed in the field and the water-level data validated the presence of very high water table on that day. We predicted that the presence of surface ponding during the May 2020 event after the P fertilization had prevented the P to be lost by drainage discharge. Therefore, the P model needs to be further modified to better simulate the partitioning of fertilizer P into different P pools, especially under ponded conditions. The partitioning of the P model can be experimentally studied in the field by collecting soil samples at different depths immediately before fertilization and after fertilization

followed by the first precipitation event. The Bray-P concentration present in different soil layers before and after fertilization would provide an understanding on the effects of fertilizer application on P partitioning. This way we can estimate the percentage of labile P present in each soil layer after each precipitation event. If several replicates showed similar percentage of labile P present in the soil layers, these percentages can be updated in the source code of the P module to better represent the P partitioning processes.

Second, the RZWQM2-P model has been evaluated only twice by Sadhukhan et al. (2019a) and Sadhukhan et al. (2019b), where fertilization practice was the only difference between the two studies. In Sadhukhan et al. (2019a), the authors evaluated the model based on flow events over four years. They aggregated their collected data into 19 different flow periods and used the first 12 of those as calibration period and the last 9 as validation period. Aggregated flow periods captured from 16 days to several months of flow and P load data, thereby dampening the visibility of rapid changes in P concentration (Dialameh & Ghane, 2022). Our study differed from Sadhukhan et al. (2019a) in the sense that we did not aggregate our data rather we used daily high-resolution observed discharge and load data to compare with the simulation. It is more difficult to obtain high NSE and PBIAS values with the daily discharge and load data compared to those aggregated over several days or months. This could be another reason for the unsatisfactory performance of the P model based on the model performance statistics.

#### 4.5.2 RZWQM2-P research need

Based on the discussion above, the P model is insensitive to fertilizer application and its inability to simulate P loss through subsurface drainage discharge under ponded situations need to be further investigated. We recommend improving the partitioning of fertilizer P into different

P pools to better represent the fertilizer P loss through drainage discharge after large rainfall events. We also recommend that the macropore flow simulation of the P model needs to be improved as the P model was not very sensitive to the macropore parameters. In RZWQM2-P, DRP is transported from the dissolved labile P in soil and leached down from topsoil to deeper soil layers. Afterward, it gets mixed with groundwater reservoir, and then leached out through subsurface drains. The same process is assumed for macropore DRP except that macropore DRP can directly enter the groundwater reservoir without being adsorbed by the soil matrix. This is a very slow process and may result in some underprediction of the P loss. On the other hand, the other available field-scale P loss model, DRAINMOD-P, assumes that DRP lost through macropores directly enters the subsurface drains. This method may significantly overestimate DRP loss from the macropores into the subsurface drains as only the macropores right above the subsurface drain may enter the pipe. For areas other than the macropores, water and nutrients will hit the groundwater reservoir rather than the pipe. Future P model development should focus on a strategy somewhere in the middle between these two methods.

The current guidelines (Moriasi et al., 2007, 2015) to evaluate the performance of P models are mostly based on watershed-scale (e.g., SWAT, HSPF, etc.) and field-scale models (ICECREAM-DB, DRAINMOD-P, RZWQM2-P, etc.). Those guidelines are based on decades-old publications when no reliable field-scale P model was available. Those performance statistics are the same for both N and P, but the P transport dynamics are more complex than the N transport dynamics. Therefore, there is a need to further modify those statistics for P alone.

#### **4.6 Conclusions**

RZWQM2-P was used in this study to assess the model's performance in simulating P loss from a subsurface-drained field. The model performed satisfactorily in simulating subsurface drainage discharge and total phosphorus (TP) load but underperformed while simulating dissolved reactive phosphorus (DRP) load. Since the model was insensitive to the fertilizer inputs, we predicted that the model needs improvement in partitioning the fertilizer P into different P pools, especially under ponded conditions. These ponding situations coupled with inefficient partitioning of fertilizer P into different P pools may have limited the model's ability to simulate P loss through subsurface drains. Additionally, previous studies used aggregated subsurface drainage discharge data which possibly did not represent the rapid fluctuation and variation of P concentration in drainage discharge. Using high-resolution daily drainage discharge and load data is a better strategy to capture the dynamic nature of P transport in a subsurface-drained field. This is the first study that used daily data to validate the RZWQM2-P model. Further testing of the P model is necessary under different climates, soil, crop varieties, and management practices.

## REFERENCES

- Ahmed, I., Rudra, R., McKague, K., Gharabaghi, B., & Ogilvie, J. (2007). Evaluation of the Root Zone Water Quality Model (RZWQM) for Southern Ontario: Part II. Simulating Long-Term Effects of Nitrogen Management Practices on Crop Yield and Subsurface Drainage Water Quality. *WATER QUALITY RESEARCH JOURNAL OF CANADA*, 42(3), 219–230. <https://doi.org/10.2166/wqrj.2007.025>
- Ahuja, L., Rojas, K. W., & Hanson, J. D. (2000). *Root zone water quality model: modelling management effects on water quality and crop production*. Water Resources Publication.
- Askar, M. H., Youssef, M. A., Hesterberg, D. L., King, K. W., Amoozegar, A., Skaggs, R. W., Chescheir, G. M., & Ghane, E. (2021). DRAINMOD-P: A Model for Simulating Phosphorus Dynamics and Transport in Drained Agricultural Lands: II. Model Testing. *Transactions of the ASABE*, 64(6), 1849–1866.
- Baker, J. L., Campbell, K. L., Johnson, H. P., & Hanway, J. J. (1975). Nitrate, phosphorus, and sulfate in subsurface drainage water. *Journal of Environmental Quality*, 4(3), 406–412. <https://doi.org/10.2134/jeq1975.00472425000400030027x> WE - Science Citation Index Expanded (SCI-EXPANDED)
- Bengston, R. L., Carter, C. E., Fous, J. L., Southwick, L. M., & Willis, G. H. (1995). Agricultural drainage and water-quality in Mississippi delta. *JOURNAL OF IRRIGATION AND DRAINAGE ENGINEERING-ASCE*, 121(National Irrigation and Drainage Conference), 292–295. [https://doi.org/10.1061/\(ASCE\)0733-9437\(1995\)121:4\(292\)](https://doi.org/10.1061/(ASCE)0733-9437(1995)121:4(292)) WE - Conference Proceedings Citation Index - Science (CPCI-S) WE - Science Citation Index Expanded (SCI-EXPANDED)
- Bouwer, H., & Van Schilfgaarde, J. (1963). Simplified method of predicting fall of water table in drained land. *Transactions of the ASAE*, 6(4), 288–291.
- Brooks, R. H., & Corey, A. T. (1964). Hydraulic properties of porous media and their relation to drainage design. *Transactions of the ASAE*, 7(1), 26–28.
- Dialameh, B., & Ghane, E. (2022). Effect of water sampling strategies on the uncertainty of phosphorus load estimation in subsurface drainage discharge. *JOURNAL OF ENVIRONMENTAL QUALITY*, 51(3), 377–388. <https://doi.org/10.1002/jeq2.20339> WE - Science Citation Index Expanded (SCI-EXPANDED)
- Dolezal, F., Kulhavy, Z., Soukup, M., & Kodesova, R. (2001). Hydrology of tile drainage runoff. *PHYSICS AND CHEMISTRY OF THE EARTH PART B-HYDROLOGY OCEANS AND ATMOSPHERE*, 26(25th General Assembly of the European-Geophysical-Society), 623–627. [https://doi.org/10.1016/S1464-1909\(01\)00059-4](https://doi.org/10.1016/S1464-1909(01)00059-4) WE - Conference Proceedings Citation Index - Science (CPCI-S) WE - Science Citation Index Expanded (SCI-EXPANDED)

- Dubrovsky, N. M., Burow, K. R., Clark, G. M., Gronberg, J. M., Hamilton, P. A., Hitt, K. J., Mueller, D. K., Munn, M. D., Nolan, B. T., & Puckett, L. J. (2010). The quality of our Nation's waters—Nutrients in the Nation's streams and groundwater, 1992–2004. *US Geological Survey Circular, 1350(2)*, 174.
- Farahani, H. J., & DeCoursey, D. G. (2000). Potential evaporation and transpiration processes in the soil-residue-canopy system. *ROOT ZONE WATER QUALITY MODEL*, 51–80.
- Ghane, E. (2022). Choice of pipe material influences drain spacing and system cost in subsurface drainage design. *APPLIED ENGINEERING IN AGRICULTURE, In Press*.
- Ghane, E., Ranaivoson, A. Z., Feyereisen, G. W., Rosen, C. J., & Moncrief, J. F. (2016). Comparison of Contaminant Transport in Agricultural Drainage Water and Urban Stormwater Runoff. *Plos One, 11(12)*. <https://doi.org/10.1371/journal.pone.0167834>
- Gilliam, J. W., Skaggs, R. W., & Weed, S. B. (1979). *Drainage control to diminish nitrate loss from agricultural fields*. Wiley Online Library.
- Green, W. H., & Ampt, G. A. (1911). Studies on soil physics Part I - The flow of air and water through soils. *JOURNAL OF AGRICULTURAL SCIENCE, 4*, 1–24. <https://doi.org/10.1017/S0021859600001441> WE - Science Citation Index Expanded (SCI-EXPANDED)
- Hanson, J. D. (2000). Generic crop production model for the root zone water quality model. *The Root Zone Water Quality Model*. Water Resource Publishing, Highland Ranch, Colorado.
- Hooghoudt, S. B. (1940). Algemeene beschouwing van het probleem van de detailontwatering en de infiltratie door middel van parallel loopende drains, greppels, slooten en kanalen. *Versl. Landbouwk. Onderz, 46(14)*, 515–707.
- Jiang, Q. J., Qi, Z. M., Madramootoo, C. A., & Singh, A. K. (2018). Simulating hydrologic cycle and crop production in a subsurface drained and sub-irrigated field in Southern Quebec using RZWQM2. *COMPUTERS AND ELECTRONICS IN AGRICULTURE, 146*, 31–42. <https://doi.org/10.1016/j.compag.2018.01.021> WE - Science Citation Index Expanded (SCI-EXPANDED)
- Jones, C. A., Cole, C. V, Sharpley, A. N., & Williams, J. R. (1984). *A simplified soil and plant phosphorus model: I. Documentation*.
- Jury, W. A., & Horton, R. (2004). *Soil physics*. John Wiley & Sons.
- King, K. W., Williams, M. R., Macrae, M. L., Fausey, N. R., Frankenberger, J., Smith, D. R., Kleinman, P. J. A., & Brown, L. C. (2015). Phosphorus Transport in Agricultural Subsurface Drainage: A

Review. *JOURNAL OF ENVIRONMENTAL QUALITY*, 44(2), 467–485.  
<https://doi.org/10.2134/jeq2014.04.0163>

- Kleinman, P., Sharpley, A., Buda, A., McDowell, R., & Allen, A. (2011). Soil controls of phosphorus in runoff: Management barriers and opportunities. *Canadian Journal of Soil Science*, 91(3), 329–338.
- Ma, L., Ahuja, L. R., Nolan, B. T., Malone, R. W., Trout, T. J., & Qi, Z. (2012). Root zone water quality model (RZWQM2): model use, calibration, and validation. *Transactions of the ASABE*, 55(4), 1425–1446.
- Ma, L., Ahuja, L. R., Saseendran, S. A., Malone, R. W., Green, T. R., Nolan, B. T., Bartling, P. N. S., Flerchinger, G. N., Boote, K. J., & Hoogenboom, G. (2011). A Protocol for Parameterization and Calibration of RZWQM2 in Field Research. In L. R. Ahuja & L. Ma (Eds.), *METHODS OF INTRODUCING SYSTEM MODELS INTO AGRICULTURAL RESEARCH* (Vol. 2, pp. 1–64).  
<https://doi.org/10.2134/advagriscystmodel2.c1>
- Ma, L., Malone, R. W., Heilman, P., Jaynes, D. B., Ahuja, L. R., Saseendran, S. A., Kanwar, R. S., & Ascough II, J. C. (2007). RZWQM simulated effects of crop rotation, tillage, and controlled drainage on crop yield and nitrate-N loss in drain flow. *Geoderma*, 140(3), 260–271.
- Macrae, M., Jarvie, H., Brouwer, R., Gunn, G., Reid, K., Joosse, P., King, K., Kleinman, P., Smith, D., & Williams, M. (2021). One size does not fit all: Toward regional conservation practice guidance to reduce phosphorus loss risk in the Lake Erie watershed. *Journal of Environmental Quality*, 50(3), 529–546.
- Malone, R. W., Kersebaum, K. C., Kaspar, T. C., Ma, L., Jaynes, D. B., & Gillette, K. (2017). Winter rye as a cover crop reduces nitrate loss to subsurface drainage as simulated by HERMES. *AGRICULTURAL WATER MANAGEMENT*, 184, 156–169.  
<https://doi.org/10.1016/j.agwat.2017.01.016> WE - Science Citation Index Expanded (SCI-EXPANDED)
- Malone, R. W., Nolan, B. T., Ma, L., Kanwar, R. S., Pederson, C., & Heilman, P. (2014). Effects of tillage and application rate on atrazine transport to subsurface drainage: Evaluation of RZWQM using a six-year field study. *Agricultural Water Management*, 132, 10–22.
- Moriasi, D. N., Arnold, J. G., Van Liew, M. W., Bingner, R. L., Harmel, R. D., & Veith, T. L. (2007). Model evaluation guidelines for systematic quantification of accuracy in watershed simulations. *TRANSACTIONS OF THE ASABE*, 50(3), 885–900.  
<https://doi.org/10.13031/2013.23153>
- Moriasi, D. N., Gitau, M. W., Pai, N., & Daggupati, P. (2015). HYDROLOGIC AND WATER QUALITY MODELS: PERFORMANCE MEASURES AND EVALUATION CRITERIA. *TRANSACTIONS OF THE ASABE*, 58(6), 1763-1785 WE-Science Citation Index Expanded (S.

- Nielsen, D. C., Ma, L. W., Ahuja, L. R., & Hoogenboom, G. (2002). Simulating soybean water stress effects with RZWQM and CROPGRO models. *AGRONOMY JOURNAL*, *94*(6), 1234–1243. <https://doi.org/10.2134/agronj2002.1234> WE - Science Citation Index Expanded (SCI-EXPANDED)
- Noack, S. R., McLaughlin, M. J., Smernik, R. J., McBeath, T. M., & Armstrong, R. D. (2012). Crop residue phosphorus: speciation and potential bio-availability. *Plant and Soil*, *359*(1), 375–385.
- Pachepsky, Y., Timlin, D., & Rawls, W. (2003). Generalized Richards' equation to simulate water transport in unsaturated soils. *Journal of Hydrology*, *272*(1–4), 3–13.
- Patton, C. J., & Kryskalla, J. R. (2003). *Methods of analysis by the US Geological Survey National Water Quality Laboratory: evaluation of alkaline persulfate digestion as an alternative to Kjeldahl digestion for determination of total and dissolved nitrogen and phosphorus in water* (Vol. 3, Issue 4174). US Department of the Interior, US Geological Survey.
- Peck, R. T. (2015). Recommended chemical soil test procedures for the north central region. *North Central Regional Research Publication No. 221 (Revised)*.
- Pferdmenges, J., Breuer, L., Julich, S., & Kraft, P. (2020). Review of soil phosphorus routines in ecosystem models. *Environmental Modelling & Software*, *126*, 104639.
- Pierzynski, G. M., Vance, G. F., & Sims, J. T. (2005). *Soils and environmental quality*. CRC press.
- Qi, H., & Qi, Z. (2016). Simulating phosphorus loss to subsurface tile drainage flow: a review. *Environmental Reviews*, *25*(2), 150–162.
- Qi, Z. M., Singh, R., Helmers, M. J., & Zhou, X. B. (2015). Evaluating the performance of DRAINMOD using soil hydraulic parameters derived by various methods. *AGRICULTURAL WATER MANAGEMENT*, *155*, 48–52. <https://doi.org/10.1016/j.agwat.2015.03.019> WE - Science Citation Index Expanded (SCI-EXPANDED)
- Radcliffe, D. E., & Cabrera, M. L. (2006). *Modeling phosphorus in the environment*. CRC Press.
- Radcliffe, D. E., Reid, D. K., Blombäck, K., Bolster, C. H., Collick, A. S., Easton, Z. M., Francesconi, W., Fuka, D. R., Johnsson, H., & King, K. (2015). Applicability of models to predict phosphorus losses in drained fields: A review. *Journal of Environmental Quality*, *44*(2), 614–628.
- Richards, L. A. (1931). Capillary conduction of liquids through porous mediums. *PHYSICS-A JOURNAL OF GENERAL AND APPLIED PHYSICS*, *1*(1), 318–333. <https://doi.org/10.1063/1.1745010> WE - Science Citation Index Expanded (SCI-EXPANDED)

- Robinson, M., & Rycroft, D. W. (1999). The impact of drainage on streamflow. *Agricultural Drainage*, 38, 767–800.
- Ryden, J. C., Syers, J. K., & Harris, R. F. (1974). Phosphorus in runoff and streams. In *Advances in agronomy* (Vol. 25, pp. 1–45). Elsevier.
- Sadhukhan, D., & Qi, Z. (2018). *RZWQM2 Phosphorus Model (Technical Report)*.
- Sadhukhan, D., Qi, Z. M., Zhang, T. Q., Tan, C. S., & Ma, L. W. (2019b). Modeling and Mitigating Phosphorus Losses from a Tile-Drained and Manured Field Using RZWQM2-P. *JOURNAL OF ENVIRONMENTAL QUALITY*, 48(4), 995–1005. <https://doi.org/10.2134/jeq2018.12.0424>.
- Sadhukhan, D., Qi, Z., Zhang, T., Tan, C. S., Ma, L., & Andales, A. A. (2019a). Development and evaluation of a phosphorus (P) module in RZWQM2 for phosphorus management in agricultural fields. *Environmental Modelling and Software*, 113, 48–58. <https://doi.org/10.1016/j.envsoft.2018.12.007>
- Sharpley, A. N., CHAPRA, S. C., WEDEPOHL, R., SIMS, J. T., DANIEL, T. C., & REDDY, K. R. (1994). MANAGING AGRICULTURAL PHOSPHORUS FOR PROTECTION OF SURFACE WATERS - ISSUES AND OPTIONS. *JOURNAL OF ENVIRONMENTAL QUALITY*, 23(3), 437–451. <https://doi.org/10.2134/jeq1994.00472425002300030006x>
- Sharpley, A. N., McDowell, R. W., & Kleinman, P. J. A. (2001). Phosphorus loss from land to water: integrating agricultural and environmental management. *PLANT AND SOIL*, 237(2), 287–307. <https://doi.org/10.1023/A:1013335814593>.
- Shokrana, M. S. Bin, & Ghane, E. (2020). Measurement of soil water characteristic curve using HYPROP2. *METHODS*, 7. <https://doi.org/10.1016/j.mex.2020.100840>
- Shokrana, M. S. B., & Ghane, E. (2021). AN EMPIRICAL V-NOTCH WEIR EQUATION AND STANDARD PROCEDURE TO ACCURATELY ESTIMATE DRAINAGE DISCHARGE. *APPLIED ENGINEERING IN AGRICULTURE*, 37(6), 1097–1105. <https://doi.org/10.13031/aea.14617> WE - Science Citation Index Expanded (SCI-EXPANDED)
- Sims, J. T., Simard, R. R., & Joern, B. C. (1998). Phosphorus Loss in Agricultural Drainage: Historical Perspective and Current Research. *Journal of Environment Quality*, 27(2), 277. <https://doi.org/10.2134/jeq1998.00472425002700020006x>
- Skaggs, R. W., Breve, M. A., & Gilliam, J. W. (1994). HYDROLOGIC AND WATER-QUALITY IMPACTS OF AGRICULTURAL DRAINAGE. *CRITICAL REVIEWS IN ENVIRONMENTAL SCIENCE AND TECHNOLOGY*, 24(1), 1–32. <https://doi.org/10.1080/10643389409388459> WE - Science Citation Index Expanded (SCI-EXPANDED)

- Skaggs, R. W., Youssef, M. A., & Chescheir, G. M. (2012). DRAINMOD: Model use, calibration, and validation. *Transactions of the ASABE*, 55(4), 1509–1522.
- Smedema, L. K., Vlotman, W. F., & Rycroft, D. (2004). *Modern land drainage: Planning, design and management of agricultural drainage systems*. CRC Press.
- Soil Survey Staff, Natural Resources Conservation Service, U. S. D. of A. (n.d.). *Web Soil survey*. Retrieved October 5, 2022, from <https://websoilsurvey.sc.egov.usda.gov/>
- Tattari, S., Bärlund, I., Rekolainen, S., Posch, M., Siimes, K., Tuhkanen, H., & Yli-Halla, M. (2001). Modeling sediment yield and phosphorus transport in Finnish clayey soils. *Transactions of the ASAE*, 44(2), 297.
- Thorp, K. R., Jaynes, D. B., & Malone, R. W. (2008). Simulating the long-term performance of drainage water management across the Midwestern United States. *Transactions of the ASABE*, 51(3), 961–976.
- Thorp, K. R., Youssef, M. A., Jaynes, D. B., Malone, R. W., & Ma, L. (2009). DRAINMOD-N II: EVALUATED FOR AN AGRICULTURAL SYSTEM IN IOWA AND COMPARED TO RZWQM-DSSAT. *TRANSACTIONS OF THE ASABE*, 52(5), 1557-1573.
- Williams, J. R., Izaurralde, R. C., & Steglich, E. M. (2008). Agricultural policy/environmental extender model. *Theoretical Documentation, Version, 604*, 2008–2017.

## **CHAPTER 5: PREDICTING THE EFFECTS OF TWO CONTROLLED DRAINAGE SCENARIOS ON DRAINAGE DISCHARGE FOR FUTURE CLIMATE**

### **5.1 Abstract**

Subsurface drainage is widely used in the Midwest United States to prevent waterlogging of the field, but this practice also serves as a medium to transport nutrients to the freshwater systems. Controlled drainage (CD) can reduce the drainage discharge and nutrient transport from the field and increase the moisture level in the root zone of the plants. It is expected that the Midwest United States will experience increased precipitation in the future, thereby requiring the need to evaluate CD under changing climate. The objective of this study was to predict the efficiency of two different CD management practices for a representative concentration pathway (RCP) 4.5 emission scenario. The common management was performed by maintaining the weir height at a lower level (i.e., 30 cm for non-growing season and 50 cm for growing season) from the ground surface and for the aggressive management, the weir height was maintained at a higher level (i.e., 15 cm for non-growing season and 40 cm for growing season). The climate projections were obtained from 21 global circulation models (GCMs). It was predicted that the precipitation in the future period (2030-2059) would increase by 5.6 %, and the fall and winter seasons are going to be warmer than the historic period (1975-2004). We performed simulations using the Root Zone Water Quality Model (RZWQM2) where the model was previously calibrated and validated in another study. The average drainage discharge obtained from 21 simulation results indicated a 11.6% increase in the 30-year average drainage discharge in future for a field with free drainage (FD). The CD with common and aggressive management practices were able to reduce drainage discharge by 60.3% and 71.9% for the historic period, respectively, and showed similar efficiency for the future period as well. The aggressive management practice

completely restricted the drainage discharge during majority of the non-growing season, which translates into a positive impact on nutrient loss. In conclusion, the aggressive management resulted in a better performance than the common management, and both managements would remain effective in reducing drainage discharge in the likely future scenario.

## **5.2 Introduction**

The Midwest United States is the largest producer of corn and soybean in the nation largely contributed by the fertile land and abundant rainfall in this region. During the last decade, this region reported an exceptional annual production of 15.1 and 3 billion bushels of corn and soybean, respectively (Morton & Abendroth, 2017; Niyogi & Mishra, 2013). Many soils in the Midwest are poorly drained, therefore, the widespread adoption of subsurface drainage has improved crop production in this area (Skaggs et al., 1994). Subsurface drainage helps reduce crop waterlogging stress by lowering the groundwater table and allowing farmers to perform timely field operations (Blann et al., 2009; Kornecki & Fouss, 2001). Although the agronomic benefits of subsurface drainage are well documented (Fraser et al., 2001; Gardner et al., 1994), there are environmental problems associated with the practice (Ghane et al., 2016b; Jaynes et al., 2001; Sims et al., 1998). The presence of excessive nutrients (e.g., nitrogen and phosphorus) in the subsurface drainage water has contributed to the harmful algal blooms (HABs) in the western Lake Erie basin (WLEB) (Macrae et al., 2021; Pease et al., 2018; Smith et al., 2015).

While several beneficial management practices (BMPs) (e.g., denitrification bioreactors, saturated buffers, cover crops, etc.) are effective in reducing nutrient loading to downstream freshwater systems (Christianson et al., 2012; Jaynes & Isenhardt, 2019; Speir et al., 2022), controlled drainage (CD) or drainage water management is a recommended BMP for the WLEB

basin because of its ability to control the subsurface drainage volume and nutrient load (Strickland et al., 2010). CD is the practice of managing the subsurface-drained water within the field by changing the outlet elevation of the drainage system. The outlet elevation is controlled with the help of stoplogs or weir boards placed inside a control structure at the edge of the field (Evans et al., 1995; Lalonde et al., 1996; Westrom et al., 2001). This practice prevents water from leaving through subsurface drains when drainage is not required, thus increasing the travel time and natural soil-water interaction within the soil matrix.

The efficiency of CD in reducing drainage discharge and nutrient loads under existing drainage design and climate has been widely tested around the world (Nash et al., 2015; Saadat et al., 2018; Tolomio & Borin, 2018; Wahba et al., 2001; Westrom & Messing, 2007; Williams et al., 2015). But the knowledge on the efficiency of CD under future climate is still limited, especially in the Midwest United States. Climate change is projected to alter the water balance in the Midwest through increased spring rainfall and higher-intensity rainfall events (Pryor et al., 2014). Additionally, the increasing population around the world demands an increase in food production for the future. Therefore, It is important to evaluate the efficiency of CD systems under climate change scenarios to ensure a sustainable and resilient agricultural system.

Few studies have evaluated the climate change impacts on subsurface drainage systems under free drainage (FD) management (Costa et al., 2021). Pease et al. (2017) found a 12.3% decrease in the annual drainage discharge for the mid-century (i.e., 2041 to 2070) and a 14.5% decrease for the late-century (i.e., 2071 to 2098) in the WLEB under a greenhouse gas emission scenario (i.e., RCP 4.5). This reduction of subsurface drainage discharge is synonymous with the findings from Poland, where the authors also found an 11% and 17% decrease in drainage

discharge in the near future (2021-2050) for 7-m and 14-m drain spacings, respectively for an RCP 4.5 emission scenario (Sojka et al., 2020). These results differ from Singh et al. (2009), where the authors discovered a 35% increase in the average annual subsurface drainage discharge in Iowa under future climate conditions (2040-2049). Two studies from Canada (Quebec and Ontario) also projected a 31.4% and 7% increase in the annual subsurface drainage discharge, respectively (Dayyani et al., 2012; Golmohammadi et al., 2021). It is important to note that all the studies mentioned above used DRAINMOD to simulate climate change scenarios. The above discussion indicates that the impact of climate change on drainage discharge varies by geographic locations as the projected precipitation and temperature patterns varies based on location. Therefore, there is a need to determine the climate change impact on drainage discharge in other locations.

While the climate change impacts on FD systems varied by location, the impacts of climate change on controlled drainage systems are scarce. Pease et al. (2017) found the CD system to be adequate in future climate conditions because of the projected reduction in annual subsurface drainage discharge as discussed above. In another study, Awad et al. (2021) found a reduction in subsurface drainage discharge in the Yangtze River basin in China. They also implemented CD management strategies but did not evaluate the performance of CD under future climate scenarios. Since they found a reduction in annual subsurface drainage discharge for the future, it is safe to assume that CD performance would be adequate for that region in the future. Sojka et al. (2020) revealed that the CD would be most effective in blocking drainage discharge in the future if it is implemented from the 1<sup>st</sup> of March. The authors also predicted that there could be a potential increase in surface runoff under future climate. In Finland, Salla et al. (2022) used the

FLUSH model and they found that different CD management decreased drainage discharge by 11% to 23% compared to free drainage under future climate scenarios.

Based on the literature review, previous studies focused on the timing of weir management under CD for future climate (Salla et al., 2021), but studies focusing on the height of weir management are scarce. Only Saadat et al., (2018) performed an on-farm experiment to evaluate the performance of CD based on the height of weir management. Those that evaluated height of weir management on CD performance, used the same weir height under CD for both non-growing and growing season (Williams et al., 2015), which is not a common practice in the Midwest USA. Therefore, there is a need to evaluate the performance of CD in reducing drainage discharge under both varying time and height managements for future climate. The objectives of this study are: (i) to evaluate the performance of FD in the WLEB under a climate change scenario, (ii) to evaluate the effects of CD weir managements on drainage discharge in a climate change scenario.

### **5.3 Materials and Methods**

#### **5.3.1 Site description**

Our study site is located in Blissfield, Michigan (figure 5.1). The soil is classified as Ziegenfuss clay loam which is a very poorly drained soil. Subsurface drains were installed at a depth of 2.68 ft (81 cm) and the drain spacing was about 33 ft (1005 cm). The drain pipes were four-row perforated type and their effective radius was estimated to be 0.7 cm (Ghane, 2022). The area of the field is about 6.7 hectares (16.6 acres) and the grade of the field is 0.1% (i.e., very flat). This is a no-till site and the farmer uses a corn-soybean rotation in this field. The agronomic management practices can be found in Shokrana and Ghane (2022). Soil samplings were

performed on 18 March 2018 and based on those samples, the average soil test phosphorus (STP) concentration was 35 ppm (Bray-P).

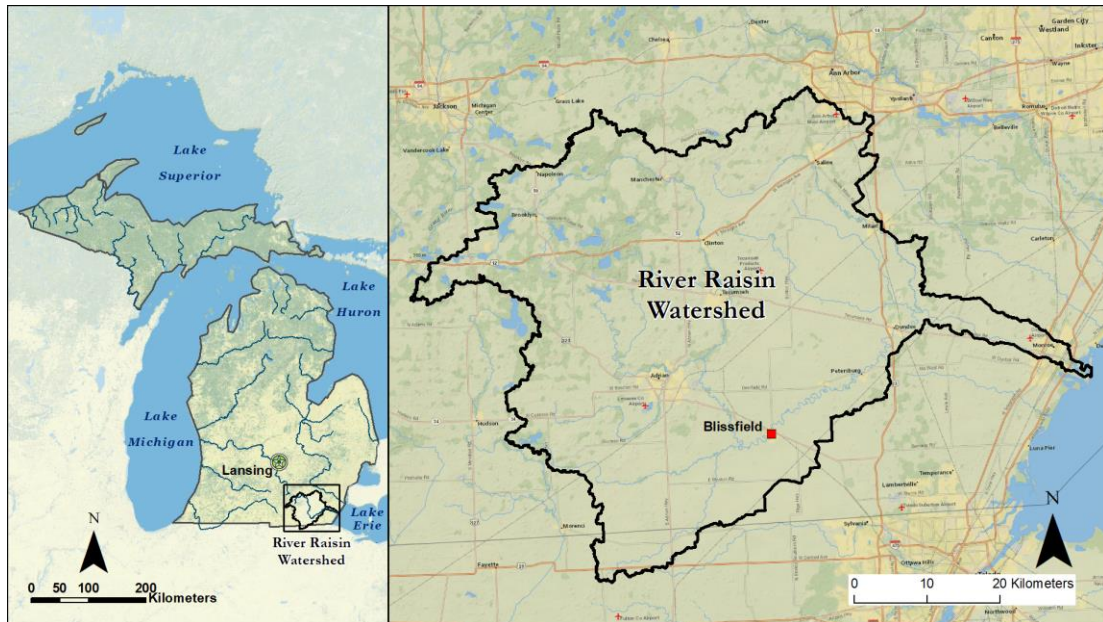


**Figure 5.1. Hydrologic boundary of the river raisin watershed. The Blissfield is part of this river raisin watershed which directly discharges into the wester Lake Erie basin at Monroe Harbor**

### 5.3.2 Flow and water quality measurements

Estimating drainage discharge is an essential part of this study because the nutrient load is directly proportional to the drainage discharge. We used our own calibrated V-notch weir flow equation as the primary method for estimating drainage discharge (Shokrana & Ghane, 2021). This equation is used until the head of water reaches the maximum height of the V-notch (i.e., 22.1 cm) for our custom-made V-notch board. Once the head of water goes above the maximum height of the V-notch, an area-velocity sensor (TIENET 350 area velocity sensor) was used to estimate the drainage discharge. HYDROS-21 sensors were used both upstream and downstream of the control structure to collect water level data. Daily water samples were collected year-round in 1000 mL plastic containers using Teledyne Isco auto sampler. Once a week, we went to

the field and brought the water samples back to the laboratory for analysis. Afterwards, the samples were analyzed for dissolved reactive phosphorus (DRP) and total phosphorus (TP). The alkaline persulfate digestion procedure was performed before analyzing the water samples for TP (Patton & Kryskalla, 2003). We used the Gallery Discrete Analyzer (Thermo Fisher Scientific) which uses the colorimetric technique for analyzing samples.

### 5.3.3 Weather data

We started monitoring the on-farm site on October 1<sup>st</sup>, 2018 and for this study, we used hourly weather data up to June 30<sup>th</sup>, 2022 (i.e., the study duration is 3.75 years). The minimum weather data required to run the RZWQM2-P are precipitation, air temperature, solar radiation, wind speed, and relative humidity. All these data were collected from our on-site ATMOS-41 weather station. Missing data were replaced from the EnviroWeather database which is the nearest weather station to our field site (<https://enviroweather.msu.edu/>). In case both ATMOS-41 and EnviroWeather databases failed to provide missing data, those were collected from the National Oceanic and Atmospheric Administration (NOAA) database (<https://www.ncei.noaa.gov/>).

After the model calibration and validation was done, we used 30 years of historic weather data (1992-2021) to run simulations for subsurface drainage discharge under various CD managements. Afterwards, we used 30 years of future weather data to simulate for subsurface drainage discharge various under CD managements.

### 5.3.4 Acquisition of future climate data

This study evaluated the performance of CD under future climate using the Root Zone Water Quality Model (RZWQM2) where the climate change data were collected from the NASA

Center for Climate Simulation (NCCS). The NASA Earth Exchange Global Daily Downscaled Projections (NEX-GDDP) dataset is a compilation of downscaled climate scenarios that are derived from 21 different general circulation models (GCMs) (table 5.1) (<https://www.nccs.nasa.gov/services/data-collections/land-based-products/nex-gddp>). The coupled model intercomparison project phase 5 (CMIP5) framework was used for analyzing the outputs from the GCMs. The CMIP5 GCM runs are supported by the fifth assessment report of the intergovernmental panel on climate change (IPCC AR5). This dataset uses a spatial resolution of 0.25 degrees (25 km x 25 km). Each GCM provides precipitation and maximum and minimum air temperature data for future climate. The NEX-GDDP dataset is generated using a statistical downscaling algorithm known as Bias-Correction Spatial Disaggregation (BCSD). The GCM runs are conducted for two greenhouse gas emission scenarios known as the representative concentration pathways (RCPs). For this study, the performance of CD was evaluated with the RCP 4.5 emission scenario for the near future (2030-2059). RCP 4.5 represents a greenhouse gas emission scenario where the radiative forces stabilize at 4.5 W/m<sup>2</sup>. Under this scenario, the policies to reduce greenhouse gas emission reaches their peak and the world population stabilizes at 9 billion (Pease et al., 2017; Thomson et al., 2011).

Changes in precipitation and temperature were calculated by subtracting the monthly average of simulated historic weather data from that of simulated future weather data. For precipitation, we used the percent change in precipitation amount between the monthly average of simulated historic and future precipitation data. Those monthly changes were then superimposed to the observed daily historic weather data from each GCM. This procedure is explained in the supplementary material of Wang et al. (2015).

We had 21 sets of climate data obtained from 21 GCMs. After running the simulations in RZWQM2 for all the GCMs, the results were processed using the equal weighting Multimodel Ensemble (MME) approach (Pease et al., 2017; Robertson et al., 2004; Tebaldi & Knutti, 2007; Weigel et al., 2010). This MME approach simply estimates the average of simulation results obtained from different GCMs. Taking an average of drainage discharge obtained from 21 GCMs will give us a better prediction compared to the drainage discharge obtained from a single model.

**Table 5.1. Summary of CMIP5 projections obtained from GCMs used in NASA NEX-GDDP database for RCP 4.5 emission scenario (Rojas-Downing et al., 2018)**

Model ID	Modeling center
inmcm4	Institute for Numerical Mathematics
bcc-csm1-1	Beijing Climate Center, China Meteorological Administration
NorESM1-M	Norwegian Climate Center
MRI-CGCM3	Meteorological Research Institute
MPI-ESM-MR	Max Planck Institute for Meteorology
MPI-ESM-LR	
MIROC5	Atmosphere and Ocean Research Institute (The University of Tokyo), National Institute for Environmental Studies, and Japan Agency for Marine-Earth Science and Technology
MIROC-ESM	
MIROC-ESM-CHEM	
IPSL-CM5A-MR	Institute Pierre-Simon Laplace
IPSL-CM5A-LR	
GFDL-ESM2M	Geophysical Fluid Dynamics Laboratory
GFDL-ESM2G	
GFDL-CM3	
CanESM2	Canadian Center for Climate Modeling and Analysis
CSIRO-Mk3-6-0	Commonwealth Scientific and Industrial Research Organization in collaboration with the Queensland Climate Change Center of Excellence
CNRM-CM5	Centre National de Recherches Meteorologiques/Centre European de Recherche et Formation Avancees en Calcul Scientifique
CESM1-BGC	National Science Foundation, Department of Energy, National Center for Atmospheric Research
CCSM4	National Center for Atmospheric Research
BNU-ESM	College of Global Change and Earth System Science, Beijing Normal University
ACCESS1-0	Commonwealth Scientific and Industrial Research Organization, Australia and Bureau of Meteorology, Australia

### 5.3.5 RZWQM2 description

The RZWQM2 model was first developed and then further improved by the USDA-ARS to simulate soil hydrological processes, crop production, and water quality effects under different agricultural management practices (Ahuja et al., 2000). The physical processes in the RZWQM2 model are defined by several mathematical equations (Ma et al., 2011; Ma et al., 2012). The soil-water characteristic curve is described by the modified forms of the Brooks-Corey equation (Brooks & Corey, 1964). The Green-Ampt equation is used to describe the infiltration process

after a rainfall, snowmelt, or irrigation event (Green & Ampt, 1911). The redistribution of water following the infiltration process is simulated by the Richards equation (Richards, 1931) and the Hooghoudt's steady-state equation is used to simulate for subsurface drainage discharge (Bouwer & Van Schilfgaarde, 1963; Smedema et al., 2004). The macropore flow is simulated using the Poiseuille's law. The Shuttleworth-Wallace equation is used to estimate the Daily potential evapotranspiration (PET) (Farahani & DeCoursey, 2000). Three crop growth simulation options are available in the model to simulate for crop yield: (i) the generic crop growth model (Hanson, 2000), (ii) the DSSAT crop growth model (Nielsen et al., 2002), and (iii) the HERMES crop growth model (R W Malone et al., 2017). For this study, we started working with the model which was already calibrated in Shokrana et al. (2022).

#### 5.3.6 Management scenarios for controlled drainage

We investigated two management scenarios for a field with a corn-soybean rotation. First scenario was the aggressive management which comprised setting the outlet elevation to 15 cm below soil surface during the non-growing season and 40 cm for the growing season. The second scenario was the common management which comprised setting the outlet elevation to 30 cm below soil surface during the non-growing season and 50 cm for the growing season. Both management scenarios were dependent on the planting and harvesting dates for corn and Soybean. Corn was planted and harvested on May 10 and October 28, respectively, during each alternative year. On the other hand, soybean was planted on May 24 and harvested on October 14 during each alternative year. For both corn and soybean, the common management during the growing season started four weeks after planting. The weir height was lowered to the drain depth (FD) two weeks before harvesting. The weir height was again raised four weeks after

harvesting and this management continued until four weeks before planting of the following year. This procedure for the timing of weir management was obtained from (Thorp et al., 2008; Youssef et al., 2018). The aggressive management for the growing season started three weeks after planting and for the non-growing season it started three weeks after harvest. The timing and height of weir boards under CD management are shown in table 5.2.

**Table 5.2. Management of weir height and timing of the common and aggressive managements used in the simulations during (1975-2004) and future (2030-2059) periods. The reference of the weir height is from the ground surface**

<b>Crop type</b>	<b>Status of management</b>	<b>Start date of common management</b>	<b>Weir height for common management (cm)</b>	<b>Start date of aggressive management</b>	<b>Weir height for aggressive management (cm)</b>
Corn	Start of free flow	12 April	88	19 April	88
	Start of managed flow	7 June	50	31 May	40
	Start of free flow	14 October	88	21 October	88
	Start of managed flow	25 November	30	18 November	15
Soybean	Start of free flow	26 April	88	3 May	88
	Start of managed flow	21 June	50	14 June	40
	Start of free flow	30 September	88	7 October	88
	Start of managed flow	11 November	30	4 November	15

### 5.3.7 Statistical Analysis

We used a paired  $t$ -test to compare changes in weather data and drainage discharge under all the management practices for both historic and future periods. We also performed comparison between the CM and IM using the paired  $t$ -test. Since we had a large sample size, the central limit theorem fulfilled the need for the normality assumption required for paired  $t$ -test. Serial correlation caused the error terms to be not independent, therefore, the standard error equation was adjusted as mentioned in Ghane et al. (2016a) and Ramsey & Schafer (2012).

## 5.4 Results and Discussions

### 5.4.1 Changes in air temperature and precipitation

The projected temperature from all 21 CMIP5 GCMs showed an increase of the maximum and minimum air temperature under future climate (2030-2059) scenario. Both the maximum and minimum temperature showed an increase in the 30-year average monthly temperature for future (figure 5.2). The 30-year average monthly maximum temperature for future is high during the months of July till December. The same is true for 30-year average monthly minimum temperature. On a seasonal basis, the 30-year average temperature in future remains stable during spring (March, April, and May), whereas the summer (June, July, and August), Fall (September, October, and November) and winter (December, January, and February) seasons were projected to be warmer (table 5.3). The highest increase in the 30-year average monthly temperature was projected during October (4.2°C increase) and it decreased during March (0.2°C decrease). The 30-year average of maximum and minimum temperature increased by 1.98°C and 1.95°C, respectively, under future climate scenario. The increase of temperature in future climate was statistically significant ( $p$ -value= $<0.001$ ).

The RCP 4.5 projections from 21 GCMs showed that future precipitation will increase by 5.6% compared to the historic scenario (1975-2004). Although this increase of precipitation in future was not statistically significant, the increasing trend of precipitation was synonymous to the results obtained in the Pease et al. (2017). Figure 5.3 showed a notable increase in the 30-year average monthly precipitation amount during spring, fall, and winter. The lowest percent increase in precipitation was projected during summer (i.e., 2.4% increase) and the highest was projected during winter (i.e., 12% increase). According to the GCMs, the percent change in precipitation amount will be the highest in December and lowest in June (table 5.3).

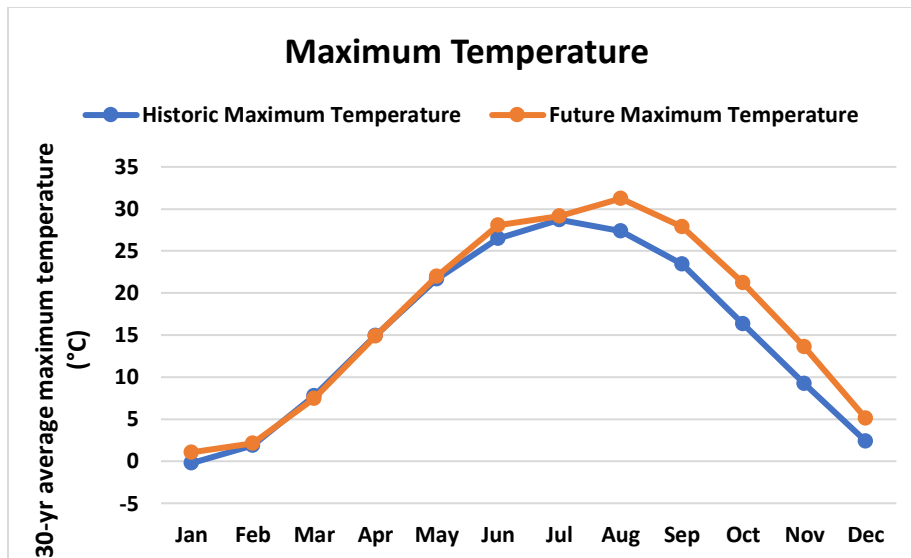
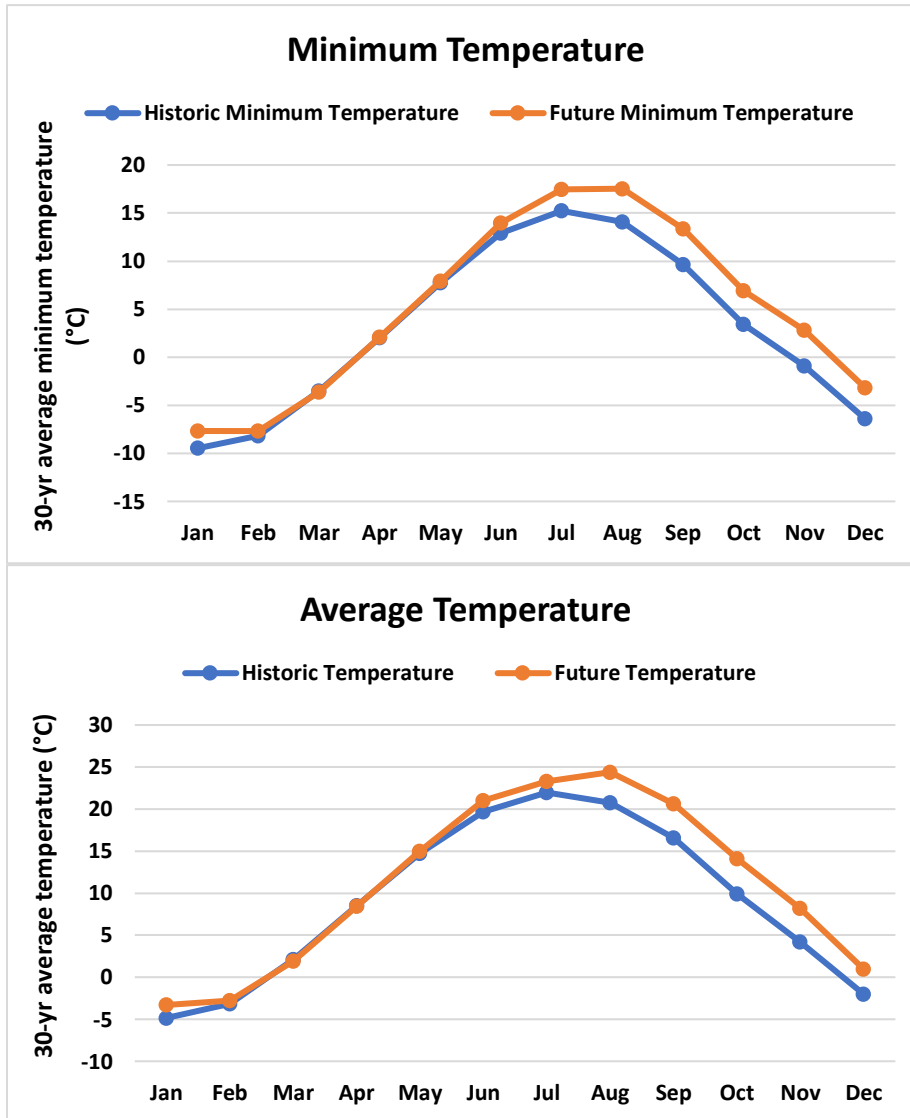


Figure 5.2. Change in the 30-year average monthly maximum, minimum, and mean temperature

Figure 5.2. (cont'd)



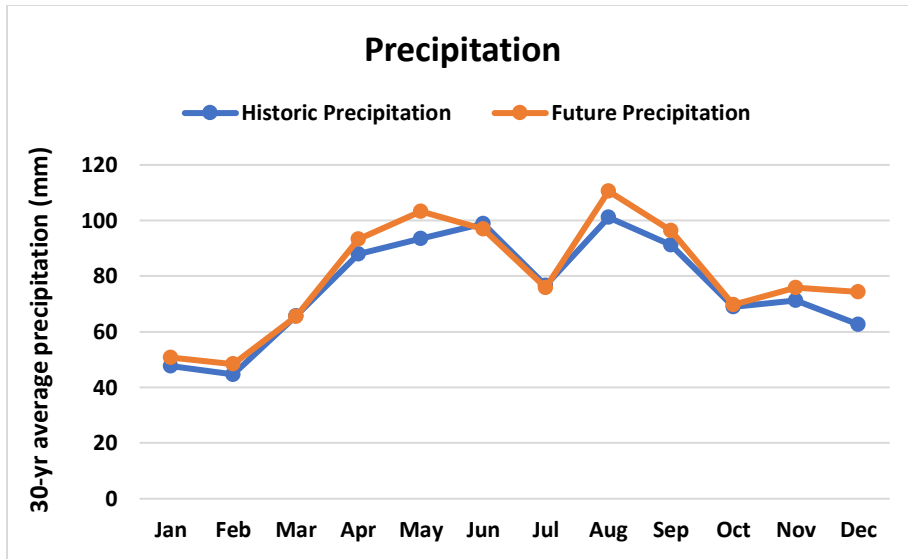


Figure 5.3. Changes in precipitation amount under historical (1975-2004) and future climate scenario (2030-2059)

**Table 5.3. The 30-year average monthly temperature and precipitation under historic (1975-2004) and future (2030-2059) climate scenarios**

	Historic weather (1975-2004)				Future weather (2030-2059)				Change in average temperature (°C)	Change in precipitation (%)
	Maximum Temperature (°C)	Minimum Temperature (°C)	Average Temperature (°C)	Precipitation (mm)	Maximum Temperature (°C)	Minimum Temperature (°C)	Average Temperature (°C)	Precipitation (mm)		
<b>Jan</b>	-0.2	-9.5	-4.8	47.6	1.1	-7.7	-3.3	50.8	1.5	6.7
<b>Feb</b>	1.8	-8.2	-3.2	44.7	2.1	-7.7	-2.8	48.4	0.4	8.2
<b>Mar</b>	7.8	-3.5	2.1	65.7	7.4	-3.6	1.9	65.5	-0.2	-0.3
<b>Apr</b>	14.9	2.0	8.5	87.9	14.8	2.1	8.5	93.3	0.0	6.1
<b>May</b>	21.7	7.8	14.7	93.5	22.0	7.9	15.0	103.3	0.2	10.4
<b>Jun</b>	26.5	12.9	19.7	98.9	28.1	14.0	21.0	97.0	1.3	-1.9
<b>Jul</b>	28.7	15.2	22.0	76.7	29.1	17.5	23.3	75.9	1.3	-1.1
<b>Aug</b>	27.4	14.1	20.7	101.1	31.2	17.5	24.4	110.6	3.7	9.4
<b>Sep</b>	23.4	9.7	16.5	91.2	27.9	13.3	20.6	96.4	4.1	5.7
<b>Oct</b>	16.4	3.5	9.9	69.0	21.2	6.9	14.1	69.8	4.2	1.2
<b>Nov</b>	9.2	-0.9	4.2	71.3	13.6	2.8	8.2	75.9	4.0	6.5
<b>Dec</b>	2.4	-6.4	-2.0	62.6	5.1	-3.2	1.0	74.3	3.0	18.7

#### 5.4.2 Climate change effects on free drainage

The predictions of drainage discharge from the GCMs showed that there will be an increase in the 30-year average drainage discharge in the future under FD (table 5.4). The drainage discharge in the future (2030-2059) increased by 11.6% compared to the discharge obtained from historic simulation (1975-2004). This increase in discharge was statistically significant ( $p$ -value= $<0.001$ ) between the historic and future period under RCP4.5 emission scenario.

Figure 5.4 showed the changes in drainage discharge under FD between historic and future period on a monthly basis. According to the GCMs projections, the increase in 30-year

average monthly drainage discharge was highest during winter and lowest during summer. The 30-year average monthly drainage discharge under FD was greater in the future period for most of the year except for the months of February, March, June, and July (figure 5.4). The reduced drainage discharge in future during March, June, and July is mainly contributed by the decrease in precipitation amount during those months. An increase in the average temperature during June and July likely has caused increased evapotranspiration (ET) which reduced the drainage discharge. Although precipitation increased by 8.2% in future for February, but drainage discharge was decreased compared to the historic period. Since the average temperature in future for February was below freezing point ( $-2.8^{\circ}\text{C}$ ), most of the increased precipitation was probably accumulated as snow. As a result, accumulated snow on ground surface reduced infiltration rate which resulted into reduced drainage discharge. On the contrary, the reason for the overall increase in drainage discharge for future period is the greater precipitation in January, April, May, August, September, October, November, and December.

During the future period, the 30-year average drainage discharge increased 1.5 cm during winter, 0.6 cm during spring, 0.2 cm during summer, and 0.8 cm during fall. This increasing trend of drainage discharge of the four seasons for future complied with the findings of Dayyani et al. (2012) and Golmohammadi et al. (2021) conducted in Canada, but does not match with King et al. (2014) and Pease et al. (2017). Since Michigan is located in the north of United States, the climate is similar to that of Canada. Therefore, the projected climate change patterns agree with the studies performed in Canada (Dayyani et al., 2012 and Golmohammadi et al., 2021). Both Pease et al. (2017) and King et al. (2014) studies were performed in Ohio. Although their studies showed an increase in average annual winter temperature, but the projected drainage discharge

decreased because the projected increase in the annual average precipitation was very low in winter. This is because Ohio does not experience extended periods of frozen soil during winter. A high increase in temperature combined with low increase in precipitation would increase ET and decrease the drainage discharge for this region under future climate (Pease et al., 2017).

For both historic and future periods, the highest drainage discharge was observed during spring and lowest during fall. The high amount of drainage discharge for both periods is likely caused by the mild temperature in Michigan around spring coupled with the high spring rainfall. On the contrary, weather predictions showed an increase in temperature and precipitation amount in winter for Michigan. Since the soils in Michigan freeze in winter, an increase in temperature would cause less snow accumulation and soils will stay frozen for shorter periods. As a result, snow will start melting leading to increased infiltration through soil and thus will increase the drainage discharge. These findings complied with the findings of Seybold et al., (2022) where the authors predicted that rain would become more frequent than snow in future. Since winter is projected to get warmer in future, the number of days below freezing point is going to reduce over time. Increased amounts of rain coupled with reduced average temperatures in winter will increase nutrient transport through drainage discharge and pose a higher risk for harmful algal bloom for the freshwater ecosystems.

**Table 5.4. Comparison between historic (1975-2004) and future period (2030-2059) for 30-year average drainage discharge under FD and CD**

Period	FD (cm)	CD under common management (cm)	CD under aggressive management (cm)
Historic (1975-2004)	26.7	10.6	7.5
Future (2030-2059)	29.8	11.6	8.4

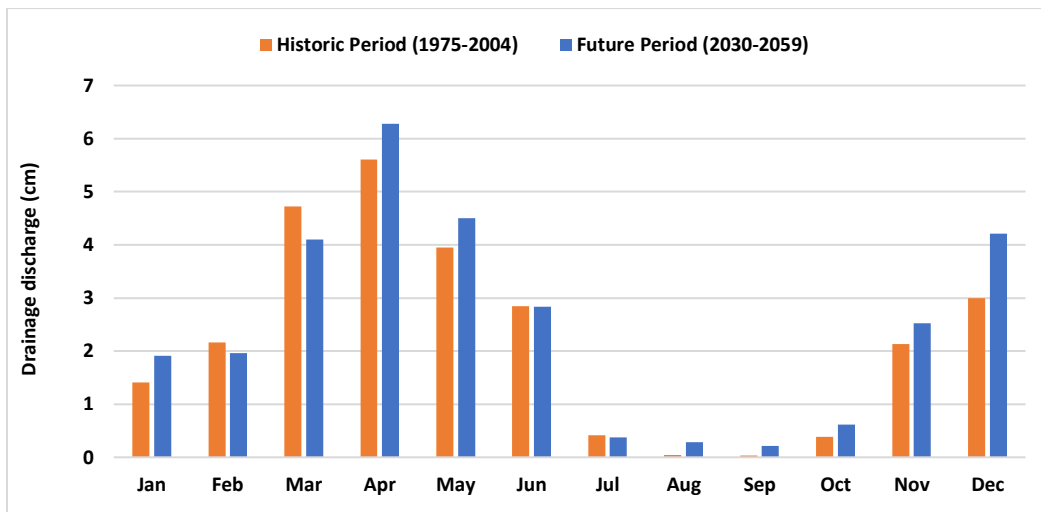


**Figure 5.4. 30-year average monthly drainage discharge for historic and future period**

### 5.4.3 Climate change effects on controlled drainage

RZWQM2 model simulations showed that CD was able to reduce drainage discharge for the historic period (table 5.4). The 30-year average drainage discharge for the historic period was reduced by 60.3% and 71.9% under common and aggressive managements, respectively. For the future period, the 30-year average drainage discharge was reduced by 61.1% under common management and 71.8% under aggressive management. The reduction of drainage discharge by both common and aggressive management was statistically significant for both historic and future periods ( $p$ -value= $<0.05$ ).

The common management performed equally well for both the historic and future period. This can be explained by combined effect of precipitation and temperature change in the future. During the non-growing season (November to mid-April), the precipitation was projected to increase by 7.5% in future, whereas the average temperature would increase by 1.4°C. Increased temperature would increase the ET, which probably would reduce the impact of increased precipitation on drainage discharge in future. For the growing season (June – September), the GCMs predicted a 3.2% increase in precipitation, but a 2.6°C increase in temperature. The combined effect of high increase in temperature a relatively low increase in precipitation would merely cause a 2.2% increase in drainage for the growing season in future. Therefore, the common management would continue to be effective for the future period.

Figure 5.5 showed that the CD with aggressive management completely stopped the drainage discharge during the entire winter (December, January, and February), early spring (March), and most of the summer season (August and September) for the historic period. CD with common management also reduced the drainage discharge during winter, early spring (March), mid-summer (August). The reason for very low or no flow under CD managements during August and September is because the subsurface drains were dry even with FD. Both CD managements showed similar drainage discharge as FD during the months of May and October. This is because the weir is lowered to represent FD to facilitate planting and harvesting operations in the field during these months for both CD managements. A sudden release of backed-up water from the entire non-growing and growing season under CD management caused a higher amount of drainage discharge compared to the FD period during these months. CD with common management showed a 45.8% reduction of drainage discharge during the summer months (June,

July, and August), whereas the aggressive management performed a 75.8% reduction. During the winter months, the common and aggressive managements caused a reduction of 98.6% and 100%, respectively.

Similar to the historic period, the CD with aggressive management was able to completely stop the drainage discharge for the months of December, January, February, and March in future (figure 5.6). Therefore, CD with aggressive management was projected to continue to be effective in completely stopping drainage discharge in future during entire winter and early spring. Drainage discharge for CD under common management increased by 9.4% in the future compared to the same management scenario during the historic period. Both CD managements for future period were able to offset the projected increase in drainage discharge by the GCMs. Therefore, it is evident that CD management will continue to be an effective practice to reduce drainage discharge in future. For regions with a much higher projected drainage discharge in future, CD with aggressive management will be the best choice because of its ability to completely restrict the drainage discharge during winter and early spring.

It is common knowledge that the nutrients (nitrogen and phosphorus) loss from agricultural fields mostly happen during the non-growing season because of the increased drainage discharge. The loss of these nutrients especially phosphorus from the agricultural fields is one of the main sources of harmful algal blooms in the WLEB. This situation is projected to worsen in future with the increased drainage discharge. Therefore, CD with aggressive management can be an effective practice to reduce the increased drainage discharge and nutrient loss from agricultural fields. Although CD managements continue to be an effective practice in reducing drainage discharge under future weather conditions, CD practice will likely

increase surface runoff. Therefore, implementing BMPs to reduce surface runoff (i.e., vegetative buffer strips, conservation tillage, etc.) from the field will be a good idea.

In future, farmers in Michigan should invest in installing drainage systems in their fields to offset the negative effects of waterlogging due to the projected increase in precipitation. A subsurface drainage system combined with a CD management could dampen the adverse water-quality effects caused by the increased rainfall and temperature in winter as reported in Seybold et al. (2022). The GCMs predicted an increase in spring rainfall for future while temperature being the same. On the contrary, early summer months (i.e., June and July) will have similar or less precipitation but increased temperature. The farmers should plant early in future to capture some of those spring rainfall and avoid the dry months in early summer.

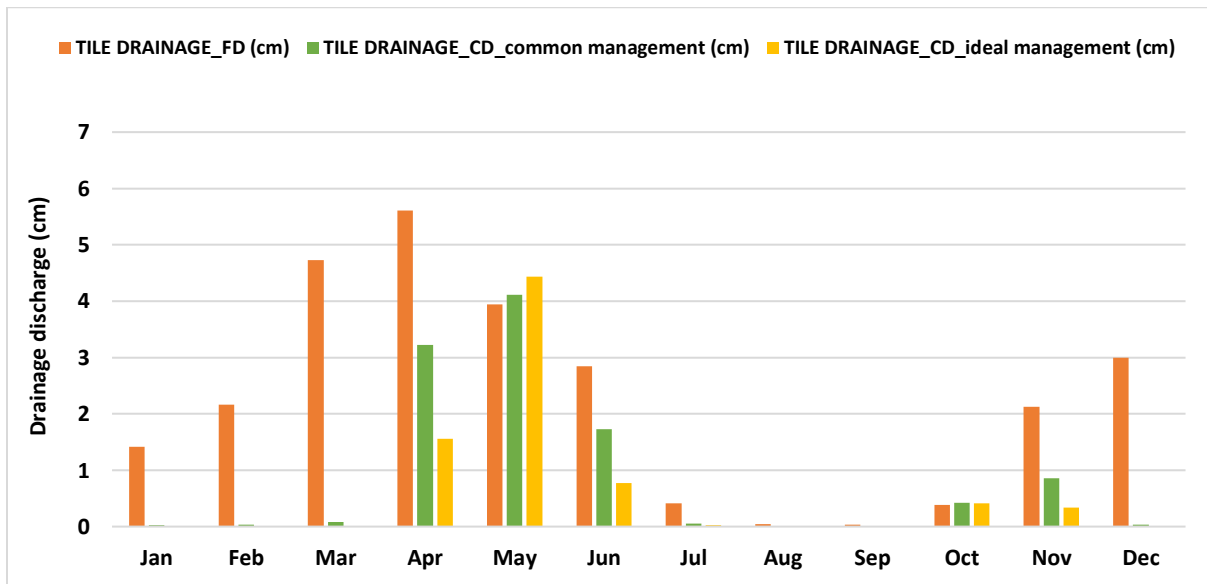


**Figure 5.5. The 30-year average monthly drainage discharge under FD, common management, and aggressive management for the historic period (1975-2004)**

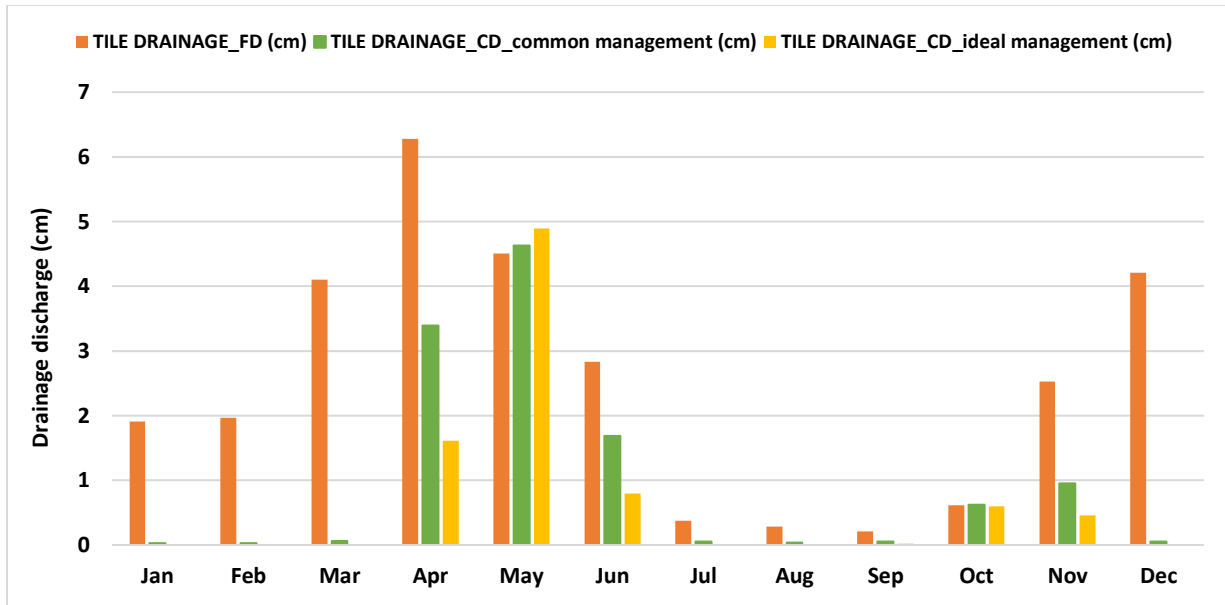


**Figure 5.6. The 30-year average monthly drainage discharge under FD, common management, and aggressive management for the future period (2030-2059)**

#### 5.4.4 Variations in drainage discharge for future climate

Section 5.4.3 demonstrated the 30-year average monthly drainage discharge obtained from 21 GCMs. In this process, the future monthly drainage discharge simulated from 21 GCMs were averaged to obtain a 30-year average monthly drainage discharge combining the GCMs. Some GCMs showed much higher variability in drainage discharge than the others and averaging them do not show the consequences of extreme drainage discharge events.

Figures 5.7, 5.8, and 5.9 showed the minimum, maximum and average future drainage discharge simulated by the 21 GCMs under free drainage, common management, and aggressive management, respectively. The variability in simulated drainage discharge is low under free drainage during the months of July, August, and September (i.e., late summer and early fall) (figure 5.7). The difference between maximum and minimum drainage discharge was high during the months of January, February, March, April, May, June, October, November, and December.

Therefore, the variation in simulated future drainage discharge were more prominent during winter, spring, and the late fall months.

Common management was able to significantly reduce the variability in drainage discharge during the months of December, January, February, and March (figure 5.8). A high difference between maximum and minimum drainage discharge under common management was observed during May and November, largely because the field was under free drainage during entire May and most of the days in November to facilitate planting and harvesting operations.

Similar to the common management, the future drainage discharge during the months of December, January, February, and March was reduced under aggressive management (figure 5.9). In comparison with the common management, the aggressive management was more efficient in reducing drainage discharge during the months of April, June, and November. From the above discussion, it is evident that both common and aggressive management were efficient in reducing future drainage discharge even if we decided to use maximum simulated drainage discharge obtained from the 21 GCMs instead of the average ones.

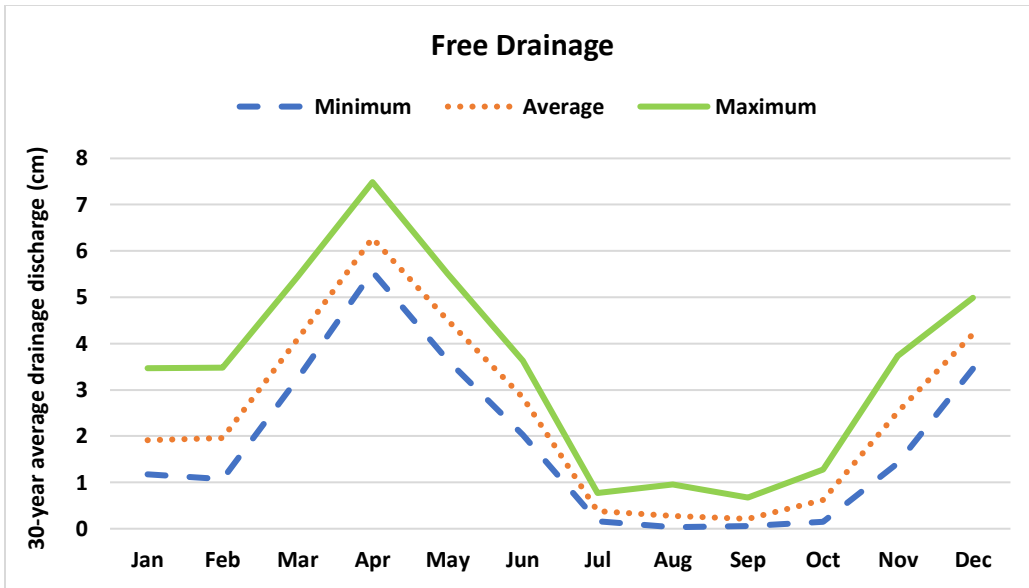


Figure 5.7. The variability in simulated future drainage discharge using 21 GCMs under FD management

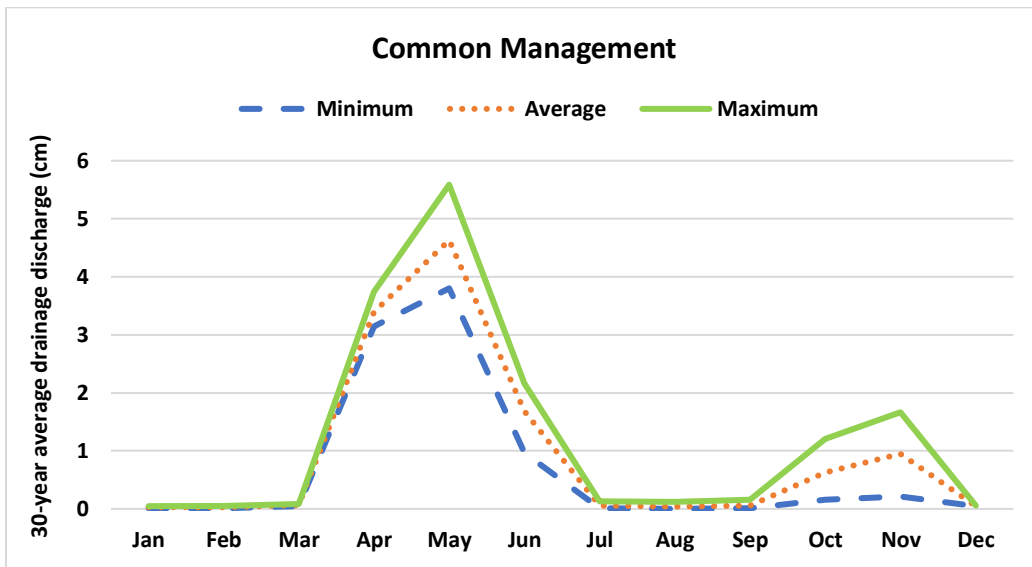
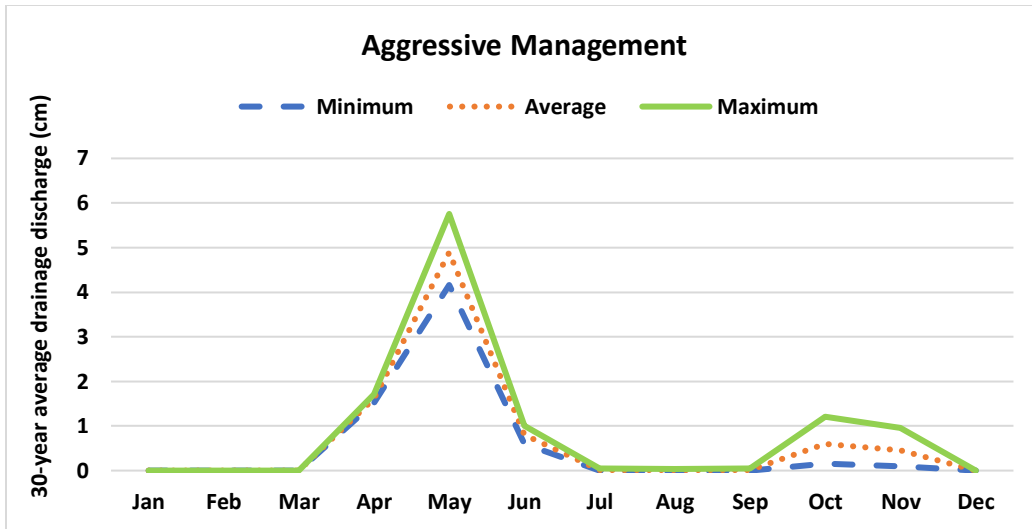


Figure 5.8. The variability in simulated future drainage discharge using 21 GCMs under common management



**Figure 5.9. The variability in simulated future drainage discharge using 21 GCMs under aggressive management**

#### 5.4.5 Limitation of the study

A limitation of this study is that it is solely hydrology based without focusing on crop yield. Although we used the RZWQM2-DSSAT crop growth model in our simulations to mimic the crop growth stages and crop water uptake, but RZWQM2 does not address wet stress on crop yield. The DSSAT model does have both crop yield and soil moisture component, but RZWQM2 only uses the crop growth component from DSSAT, which makes the model vulnerable to lack of crop wet stress. When subsurface-drained fields are put into CD management, it may induce wet stress on crops depending on the soil type and drainage design. We recommend using a different field-scale hydrologic model that accounts for wet stress on crop yield. Stacking other management practices with CD to see the effects on hydrology and water quality will also add value to the existing knowledge.

The methodology used in this study while processing climate data is limited to using the monthly averaged weather parameters obtained from the 21 GCMs. The method of

superimposing the difference between projected historic and future monthly average weather data to the daily observed weather data suppressed the effects of extreme weather events. Since future climate will be most affected by the extreme events, running separate weather simulations obtained from the 21 GCMs without superimposing the data would provide a better understating of the patterns of extreme events in future.

## **5.5 Conclusions**

We predicted the impacts of two different CD management (i.e., common and aggressive) practices on drainage discharge for a changing climate. We used 21 GCMs to generate climate projections for future. The projections indicated an increase in temperature and precipitation during fall and winter, whereas an increase in precipitation was also predicted in spring. Although the drainage discharge under FD increased for future climate, both common and aggressive CD managements were effective in reducing drainage discharge for both historic and future periods. CD with aggressive management were able to completely restrict the drainage discharge during winter or majority of the non-growing season. Since, drainage discharge under FD is projected to increase the most during winter, implementing CD with aggressive management will be the most effective practice to reduce drainage discharge and nutrient load. Farmers should invest in installing drainage systems in their field to avoid waterlogging under increased future precipitation. In future, planting early in spring would improve the crop yield because farmers would be able to capture the increased spring rainfall and avoid dry summers. In conclusion, both CD with common and aggressive management remained to be an effective practice in reducing drainage discharge for future climate.

## REFERENCES

- Ahuja, L., Rojas, K. W., & Hanson, J. D. (2000). *Root zone water quality model: modelling management effects on water quality and crop production*. Water Resources Publication.
- Awad, A., Luo, W., & Zou, J. R. (2021). DRAINMOD simulation of paddy field drainage strategies and adaptation to future climate change in lower reaches of the Yangtze river basin. *IRRIGATION AND DRAINAGE*, 70(4), 819–831. <https://doi.org/10.1002/ird.2564>
- Blann, K. L., Anderson, J. L., Sands, G. R., & Vondracek, B. (2009). Effects of Agricultural Drainage on Aquatic Ecosystems: A Review. *CRITICAL REVIEWS IN ENVIRONMENTAL SCIENCE AND TECHNOLOGY*, 39(11), 909–1001. <https://doi.org/10.1080/10643380801977966>
- Bouwer, H., & Van Schilfgaarde, J. (1963). Simplified method of predicting fall of water table in drained land. *Transactions of the ASAE*, 6(4), 288–291.
- Brooks, R. H., & Corey, A. T. (1964). Hydraulic properties of porous media and their relation to drainage design. *Transactions of the ASAE*, 7(1), 26–28.
- Christianson, L., Bhandari, A., Helmers, M., Kult, K., Sutphin, T., & Wolf, R. (2012). Performance evaluation of four field-scale agricultural drainage denitrification bioreactors in Iowa. *Transactions of the ASABE*, 55(6), 2163–2174.
- Costa, D., Zhang, H., & Levison, J. (2021). Impacts of climate change on groundwater in the Great Lakes Basin: A review. *JOURNAL OF GREAT LAKES RESEARCH*, 47(6), 1613–1625. <https://doi.org/10.1016/j.jglr.2021.10.011>
- Dayyani, S., Prasher, S. O., Madani, A., & Madramootoo, C. A. (2012). IMPACT OF CLIMATE CHANGE ON THE HYDROLOGY AND NITROGEN POLLUTION IN A TILE-DRAINED AGRICULTURAL WATERSHED IN EASTERN CANADA. *TRANSACTIONS OF THE ASABE*, 55(2), 389–401.
- Evans, R. O., Skaggs, R. W., & Gilliam, J. W. (1995). CONTROLLED VERSUS CONVENTIONAL DRAINAGE EFFECTS ON WATER-QUALITY. *JOURNAL OF IRRIGATION AND DRAINAGE ENGINEERING-ASCE*, 121(4), 271–276. [https://doi.org/10.1061/\(ASCE\)0733-9437\(1995\)121:4\(271\)](https://doi.org/10.1061/(ASCE)0733-9437(1995)121:4(271))
- Farahani, H. J., & DeCoursey, D. G. (2000). Potential evaporation and transpiration processes in the soil-residue-canopy system. *ROOT ZONE WATER QUALITY MODEL*, 51–80.
- Fraser, H., Fleming, R., & Eng, P. (2001). Environmental benefits of tile drainage. *Prepared for: LICO. Land Improvement Contractors of Ontario. Ridgetown College, University of Guelph.*

- Gardner, W. K., Drendel, M. F., & McDonald, G. K. (1994). Effects of subsurface drainage, cultivation, and stubble retention on soil porosity and crop growth in a high rainfall area. *Australian Journal of Experimental Agriculture*, 34(3), 411–418.
- Ghane, E. (2022). Choice of pipe material influences drain spacing and system cost in subsurface drainage design. *Applied Engineering in Agriculture*, 38(4), 685–695.
- Ghane, E., Ranaivoson, A. Z., Feyereisen, G. W., Rosen, C. J., & Moncrief, J. F. (2016a). Comparison of contaminant transport in agricultural drainage water and urban stormwater runoff. *Plos One*, 11(12), e0167834.
- Ghane, E., Ranaivoson, A. Z., Feyereisen, G. W., Rosen, C. J., & Moncrief, J. F. (2016b). Comparison of Contaminant Transport in Agricultural Drainage Water and Urban Stormwater Runoff. *Plos One*, 11(12). <https://doi.org/10.1371/journal.pone.0167834>
- Golmohammadi, G., Rudra, R. P., Parkin, G. W., Kulasekera, P. B., Macrae, M., & Goel, P. K. (2021). Assessment of Impacts of Climate Change on Tile Discharge and Nitrogen Yield Using the DRAINMOD Model. *HYDROLOGY*, 8(1). <https://doi.org/10.3390/hydrology8010001>
- Green, W. H., & Ampt, G. A. (1911). Studies on soil physics Part I - The flow of air and water through soils. *JOURNAL OF AGRICULTURAL SCIENCE*, 4, 1–24. <https://doi.org/10.1017/S0021859600001441> WE - Science Citation Index Expanded (SCI-EXPANDED)
- Hanson, J. D. (2000). Generic crop production model for the root zone water quality model. *The Root Zone Water Quality Model*. Water Resource Publishing, Highland Ranch, Colorado.
- Jaynes, D. B., Colvin, T. S., Karlen, D. L., Cambardella, C. A., & Meek, D. W. (2001). Nitrate loss in subsurface drainage as affected by nitrogen fertilizer rate. *Journal of Environmental Quality*, 30(4), 1305–1314.
- Jaynes, D. B., & Isenhardt, T. M. (2019). Performance of Saturated Riparian Buffers in Iowa, USA. *JOURNAL OF ENVIRONMENTAL QUALITY*, 48(2), 289–296. <https://doi.org/10.2134/jeq2018.03.0115>
- King, K. W., Fausey, N. R., & Williams, M. R. (2014). Effect of subsurface drainage on streamflow in an agricultural headwater watershed. *Journal of Hydrology*, 519(A), 438–445. <https://doi.org/10.1016/j.jhydrol.2014.07.035>
- Kornecki, T. S., & Fouss, J. L. (2001). Quantifying soil trafficability improvements provided by subsurface drainage for field crop operations in Louisiana. *APPLIED ENGINEERING IN AGRICULTURE*, 17(6), 777–781.

- Lalonde, V., Madramootoo, C. A., Trenholm, L., & Broughton, R. S. (1996). Effects of controlled drainage on nitrate concentrations in subsurface drain discharge. *Agricultural Water Management*, 29(2), 187–199.
- Ma, L., Ahuja, L. R., Nolan, B. T., Malone, R. W., Trout, T. J., & Qi, Z. (2012). Root zone water quality model (RZWQM2): model use, calibration, and validation. *Transactions of the ASABE*, 55(4), 1425–1446.
- Ma, L., Ahuja, L. R., Saseendran, S. A., Malone, R. W., Green, T. R., Nolan, B. T., Bartling, P. N. S., Flerchinger, G. N., Boote, K. J., & Hoogenboom, G. (2011). A Protocol for Parameterization and Calibration of RZWQM2 in Field Research. In L. R. Ahuja & L. Ma (Eds.), *METHODS OF INTRODUCING SYSTEM MODELS INTO AGRICULTURAL RESEARCH* (Vol. 2, pp. 1–64). <https://doi.org/10.2134/advagriscystmodel2.c1>
- Macrae, M., Jarvie, H., Brouwer, R., Gunn, G., Reid, K., Joosse, P., King, K., Kleinman, P., Smith, D., & Williams, M. (2021). One size does not fit all: Toward regional conservation practice guidance to reduce phosphorus loss risk in the Lake Erie watershed. *Journal of Environmental Quality*, 50(3), 529–546.
- Malone, R. W., Kersebaum, K. C., Kaspar, T. C., Ma, L., Jaynes, D. B., & Gillette, K. (2017). Winter rye as a cover crop reduces nitrate loss to subsurface drainage as simulated by HERMES. *AGRICULTURAL WATER MANAGEMENT*, 184, 156–169. <https://doi.org/10.1016/j.agwat.2017.01.016> WE - Science Citation Index Expanded (SCI-EXPANDED)
- Morton, L. W., & Abendroth, L. J. (2017). Crops, climate, culture, and change. *JOURNAL OF SOIL AND WATER CONSERVATION*, 72(3), 47A-52A. <https://doi.org/10.2489/jswc.72.3.47A> WE - Science Citation Index Expanded (SCI-EXPANDED)
- Nash, P. R., Nelson, K. A., Motavalli, P. P., Nathan, M., & Dudenhoefter, C. (2015). Reducing Phosphorus Loss in Tile Water with Managed Drainage in a Claypan Soil. *JOURNAL OF ENVIRONMENTAL QUALITY*, 44(2), 585–593. <https://doi.org/10.2134/jeq2014.04.0146>
- Nielsen, D. C., Ma, L. W., Ahuja, L. R., & Hoogenboom, G. (2002). Simulating soybean water stress effects with RZWQM and CROPGRO models. *AGRONOMY JOURNAL*, 94(6), 1234–1243. <https://doi.org/10.2134/agronj2002.1234> WE - Science Citation Index Expanded (SCI-EXPANDED)
- Niyogi, D., & Mishra, V. (2013). Climate-agriculture vulnerability assessment for the midwestern United States. *Climate Change in the Midwest: Impacts, Risks, Vulnerability and Adaptation*. Indiana University Press, Bloomington, 69–81.
- Patton, C. J., & Kryskalla, J. R. (2003). *Methods of analysis by the US Geological Survey National Water Quality Laboratory: evaluation of alkaline persulfate digestion as an alternative to*

*Kjeldahl digestion for determination of total and dissolved nitrogen and phosphorus in water* (Vol. 3, Issue 4174). US Department of the Interior, US Geological Survey.

- Pease, L. A., Fausey, N. R., Martin, J. F., & Brown, L. C. (2017). Projected climate change effects on subsurface drainage and the performance of controlled drainage in the Western Lake Erie Basin. *Journal of Soil and Water Conservation*. <https://doi.org/10.2489/jswc.72.3.240>
- Pease, L. A., King, K. W., Williams, M. R., LaBarge, G. A., Duncan, E. W., & Fausey, N. R. (2018). Phosphorus export from artificially drained fields across the Eastern Corn Belt. *Journal of Great Lakes Research*, 44(1), 43–53. <https://doi.org/10.1016/j.jglr.2017.11.009>
- Pryor, S. C., Scavia, D., Downer, C., Gaden, M., Iverson, L., Nordstrom, R., Patz, J., & Robertson, G. P. (2014). Midwest. Climate change impacts in the United States: The third national climate assessment. In: Melillo, JM; Richmond, TC; Yohe, GW, Eds. *National Climate Assessment Report. Washington, DC: US Global Change Research Program: 418-440.*, 418–440.
- Ramsey, F., & Schafer, D. (2012). *The statistical sleuth: a course in methods of data analysis*. Cengage Learning.
- Richards, L. A. (1931). Capillary conduction of liquids through porous mediums. *PHYSICS-A JOURNAL OF GENERAL AND APPLIED PHYSICS*, 1(1), 318–333. <https://doi.org/10.1063/1.1745010> WE - Science Citation Index Expanded (SCI-EXPANDED)
- Robertson, A. W., Lall, U., Zebiak, S. E., & Goddard, L. (2004). Improved combination of multiple atmospheric GCM ensembles for seasonal prediction. *Monthly Weather Review*, 132(12), 2732–2744.
- Rojas-Downing, M. M., Nejadhashemi, A. P., Abouali, M., Daneshvar, F., Masraf, A., Dawood, S. A., Herman, M. R., Harrigan, T., & Zhang, Z. (2018). Pasture diversification to combat climate change impacts on grazing dairy production. *Mitigation and Adaptation Strategies for Global Change*, 23(3), 405–431.
- Saadat, S., Bowling, L., Frankenberger, J., & Kladvik, E. (2018). Nitrate and phosphorus transport through subsurface drains under free and controlled drainage. *Water Research*, 142, 196–207. <https://doi.org/10.1016/j.watres.2018.05.040>
- Salla, A., Salo, H., & Koivusalo, H. (2022). Controlled drainage under two climate change scenarios in a flat high-latitude field. *HYDROLOGY RESEARCH*, 53(1), 14–28. <https://doi.org/10.2166/nh.2021.058>
- Seybold, E. C., Dwivedi, R., Musselman, K. N., Kincaid, D. W., Schroth, A. W., Classen, A. T., Perdrial, J. N., & Adair, E. C. (2022). Winter runoff events pose an unquantified continental-

- scale risk of high wintertime nutrient export. *Environmental Research Letters*, 17(10), 104044.
- Shokrana, M. S. B., & Ghane, E. (2021). AN EMPIRICAL V-NOTCH WEIR EQUATION AND STANDARD PROCEDURE TO ACCURATELY ESTIMATE DRAINAGE DISCHARGE. *APPLIED ENGINEERING IN AGRICULTURE*, 37(6), 1097–1105. <https://doi.org/10.13031/aea.14617> WE - Science Citation Index Expanded (SCI-EXPANDED)
- Sims, J. T., Simard, R. R., & Joern, B. C. (1998). Phosphorus loss in agricultural drainage: Historical perspective and current research. *Journal of Environmental Quality*, 27(2), 277–293.
- Singh, R., Helmers, M. J., Kaleita, A. L., & Takle, E. S. (2009). Potential Impact of Climate Change on Subsurface Drainage in Iowa's Subsurface Drained Landscapes. *JOURNAL OF IRRIGATION AND DRAINAGE ENGINEERING*, 135(4), 459–466. [https://doi.org/10.1061/\(ASCE\)IR.1943-4774.0000009](https://doi.org/10.1061/(ASCE)IR.1943-4774.0000009)
- Skaggs, R. W., Breve, M. A., & Gilliam, J. W. (1994). HYDROLOGIC AND WATER-QUALITY IMPACTS OF AGRICULTURAL DRAINAGE. *CRITICAL REVIEWS IN ENVIRONMENTAL SCIENCE AND TECHNOLOGY*, 24(1), 1–32. <https://doi.org/10.1080/10643389409388459> WE - Science Citation Index Expanded (SCI-EXPANDED)
- Smedema, L. K., Vlotman, W. F., & Rycroft, D. (2004). *Modern land drainage: Planning, design and management of agricultural drainage systems*. CRC Press.
- Smith, D. R., King, K. W., & Williams, M. R. (2015). What is causing the harmful algal blooms in Lake Erie? *Journal of Soil and Water Conservation*, 70(2), 27A-29A.
- Sojka, M., Kozłowski, M., Kesicka, B., Wrozyński, R., Stasik, R., Napierala, M., Jaskula, J., & Liberacki, D. (2020). The Effect of Climate Change on Controlled Drainage Effectiveness in the Context of Groundwater Dynamics, Surface, and Drainage Outflows. Central-Western Poland Case Study. *AGRONOMY-BASEL*, 10(5). <https://doi.org/10.3390/agronomy10050625>
- Speir, S. L., Tank, J. L., Trentman, M. T., Mahl, U. H., Sethna, L. R., Hanrahan, B. R., & Royer, T. v. (2022). Cover crops control nitrogen and phosphorus transport from two agricultural watersheds at multiple measurement scales. *AGRICULTURE ECOSYSTEMS & ENVIRONMENT*, 326. <https://doi.org/10.1016/j.agee.2021.107765>
- Strickland, T., Fisher, L., & Korleski, C. (2010). *Ohio Lake Erie phosphorus task force final report*. Ohio Environmental Protection Agency, Division of Surface Water.
- Tebaldi, C., & Knutti, R. (2007). The use of the multi-model ensemble in probabilistic climate projections. *Philosophical Transactions of the Royal Society A: Mathematical, Physical and Engineering Sciences*, 365(1857), 2053–2075.

- Thomson, A. M., Calvin, K. v, Smith, S. J., Kyle, G. P., Volke, A., Patel, P., Delgado-Arias, S., Bond-Lamberty, B., Wise, M. A., & Clarke, L. E. (2011). RCP4. 5: a pathway for stabilization of radiative forcing by 2100. *Climatic Change*, *109*(1), 77–94.
- Thorp, K. R., Jaynes, D. B., & Malone, R. W. (2008). Simulating the long-term performance of drainage water management across the Midwestern United States. *Transactions of the ASABE*, *51*(3), 961–976.
- Tolomio, M., & Borin, M. (2018). Water table management to save water and reduce nutrient losses from agricultural fields: 6 years of experience in North-Eastern Italy. *Agricultural Water Management*, *201*(January), 1–10. <https://doi.org/10.1016/j.agwat.2018.01.009>
- Wahba, M. A. S., El-Ganainy, M., Abdel-Dayem, M. S., Gobran, A., & Kandil, H. (2001). Controlled drainage effects on water quality under semi-arid conditions in the Western Delta of Egypt. *IRRIGATION AND DRAINAGE*, *50*(4), 295–308. <https://doi.org/10.1002/ird.29>
- Wang, Z., Qi, Z., Xue, L., Bukovsky, M., & Helmers, M. J. (2015). Modeling the impacts of climate change on nitrogen losses and crop yield in a subsurface drained field. *Climatic Change*, *129*(1), 323–335.
- Weigel, A. P., Knutti, R., Liniger, M. A., & Appenzeller, C. (2010). Risks of model weighting in multimodel climate projections. *Journal of Climate*, *23*(15), 4175–4191.
- Wesstrom, I., & Messing, I. (2007). Effects of controlled drainage on N and P losses and N dynamics in a loamy sand with spring crops. *AGRICULTURAL WATER MANAGEMENT*, *87*(3), 229–240. <https://doi.org/10.1016/j.agwat.2006.07.005>
- Wesstrom, I., Messing, I., Linner, H., & Lindstrom, J. (2001). Controlled drainage - effects on drain outflow and water quality. *AGRICULTURAL WATER MANAGEMENT*, *47*(2), 85–100. [https://doi.org/10.1016/S0378-3774\(00\)00104-9](https://doi.org/10.1016/S0378-3774(00)00104-9)
- Williams, M. R., King, K. W., & Fausey, N. R. (2015). Drainage water management effects on tile discharge and water quality. *AGRICULTURAL WATER MANAGEMENT*, *148*, 43–51. <https://doi.org/10.1016/j.agwat.2014.09.017>
- Youssef, M. A., Abdelbaki, A. M., Negm, L. M., Skaggs, R. W., Thorp, K. R., & Jaynes, D. B. (2018). DRAINMOD-simulated performance of controlled drainage across the U.S. Midwest. *Agricultural Water Management*. <https://doi.org/10.1016/j.agwat.2017.11.012>

## APPENDIX A: CHAPTER 3

### Supplementary Figures S1



**Figure S1a. Pumping water from the pond using a flexible PVC pipe. A blue lay flat discharge hose was connected to the discharge side of the pump to convey water through the flow meter and the control structure. Finally, the pumped water flowed through the outlet of the control structure back to the pond.**



**Figure S1b.** We used a centrifugal pump (Pacer pumps, model number SEB2ULE51C) to collect water from the pond. A box quarter turn ball valve was used to regulate the flow rate.



**Figure S1c.** A 100-ft long lay flat discharge hose was used to convey water from the pond. The lay flat discharge hose was attached to a PVC pipe upstream of the flow meter. An additional ball valve was connected to the PVC pipe to adjust the flow rates as per the need of the experiment.



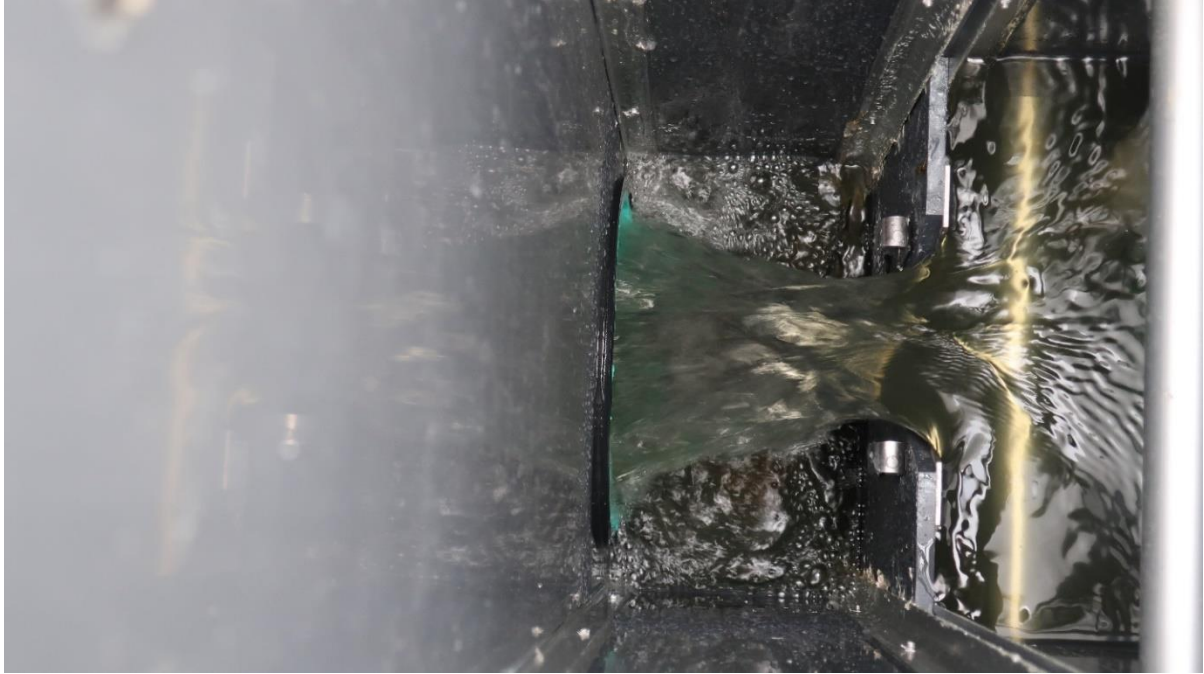
**Figure S1d.** We maintained the optimum pipe length for the turbine flow meter. Based on the turbine flow meter manual, the upstream and downstream pipe lengths of the flow meter should be at least ten (10) times and five (5) times the diameter of the turbine (i.e., 5 cm), respectively. In our experiment, the upstream pipe length of the flow meter was 101.6 cm (20 times the turbine's diameter) and the downstream pipe length was 50.8 cm (10 times the turbine's diameter). The upstream and downstream pipes were level throughout the experiment.



Figure S1e. A reading from the turbine flow meter taken during a practice run of the experiment, hence not included in the experimental data.



Figure S1f. The pumped water from the pond flowed through the flow meter, then to the control structure, where a metal-edge sharp-crest 45° V-notch weir was placed



**Figure S1g. An image of water flowing through the metal-edge sharp-crest 45° V-notch weir**

## Supplementary Figures S2

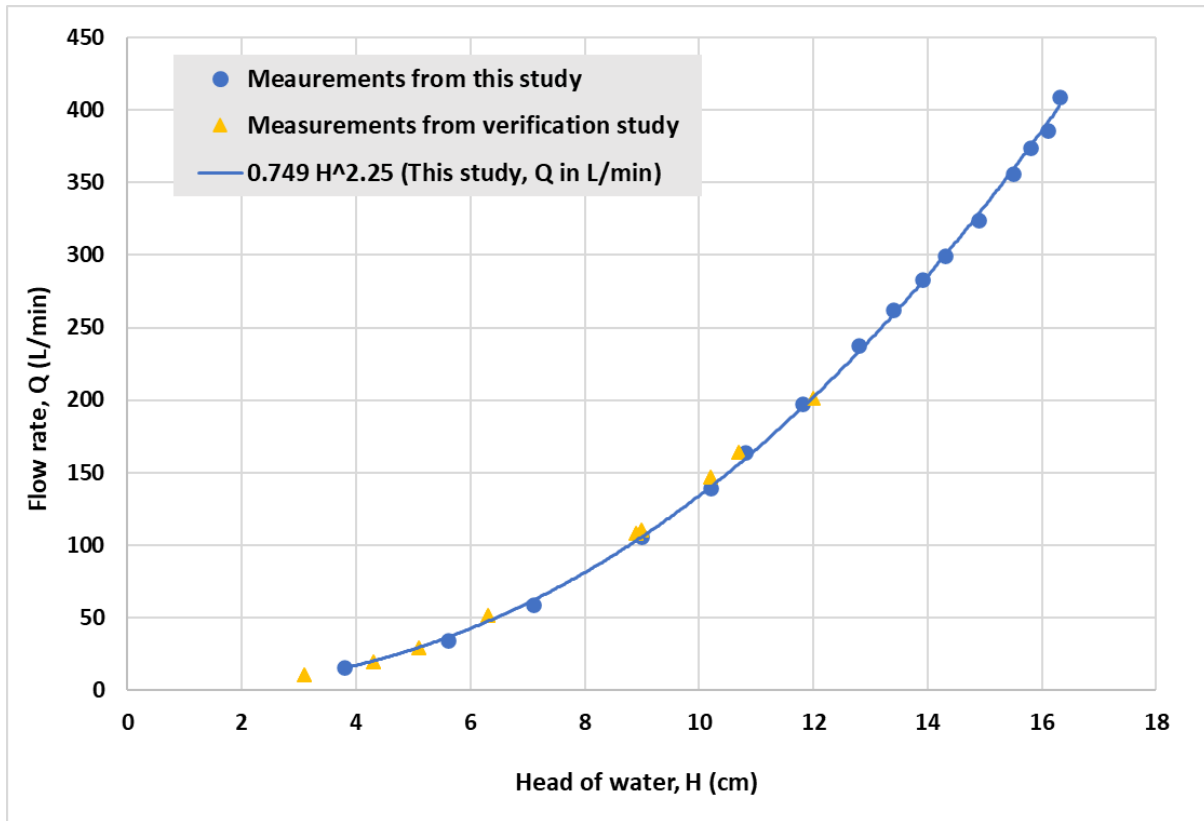
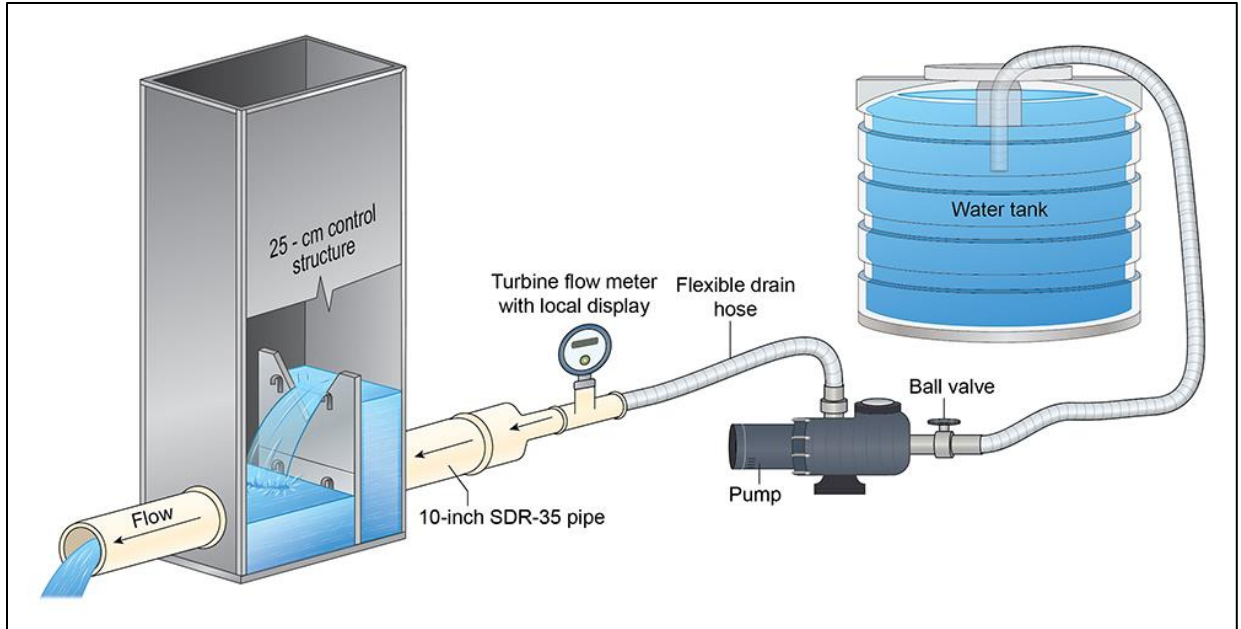
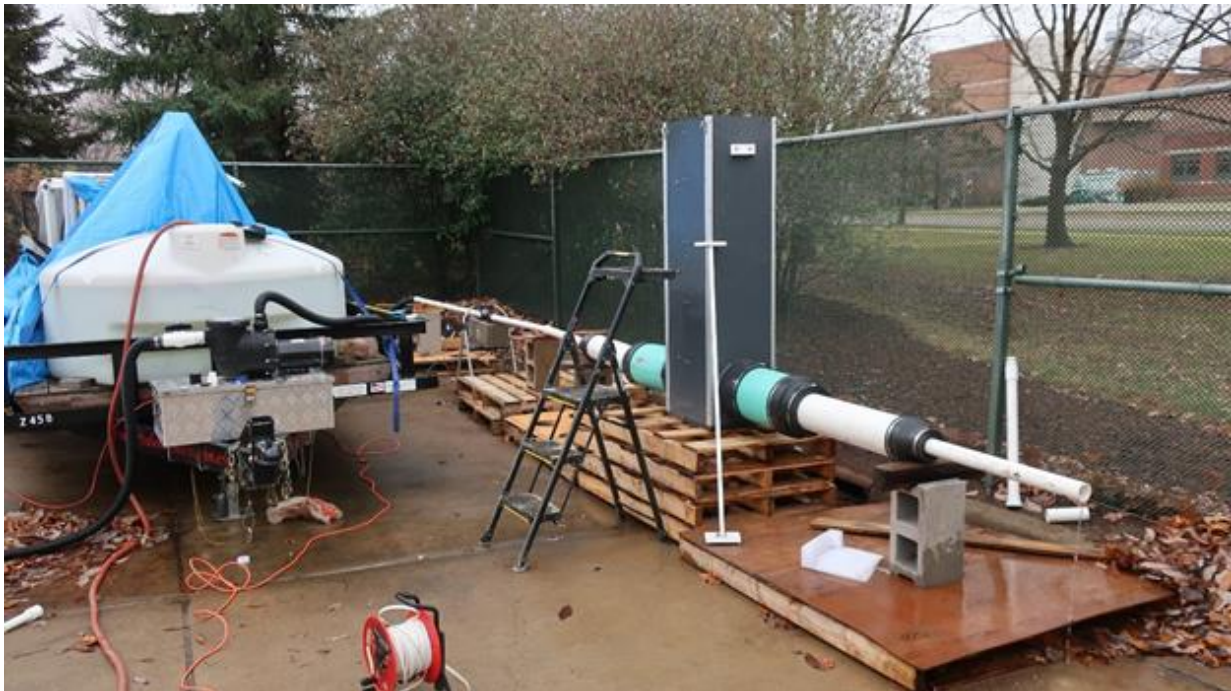


Figure S2a. A combined plot of measurements obtained from this study and the verification study, each conducted under a different setting. The former was conducted using pond water and the latter was conducted using tank water. This graph proves that the flow meters were not overestimating compared to the weighing method.



**Figure S2b. A schematic diagram of the experimental setup of the verification study. A 300-gallon water tank was used instead of a pond during this experiment**



**Figure S2c. An image of the experimental setup of the verification study conducted at Michigan State University**

## APPENDIX B: CHAPTER 4



**Figure S1. Surface ponding near the edge of the field on May 18, 2020. This was the first precipitation event after fertilization on May 13, 2020. Unfortunately, we did not have time-lapse cameras or observation wells installed in the field during the first fertilization event on April 9, 2019, but we assume that a similar ponding condition as May 18, 2020 may have existed in April 2019.**



**Figure S2. Surface ponding on the field on 28 May, 2020. Ponding was also observed on 26 and 27 May, 2020.**

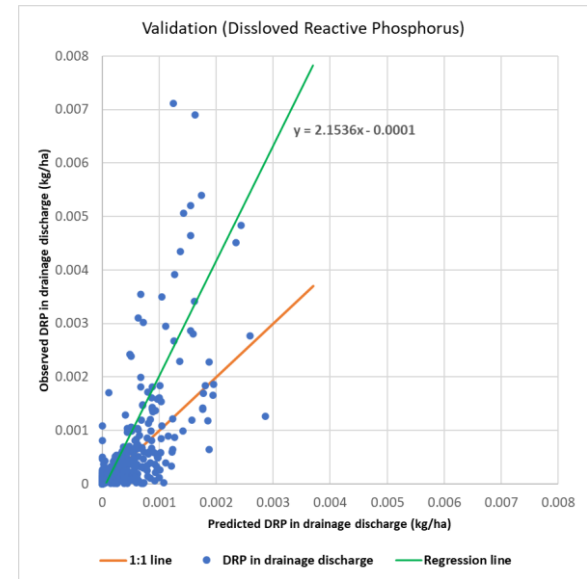
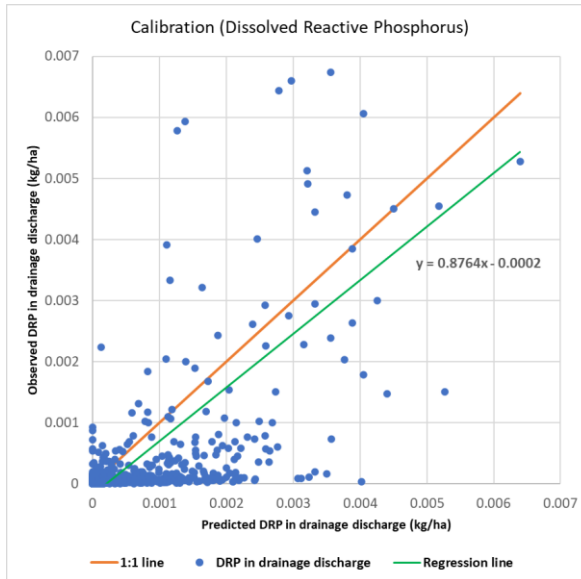
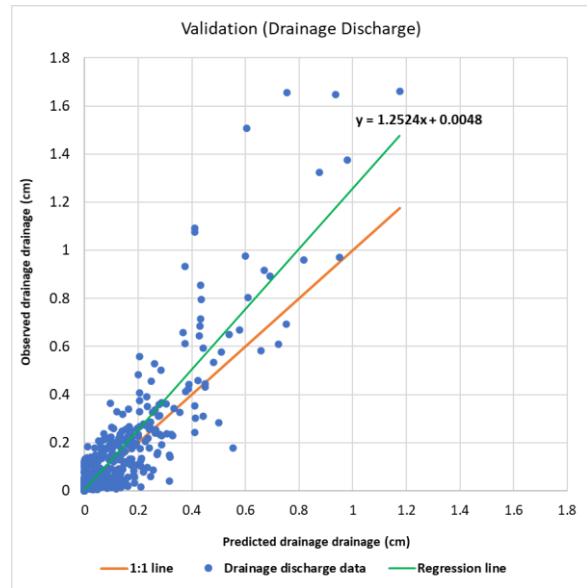
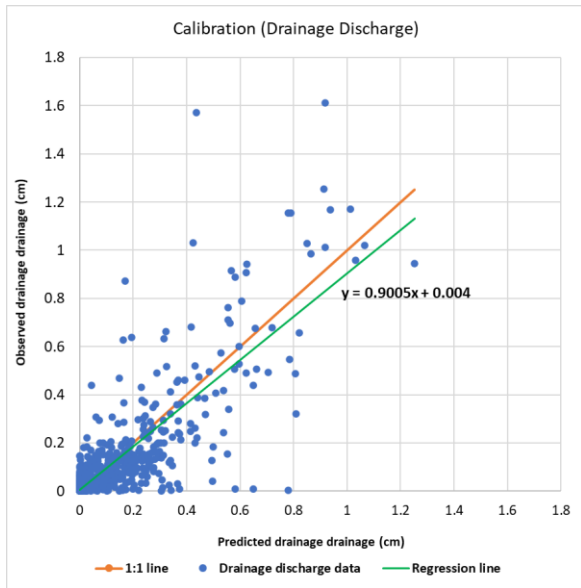


Figure S3. Scatterplot of drainage discharge, TP, and DRP for the calibration and validation period

Figure S3. (cont'd)

